Autonomous Structural Materials with Controlled Toughening and Healing

by

Michael Garcia

A Thesis Presented in Partial Fulfillment
of the Requirements for the Degree
Master of Science

Approved November 2010 by the
Graduate Supervisory Committee

Henry Sodano, Chair
Hanqing Jiang
Yirong Lin

ARIZONA STATE UNIVERSITY

December 2010

ABSTRACT

The field of Structural Health Monitoring (SHM) has grown significantly over the past few years due to safety and performance enhancing benefits as well as potential life saving capabilities offered by technology. Current advances in SHM systems have lead to a variety of techniques capable of identifying damage. However, few strategies exist for using this information to quickly react to environmental or material conditions needed to repair or protect the system. Rather, current systems simply relay this information to a central processor or human operator who then decides on a course of action, such as altering the mission or scheduling a repair operation.

Biological systems exhibit many advanced sensory and healing traits that can be applied to the design of material systems. For instance, bones are the major structural component in vertebrates; however, unlike modern structural materials, bones have many properties that make it effective for arresting the development and propagation of cracks and subsequent healing of the damaged region.

Mimicking biological materials, an autonomous material system was developed that uses Shape Memory Polymers (SMPs) with an embedded fiber optic network. This thesis researches a novel system that uses SMPs and employs an optical fiber network as both a damage detection sensor and a network to deliver stimulus to the damage site, initiating active toughening and healing algorithms. In the presence of damage, the fiber optic fractures, which allowed a high power laser diode to deposit a controlled level of thermal energy at the damage site, locally reducing the modulus and blunting the crack tip. The shape

memory polymer not only provided a sharp glass transition, but also allowed for the application of an programmed global pre-strain, which under thermal loads induced the shape memory effect to close the crack and adequately heal the polymer to its designed operational conditions recovering full strength. It will be shown that the material can be significantly toughened and that control algorithms combined with the shape memory properties can further increase the toughening and healing effect. The entire system will be able to effectively sense damage, defend its propagation by actively toughening, and subsequently heal the structure, autonomously in a real time operational environment.

DEDICATION

To my future wife, my family, and my friends. Without your love and support this would not have been possible.

ACKNOWLEDGMENTS

First and foremost I would like to thank my advisor and chair, Dr. Henry Sodano. His guidance and support led me to surmount obstacles which I would otherwise not have overcome. The result is that I am now certain of the best direction for my career. I would also like to extend my thanks to all the members of my thesis committee, Dr. Hanqing Jiang and Dr. Yirong Lin. Their constructive criticism truly polished the work of this thesis.

Much thanks to all of the members of MASS Lab, who provided me with insightful discussion about the direction of my research. I would like to generously thank Mr. Greg "Boss" Ehlert for his patience and willingness to teach. Without his mentorship, I am confident that this research would not have been completed so quickly. Also, I would like to thank Mr. Joe Shafer for sharing his copious amount of knowledge in finite element modeling, as well as being a big brother to me allowing me to vent about all the hardships that came throughout these past years. Lastly, I would like to thank the National Science Foundation (Grant # CMMI-0707309) for supporting this research.

TABLE OF CONTENTS

Page

CHAPTER Page

CHAPTER Page

LIST OF FIGURES

Figure Page

CHAPTER 1

Introduction

1.1 Motivation for Research

As critical structures age and deteriorate, it is imperative that an effective maintenance and monitoring system be implemented not only to protect the enormous monetary investment in the world's infrastructure, but more importantly, to offer protection and safety to the general public. Over the past decade, the field of Structural Health Monitoring (SHM) has led to the advancement of sensor and signal processing techniques which provide numerous methods for the detection of damage in both simple and complex structures [1-3]. Although the field of SHM has received much interest, the current techniques are limited strictly to damage detection, and simply relay the information to an outside source to schedule maintenance and repair, thus requiring the structure to undergo unwanted downtime. To mitigate this issue, there is a demand for structures that can detect as well as respond to damage in an autonomous manner.

As a source of inspiration, numerous research efforts have looked to understand the various autonomous sensing and healing mechanisms found in biological systems, and attempted to mimic these techniques in state of the art material systems. For example, a cut in human tissue is able to fully mend itself through cell proliferation, where a collagen fiber matrix creates a reinforcement network to heal the location of damage [4]. This is continued in the remodeling stage as new, stronger collagen replaces the original damaged area, followed by cells forming the outer layer of the skin leaving behind a small scar [4, 5]. The

phenomenon described is a self-healing mechanism, as the material (i.e. skin) is able to restore the initial properties without any degradation in performance. Bone offers a different response by applying toughening mechanisms to help prevent damage from propagating further into the system (Figure 1.1) [6]. Bone is able to dissipate energy around the crack's microstructure through various techniques such as viscoplastic flow [7, 8], microcracking and crazing [9-11], crack bridging [12-14], and crack deflection [15]. These methods inherently increase the toughness of the material once damage has been initiated, and prevent its further progression into the material. This toughening response is performed in operation, preventing catastrophic failure, and stalling the damage progression while the healing process is initiated.

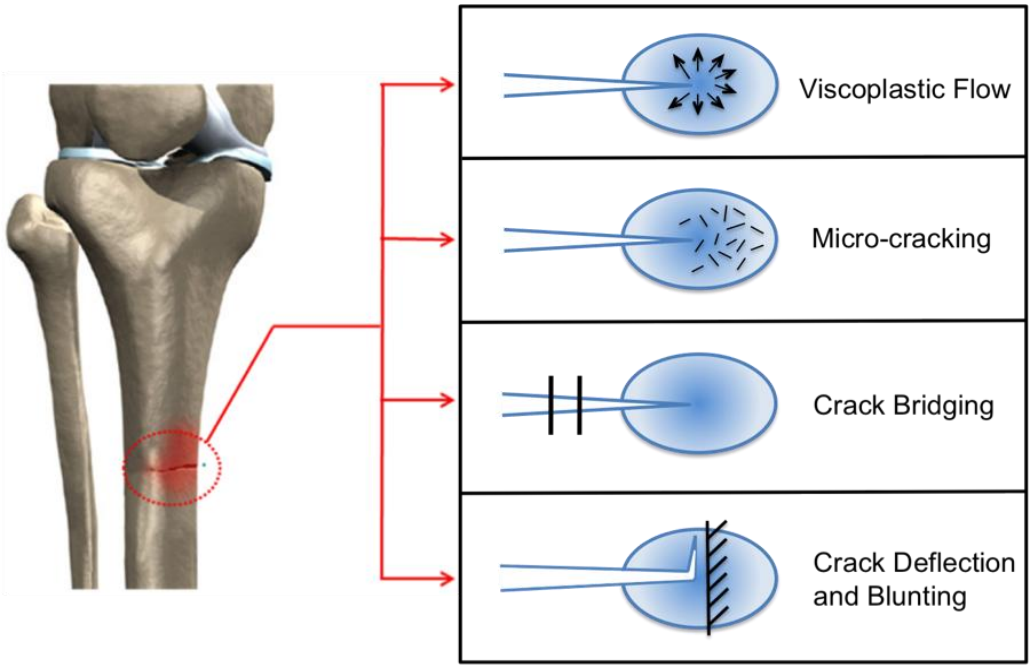

Figure 1.1 *The various natural toughening mechanisms reported for human bone. These defense mechanisms prevent the crack from propogating further into the material, and have not been implemted in structures such that the system can remain opperational by stalling damage until it can be healed (Adapted from Peterlik et al [6]).*

Recently a new class of materials have emerged that attempt to re-mend themselves in the presence of damage using chemistry based self healing techniques [5,16]. Much of the work performed in this area has focused on the development of self-healing polymers due to the reactivity of these structures and their unique response to thermal energy. White *et al.* successfully developed a self-healing polymer through the integration of two-part epoxy into the bulk polymer with the resin phase encapsulated [17]. Upon fracture, the encapsulated resin is released, reacting with a catalyst dispersed throughout the polymer leading to recovery of as much as 75% of the original strength. Chen *et al.* used a separate approach that takes advantage of the thermally reversible Diels-Alder cycloaddition reaction to break and reconnect the polymer's intermonomer linkages when subjected to thermal energy [18]. Due to the fully reversible nature of the process, the polymer can be healed multiple times, and was shown to recover nearly 57% of the original fracture load without changing the material's original properties. Although these polymeric materials have shown great achievements in self-healing, the time required to heal and repair the cracked polymer is critical, especially if the system is to continue operation. Current methods do not prevent damage from propagating, and are only effective after an adequate recovery time is provided to allow the polymerization reaction to repair the damaged site.

To overcome current limitations, this thesis focuses on the development of a novel system that couples the advantages mechanical properties of SMPs, namely, shape recovery and sharp decrease in modulus with applied heat, with a fiber

optic network to sense the presence of damage and deliver thermal energy to the damage site. As damage progresses through the polymer, the fiber optic fractures allowing a controlled amount of thermal energy to be deposited at the crack location locally reducing the modulus. The transmission loss from the fiber not only signifies a crack in the material, but initiates a control algorithm to adjust the amount of thermal energy applied and thus the modulus at the crack location such that strain energy is dissipated. This method blunts the crack, slowing its growth rate and allowing the polymer to achieve immense strains without fracture. The shape memory property of the SMP also allows the crack to be closed, and when programmed before crack initiation, can geometrically enhance the crack site to recover the original strength and heal the polymer matrix. This novel autonomous material system provides the missing link in SHM and self healing materials as it able to (1) detect damage, (2) respond and actively toughen at the crack location impeding crack propagation, and (3) recover the induced strain energy, subsequently healing the structure to its designed conditions. The system is able to adapt to different loading scenarios using autonomous control in a real time atmosphere.

1.2 Review of Previous Work

The following section presents a literature review of research relevant to each sub-component of the aforementioned self-healing system developed in this thesis. The first section briefly surveys current SHM applications using fiber optic sensors in polymer composite materials. The second section introduces the current state of the art of various healing mechanisms of both thermoplastic and

thermoset polymers. The final section discusses the advantageous mechanical properties of shape memory polymers based on A-B type polymer synthesis.

1.2.1 SHM Monitoring Systems with Embedded Fiber Optics – Overview

The majority of SHM techniques operate by interrogating the structure with a known damage scenario and correlating the measured response of different sensors to predict the state of health of the structure. Currently the two main sensors used in SHM are piezoelectric and fiber optic sensors. Piezoelectric sensor arrays are used for vibration based structural health monitoring, such that a change in the structures natural vibrating modes (global, local, or traveling waves) can be captured to locate a specific damage [19]. Fiber optic sensors offer a uniquely different response, traditionally outputting strain or temperature in a particular region, which is then correlated to a specific type of damage based on constitutive relationships [20, 21]. Another emerging approach is characterizing the transmission signal through the fiber optic to direct damage. One of the advantages of using fiber optics as the main structural sensor is that the transmission output is continuous, such that real time health monitoring can be achieved during operational loading. Unlike its piezoelectric counterparts, which reconstructs a frequency (or impedance based) response after a specified time interval and sweep of various force excitations to capture the change in structural behavior to characterize the damage being induced.

Further, fiber optic sensor arrays are easily embedded into key structural materials like metals [22], concrete [23] and advanced composite materials [24]. This allows the structural material to gain a new function, sensing, known as an

emerging smart composite materials, inspired form the central nervous system from most biological systems. As such, the integration of optical fibers into a fiber reinforced polymer composite has achieved immense attention. Although the use of fiber reinforced polymer composites are growing rapidly in the aerospace industry due to their attractive strength-to-weight ratio and controllable mechanical properties, the anisotropic material properties lead to unique damage modes not seen in their metallic counterparts such as delamination, matrix cracking, and fiber fracture [25]. Due to the complex nature of the fiber/polymer interface the damage modes are not well understood and are currently not predictable for various loading condition and extreme atmospheres, thus there has been a demand for a structurally fiber optic damage evaluation system to be embedded into fiber reinforced polymer composites.

Although embedded fiber optics networks have numerous attractive properties, there is concern that embedding fiber optics into composite materials could compromise the overall mechanical strength. A study conducted by *Measures et al.* investigated the influence of surface treated embedded fiber optics into Kevlar/epoxy panels [26]. They created two mechanical coupons that were placed in a load frame measuring the axial load and displacement in compression and tension. The two samples consisted of a 5-ply $[0_2\{90\}0_2]$ Kevlar sample, and the other with an array of optical fibers embedded between the two middle plies and orthogonal to the Kevlar fibers. They concluded that the use of embedded fiber optics did not compromise the overall compressive and tensile strength, with both types of samples with and without fiber optics, both were reported within

10% error of the manufactures reported strength values. Additionally, *Measures et al.* has demonstrated that the use of fiber optics grids in-between immediate plies of fiber do not have a detrimental influence to the resistance of delamination, ensuring the structural integrity of the composite material [27].

There are numerous types of fiber optic sensors currently used in smart structures, including fiber Bragg gratings, intensity-based optical fibers, polarimetric sensors, and a range of optical interferometric sensors [28, 29]. Within their specific limitations these sensors have shown the capability of providing the necessary sensing technologies to aid in health monitoring systems of composite materials. SHM fiber optic systems have demonstrated the ability to detect impact damage and delamination [30], measurement of structural strains in hot spots [31], the monitoring of crack propagation in bonded repair systems [32-34], the detection of transverse cracks [35], and the detection of fatigue induced damage [36]. Also, fiber optic systems have shown promise as a real time direct measurement system of the structures important mechanical properties such as tensile and compressive strengths [37, 38], stiffness [39, 40], interlaminar fracture toughness [41], and fatigue resistance [42].

1.2.1.1 Intensity Based Fiber Optic SHM Systems

Intensity based fiber optic sensors are one of the simplest designs, yet are effective for monitoring the structural integrity of a material. First developed in 1976, *Hale et al* fabricated a uni-axial patch composed up several multi-mode fiber optics embedded into an epoxy matrix. They bonded the patch with structural adhesive to a steel beam and monitored the continuity of light

transmitted through the fibers [43]. As a crack penetrated into the steel structure underneath the fiber optic patch, the crack opening displacement strained the optical fibers leading to their failure resulting in a lower light transmission, signifying a state of damage.

Shortly after *Hale et al*, a sleuth of researchers integrated the intensity based fiber optics into composite materials as a damage detection and location sensor. Some of the key work included creating large orthogonal fiber optic arrays for locating damage [44], optimization of fiber orientation for specified damage [44-45], chemically treated optical fibers to modify the surface to maximize the sensitivity [46], and altering the shape of the transmission path for increased sensitivity [47]. Each of these systems were developed and modified for a particular source of damage (i.e. impact, fatigue).

Specific to this thesis, crack propagation in an epoxy matrix is the main damage mode of interest. *Kitade et al* [48, 49] embedded intensity based fiber optics in carbon-epoxy composites with two different configurations as shown in Figure 1.2. The configuration shown in Figure 1.2a, shows the fiber optic longitudinal axis along the out of plane crack axis. This orientation was effective for detecting the delamination of the plies. By re-orientating the fiber perpendicular to the direction of the crack axis, as shown in Figure 1.2b, the system was demonstrated to be a successful method to determine crack propagation. The experiment showed that as the crack penetrates closer to the fiber optic area, the local tensile strains induced on the fiber by the matrix cracking caused the fiber optic to fail. It has been reported that in this type of

configuration, the fiber optic transmission drops by at least 90% due to light bleeding out of the fractured fiber optic, clearly indicating that failure has occurred in the system [50]. Although this method is simplistic in nature, this system is effective for monitoring crack propagation in a real time environment because the loss in transmission is measured by a continuous signal.

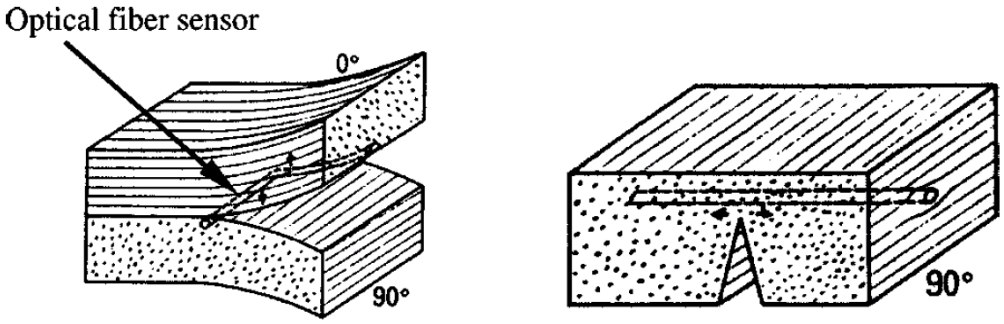

Figure 1.2. *Different fiber optic orentations used in intensity based structural health monitoring to a) detect delamination and b) detection of cracking. (Figure from Kitade et al [48,49]).*

1.2.2 Self-Healing Polymeric Materials

The use of polymers and structural composites are increasingly used in a range of applications including civil structures, transport vehicles, sports equipment, and electronics [51]. All of these polymer based systems operate in under vastly different environments, making them susceptible to various damage sources including mechanical, chemical, thermal, UV radiation, or a combination of the above [51]. It has been shown by numerous researchers that micro-cracking of the polymer matrix is the precursor to catastrophic failure in structural composites. As a crack propagating through the polymer matrix causes a drastic decrease in tensile and compressive strength [52], shorter fatigue life [53], delamination [54], and fiber fracture [55]. Current repair methods include

wielding, patching, in-situ curing of new resin, fusion bonding, adhesive bonding, and mechanical fastening, all which require the structure to schedule maintenance with a human operator and a location of the damage site. Microcracks can often penetrate deep into the laminate layers such that detection and repair methods are difficult, not cost effective, or difficult to detect.

To overcome this issue, research has looked into mimicking the autonomous self-healing response found in biological systems. The first self-healing polymer concept was demonstrated in 1980s [56], with the criteria that the polymer must be able to autonomously respond to a stimulus to recover the strength due to operational damage and continually sense and respond to damage over the components lifetime. Although various sources of damage can exist in polymer material, Mode I toughness and tensile strength are the two recoverable properties that have attracted the most interest due to their direct relation to crack propagation. Intrinsic methods exist to retard crack growth by tailoring the monomer-curing agent system [57], varying the molecular ratios [58, 59], or using additives [60, 61], allowing energy to be dissipated in the local crack region by crack deflection, zone shielding, wedging, or bridging. These methods offer overall increase the properties of the virgin sample but do not provide self-healing capabilities.

Most of the emerging research in self-healing polymers has looked into thermoplastics and thermoset polymer materials, each with their own unique properties and self-healing system. The following section will discuss the methods and concepts used for autonomous repair of damage for both thermoset

and thermoplastic materials as well as explore other methods recently demonstrating potential.

1.2.2.1 Self-Healing of Thermoplastic Materials

Molecular interdiffusion was the first self-healing concept discovered for thermoplastic materials. The concept is that as two pieces of the same polymer material are placed in conformal contact above the T_g, the molecules will diffuse across the interface causing the polymer chain segments to re-bond the two surfaces. *Jud et al* applied this concept to poly(methyl methacrylate) (PMMA) and PMMA-poly(methoxyethylate) (PMEA) bulk copolymer by fracturing single-edge notch and compact test specimens, and studied the effects of various parameters such as clamping pressures, temperatures, and healing time [62]. They discovered that visually the fracture line had disappeared, but low strength recovery was achieved due to only a diffusion length of only a few chain segments, not the complete molecular chain. Expanding on this work, *Lin et al* applied a methanol treatment to the PMMA cracked surface to promote chain mobility during diffusion with minimal heat [63]. Using the methanol treatment and allowing an appropriate time the tensile strength was fully recovered as compared to that of the virgin sample. Ethanol was also investigated as a treatment source in the same context as methanol, but showed to cause over swelling in the PMMA matrix leading to only partial recovery of mechanical strength [64].

The first demonstration of photo-induced healing in PMMA was introduced by *Chung et al*. Photochemical [2+2] cycloaddition reaction of cinnamoyl groups

was used since the photocycloaddition formed a cyclobutane structure, and upon crack propagation would revert to the original cinnamoyl structure [65]. Thus, crack healing could be performed by the re-cycloaddition of the fractured cinnamoyl groups that could be induced by pohoto-irradiation. The polymer was synthesized using a blend of 1,1,1-tris-(cinnamoyloxymethyl) ethane (TCE) with urethane dimethacrylate (UDME), triethyleneglycol dimethylacrylate (TEGDMA)-based monomers, and a visible-light photoinitiator camphorquinone (CQ) and were radically polymerized by exposing the mixture to a wavelength of light $\lambda > 280$ nm for 10 min. Healing efficiency was characterized by randomly fracturing plate specimens, followed by exposing the fractured surfaces to a wavelength of light $\lambda > 280$ nm for 10 min to initiate healing. Their results reported as high as 14% flexural strength recovery for simple irradiation and 26% for a combination of irradiation and heat addition respectively. One of the limiting factors of this method is that light must be able to penetrate past the exposed surface and transmit throughout the entire polymer structure, thus cracks in thick structures are unlikely to be exposed and heal.

Self healing through reversible bond formation was demonstrated by *Herrald et al* by grafting a secondary network of peptides to the primary polymdimethylsiloxane (PMDS) polymer [66]. The crosslinking components were formed by ionic and/or hydrogen bonding (not covalent bonding as shown in the molecular diffusion method). This not only increased the virgin toughness of the polymer, but allowed a self-healing capability due to their reversible cross linking. Healing was initiated when the surfaces came into conformal contact

with one another or with the addition of a solvent to promote chain mobility, with no additional energy or stimulus. Few experimental details are published due to patient disclosures, but claimed that healing can be achieved instantaneously and the healing efficiency can be controlled by adjusting the crosslinking structure of the polymer.

Embedding nano-particles into the polymer matrix to diffuse and/or repair the fracture is another emerging self healing technique. Mechanics modeling [67] and molecular dynamics modeling [68] demonstrated that as a crack penetrates the matrix, the embedded particles tend to migrate to the crack location autonomously applying a filler to the crack location. One of the attractive features of this method is that it does not focus on the breaking and re-joining of the polymer chains, but reinforcement of mechanical properties at the cracked site. *Gupta et al* was able to experimentally demonstrate this phenomenon by depositing a 50 nm silicon oxide layer on the top surface of a PMMA film with embedded CdSe/ZnS nanoparticles [69]. As cracks penetrated into the bulk SiO_2 layer, the nanoparticles autonomously clustered around the crack location due to the enthalpy and endotropic relations between the nanoparticles and PMMA matrix. It is believed that this process is repeatable if there is a large enough quantity of nanoparticles exists in the polymer matrix. Due to the nano-scale sample size, quantifying the healing efficiency in terms of toughness and strength was not possible and further research is required to determine the feasibly of such methods in thick structures.

1.2.2.2 Self-Healing of Thermoset Materials

The high cross linking density of thermoset materials inherently makes them more rigid and thermally stabile than thermoplastics and are thus widely used in fiber reinforced polymer composites. Due to the strong bonding between the polymer chains, they do not have chain mobility like their thermoplastic counterparts and thus diffusion and solvents cannot be used as healing mechanisms. Thus, self-healing methods in thermosets typically consist of embedded vessels containing self-healing agents into the polymer matrix, which, upon fracture autonomously release healing agents into the crack site that cure and fill the damage path.

One of the original concepts was to embed hollow fibers filled with healing agent into the polymer matrix. *Dry et al* originated this concept and first demonstrated its feasibility in cement structures [70] and successfully altered the cement matrix permeability, repaired cracks, and prevented corrosion. Although promising, transferring this method to a softer polymer based matrix was not trivial. First, they tested a single repair fiber coated with a specific polymer stiffness and thickness to control the release rate of the healing chemicals into the cracked surface [71]. This assessment was characterized by optical microscopy and photo elasticity and later visual inspections were further confirmed by *Belay et al*, but no assessment on healing efficiency was performed [72]. Expanding on the work *Pang et al* filled 60 μm diameter glass fibers with 50% volume fraction of the healing solution embedded into a conventional E-glass/epoxy laminate [73]. The healing solution consisted of varying tubes of hardener and curing

agent with a UV dye (used in X rays to detect the damage location) mixed with 40% acetone to control the viscosity for easy filling of the tubes. Although they reported difficulties in filling and releasing the healing agent in the hollow fibers, the laminate composites were successfully able to recover 93% of the flexural strength when subjected to impact damage. Further research indicated that the specimens lost their healing ability after 9 weeks due to matrix deterioration caused by the influence of acetone and the UV dye. Another attempt was to orientate 4-plys of glass fibers between 16-plys E glass/epoxy laminates, to protect intermediate cracking and delamination through the thickness of the composite during impact damage [74]. Unfortunately, by incorporating glass fibers into the structure, the flexural strength was consequently lowered by 16% due to the impact locally crushing the fibers. *Bond et al* also tried to apply heat at the crack source, in attempt to quickly cure the epoxy. However, curing occurred too rapidly and the epoxy could not disperse evenly into the crack only granting a 10% healing efficiency [75]. While an original approach, much work is needed to improve the hollow fiber method. Although healing was able to be achieved, there was a significant loss in the virgin properties of the polymer by incorporating glass fibers into the matrix. In addition, the manufacturing ability is questionable and difficulties still arise to initially fill such small diameter tubes with a high viscosity liquid.

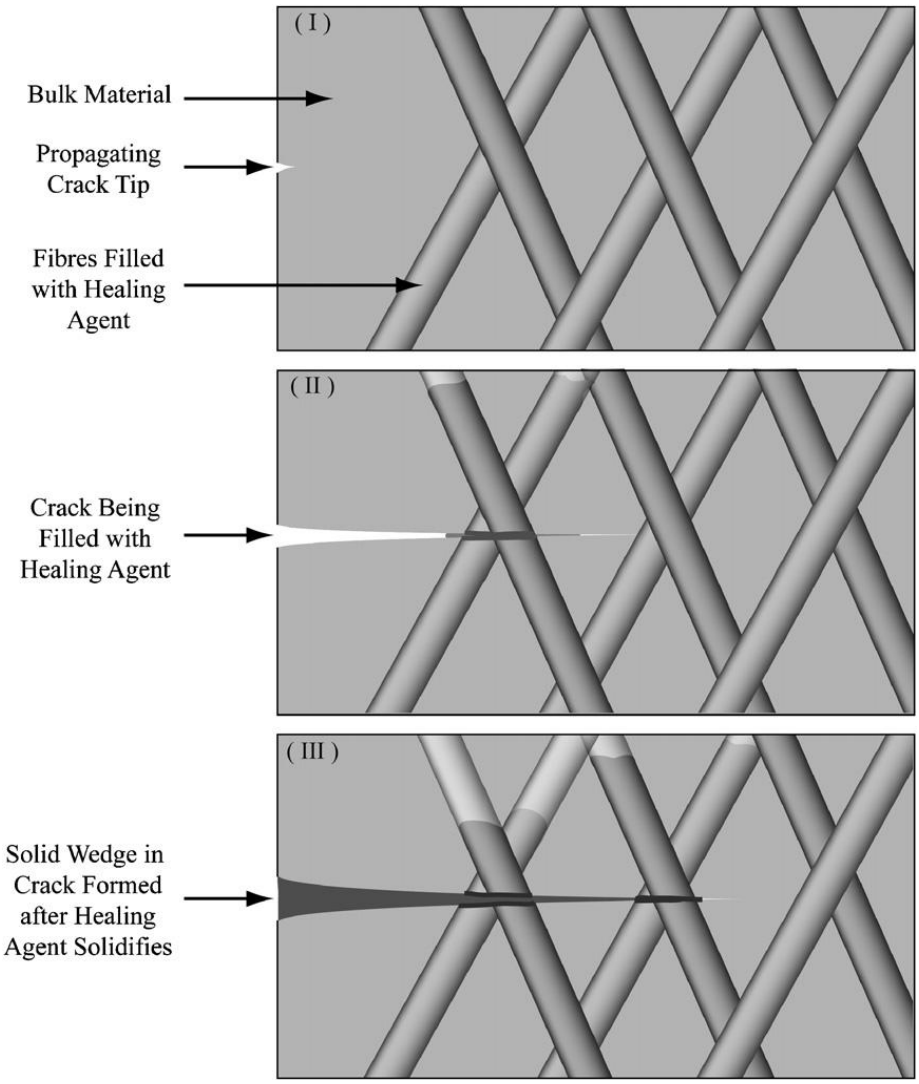

Figure 1.3. *Illustration showing the self-healing concept for the hollow fiber method (Figure from Dry et al [70]).*

The microencapsulation approach is by far the most researched self-healing concept in recent years. In the microencapsulation approach, microcapsules filled with a healing agent (in the range of 60-150μm in diameter) are incorporated into a polymer matrix with a catalysis dispersed within the matrix. Upon fracture, the capsule ruptures releasing the healing agent into the crack location by capillary action. The healing agent then reacts with the embedded catalysis to

autonomously heal the cracked site. Although various healing agent-catalyst combinations have been synthesized, the diclopentadine (DCPD) healing agent with a Bis(tricylohexylphosphine) benzylidine ruthenium (IV) (or more commonly noted as the Grubb's catalysts) self healing system is the most promising due to its numerous advantages including long shelf life, low monomer viscosity and volality, polymerization within minutes at room temperature, and formation of highly cross linked crack fillers [76]. *Sanada et al* investigated the use of the DCPD/Grubbs catalyst for healing of deboned plies in a neat epoxy and uni-directional carbon fiber matrix when undergoing tension [77]. The composite consisted of a 30 wt% of DCPD microcapsules and 2.5 wt% Grubbs' catalyst. However after fracture, the maximum tensile strength recovery after a curing schedule of 48 hours was only 14%. *White et al* showed the encapsulated approach to be beneficial for fracture healing. They prepared tapered double-cantilever beam (TDCB) specimens composed of Epon 862 resin with 2.5 wt% Grubbs' catalyst and 10 wt% DCPD filled microcapsules, and reported a toughness recovery of 75% [76]. *Brown et al* discovered that the ratio of Grubbs'/DCPD reported by *White et al* required a minimum of 25 mins (the geletation time of poly(DCPD) at room temperature) in order to recover any mechanical properties [78]. Characterization of fatigue crack growth by the microencapsulated method has been further explored by *Brown et al*. Similar specimens were prepared, in a TDCB geometric configuration with Epon 862 epoxy dispersed with 180 μm diameter 20 wt% DCPD microcapsules and 2.5 wt% Grubbs' catalyist [79]. They showed that under low-cycle fatigue conditions

the healing-method achieved 73-118% increase in fatigue life, where in high cycle fatigue conditions the range reported was 89-213% increase.

Adding microcapsules or embedding catalyst could potentially have negative effect on the virgin mechanical properties of the polymer. The effect of this change depends on the volume fraction of additives, the level of interfacial interaction, and the mechanical properties of the additives itself. *Brown et al* showed for the DCPD/Grubbs' embedded in epoxy matrices, both the modulus and ultimate strength decreased based on increasing the microcapsule diameter for a fixed volume fraction [80]. Further, they demonstrated that the addition of more than 3 wt% Grubbs' catalyst significantly reduced the fracture toughness of the original epoxy matrix [81]. Although increasing the ratio of catalyst to healing agent would speed up the critical time to heal the structure, but significantly weaken the original virgin properties.

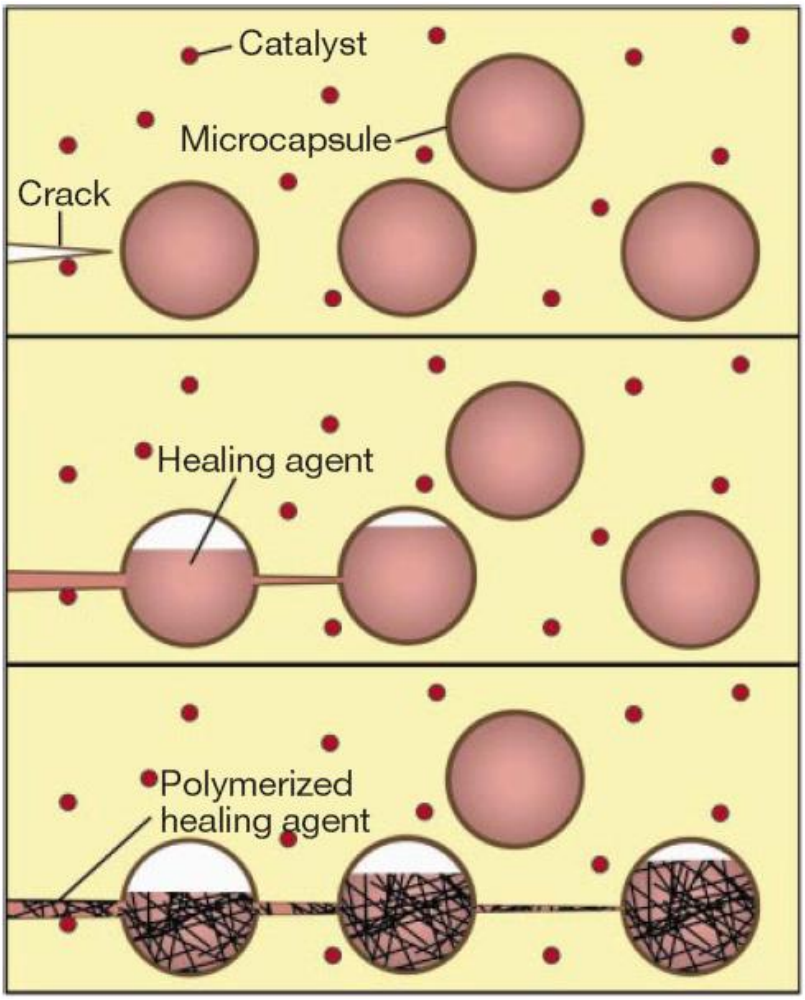

Figure 1.4. *Illustration showing the self-healing concept for the microencapsulation method (Figure from White et al [17]).*

Another self healing method involves developing thermally reversible cross linked polymers with similar mechanical properties as epoxy and thermoset resins. *Chen et al* engineered such a polymer by incorporating thermally reversible Diels-Alder (DA) reaction for linear chained polymers [82, 83]. Synthesizing a thermally reversible DA cycloaddition of a multi-diene (multi-furan, F) and multi-dienophile (multi-malemide, M) revealed a structure similar to the photo-reversible polymer network mentioned previously. Upon fracture, the

weaker non-covalent bonds between the furan and malemide split apart across the wake of the crack profile. Upon the application of heat, the inner-monomer linkages disconnect throughout the matrix, and by allowing the fractured surfaces to coincide during cooling will subsequently rejoin the molecular chains across the interface. *Chen et al* experimentally demonstrated the healing efficiencies by fabricating compact tension specimens and testing the samples to failure. The fractured surfaces were clamped and heated to 150 °C and 120 °C allowing the surfaces to rejoin and achieved a healing efficiency of 50% and 41% respectively. A study of multiple healing (i.e. fracture and re-heat) cycles was also conducted, and showed an 80% drop in critical fracture load from the 2^{nd} to 3^{rd} cycle. It is hypothesized that the healing region consisted of weaker mechanical properties than the original material because not all of the fractured bonds were repolymerized due to miss-alignment of the surfaces. Expanding on their previous work, *Chen et al* created a second generation of polymers, mitigating all solvents from the synthesis procedure, ultimately lowering the glass transition temperature (requiring less energy to heal) as well as created a harder and transparent polymer [84]. Under these adjustments higher healing efficiencies were achieved up to 80% for the first crack-heal process, followed by 78% for the second one.

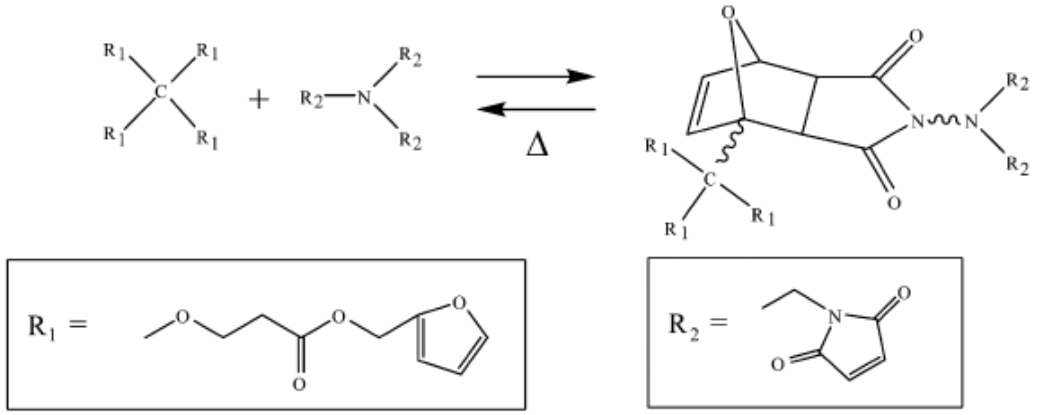

Figure 1.5. *The thermally reversible crosslinking reactions under fracture and re-heating (Figure from Chen et al [82]).*

Other less studied self-healing methods have also been developed such as the addition of thermoplastic additives within in the polymer matrix [85], chain rearrangement [86], and metal-ion-mediated healing [87]. Thermoplastic additives embedded in the polymer matrix are subjected to heat locally provide a crack filler and rebound the fractured surfaces, but challenges of this method lie in the blending of a thermoplastic into a thermoset material without degrading the matrix properties [85]. Rearrangement of polymer chains by applying a temperature source equal or greater then room temperature has shown to cause interdiffusion of dangling chains or chain slippage in the polymer network. *Yamaguchi et al*. first demonstrated this healing candidate in a thermoset epoxy by visual inspection, but has yet to perform any mechanical testing [86]. *Varghese et al*. used metal-ion-mediated reactions to repair lightly cross-linked hydrophobic gels [87]. This method involves dispersing metal ions into an aqueous solution and is absorbed into a gel through diffusion. As diffusion progresses, tensile strength recovery was shown to increase from 75% to 100%

from 6 hours to 12 hours respectively. Although high recovery is achieved, researchers speculate whether the material is "healed" because after diffusion the gel obtains a vastly different physical structure and properties making comparisons difficult.

1.2.2.3 Self-Healing via the Shape Memory Effect

A limited amount of research has been conducted in which the shape memory effect is utilized as a "healing" mechanism. This process takes a different approach applying the shape control and rapid transition from a glassy to an elastic polymer to modify the mechanical properties. The shape memory effect also allows the material to recover large mechanical deformations by applying thermal energy [88-90]. The multifunctional use of shape memory materials has great potential for various applications as it is able to tune mechanical properties and adapt to environmental changes [91]. Cheng *et al* first demonstrated the self healing aspect of the shape memory effect by microindenting shape memory alloys (SMAs) with different deformation geometries via a spherical and pyramid indenter [92]. They showed that the SMAs were able to recover nearly all of the induced strain by simply heating the material from room temperature to 150°C. Burton *et al* developed a finite element model, in which SMA wires were embedded into a polymer matrix perpendicular to the induced crack [93]. Upon loading, the SMA wires transformed to the martensite phase needed for shape recovery. By simply heating the SMA wires, the wires contracted closing the crack location and ultimately toughening the polymer matrix. Recently, *Li et al* fabricated a three dimensional woven fabric reinforced shape memory polymer

composite for impact mitigation [94]. By programming a prestrain in the composite structure, upon impact, dents could be fully recovered by applying thermal energy. The use of the shape memory effect shows great potential in assisting with crack closure techniques, providing the missing link for self-toughening materials that can halt the propagation of damage to allow the healing process to finish.

1.2.3 Shape Memory Polyurethane

The shape memory effect describes the ability of a material to return to a prescribed shape under the influence of an outside stimulus. The shape memory effect was first demonstrated in metallic alloys, such as gold-cadium alloy [95] and the more popular nickel-titanium alloy [96]. SMAs shape memory effect is governed by its phase transformation during heating and cooling. Typical programming consists of cooling the SMA from its cubic symmetry austenitic phase down to lower symmetry martensitic phase. While in this state, the material may mechanically deform (within the limitations of plastic deformation) to the desired secondary shape. Heating the SMA above the phase transition temperature allows the material to recover back to the austenitic phase and shape recovery can be achieved up to 8% of deformed strain. Although SMAs offer great recovery force that may be used in actuators, the low recovery strain makes them unsuitable for large geometric changes from the primary shape limiting their possible applications.

To overcome the limitations posed by SMAs, responsive shape memory polymers have the ability to re-cover large strains, reported as high as 300 % [97],

and have shown the ability to have more than one temporary shape opening a wide range of applications such as smart textile and apparels [98], intelligent medical instruments [99], biomimetic devices and artificial muscles [100], electrochecmical devices [101], micro-electro-mechanical systems [102], self-deployable solar sails [103], active sound absorbers and flexible speakers [104], and many more. Over the past couple of decades, numerous researchers have investigated different sources of stimuli including heat, electricity, magnetic field, moisture, and pH value (drug delivery system) each tailored to its own polymer based structure (i.e. styrene, PMMA, polyurethane) as well as tailoring the responsive behavior (i.e. recovery of mechanical deformation).

Of these polymers, thermally responsive polyurethanes have received the most interest because their properties can be controlled by simple co-polymer selection. Further, the linear A-B type synthesis have been extensively researched and have shown to have many attractive properties, such as controllable high cross linking density for increased mechanical properties, optical clarity, and controllable glass transition temperature governing the input energy for shape recovery [105]. The following section discusses the thermal response of shape memory polyurethane on the molecular level, followed by the constitutive relationships based upon copolymer selection, and lastly current relevant applications using thermally responsive SMPs in particular using photo-thermal heating.

1.2.3.1 Molecular Properties of Thermally Responsive Polyurethane

SMPs have a unique molecular structure which allows for mechanical properties such as shape recovery and rapid changes in elastic modulus. Figure

1.6 shows the shape recovery on a molecular level during a thermodynamic cycle. Typically, SMPs consist of segregated linear block copolymers consisting of hard and soft segments [106]. The hard phase acts at the primary shape, which produces a hard domain in the initial casted state which is either single crystal or physically crosslinked. The amorphous soft phase is responsible for the shape memory phenomenon. When heated past the glass transition temperature T_g (glassy to rubbery state) of the soft segments, the coiled chain segments become flexible. By applying an external stress in this heated state, the soft chains stretch in the direction of applied strain. Allowing the stretched chains to cool below the T_g in the deformed configuration will lock the chains in place, freezing the polymer into a new deformed shape. To recover the original shape, heating past T_g causes the chains to relax back to the low entropy configuration, thus remembering its original shape in which it was molded.

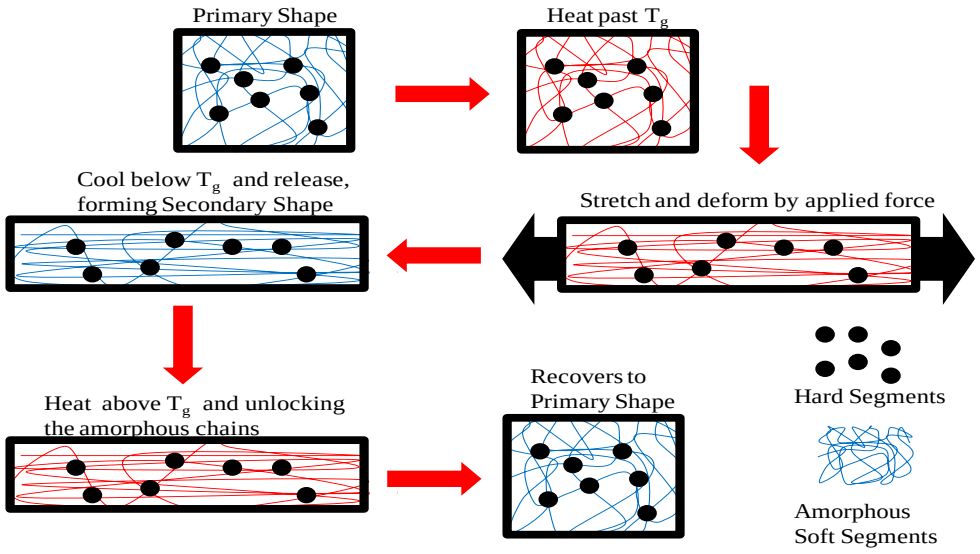

Figure 1.6. *Shematic of the the molecular structure of a segmented polymer demonstrating shape memory recovery during a thermodynamic cycle.*

Segmented polyurethane using A-B type condensation has shown to produce a promising network for shape memory polymers [106]. A-B shape memory polyurethane synthesis combines two copolymers, respectively the hard and soft segmented domains. Shape Memory Polyurethane is composed of three starting materials, (1) long chain polyol, (2) diisocyanate, and (3) a chain extender in combination of the correct 1:1 molar ratio of issocayate (-N=C=0) groups to hydroxyl (-OH) groups. The long chain polyol makes up the soft segment with the chain extender and diisocyanate forming the hard segment. By varying the ratio of soft and hard copolymers, the mechanical properties such as amount of shape memory recovery and glass transition temperature can be adjusted.

1.2.3.2 Mechanical Properties of Thermally Responsive Polyurethane

The constitutive stress-strain relations for SMPs have been formulated by *Liu et al* based on the inhomogeneous volume fractions of frozen and active phases (ϕ_f and ϕ_a respectively) which are defined as

$$\phi_f = V_f / V \tag{1.1}$$

$$\phi_a = V_a / V \tag{1.2}$$

where V is the total volume, and V_f and V_a are the frozen and active volumes respectively, allowing $\phi_f + \phi_a = 1$ [107]. The frozen phase refers to the hard segment modeling the polymer bonds during energetic change such as deformation due to an applied stress and includes the thermal deformation when subjected to a temperature gradient. The active phase corresponds to the soft amorphous segments capturing the influence of free conformational motion when

the polymer is heated to the full rubbery state. By changing the ratio of active to soft phases during a thermodynamic loading cycle allows the shape memory effect to be captured. The small strain 1D constitutive equations are given as

$$\sigma = E\left(\varepsilon - \varepsilon_s - \int_{T_o}^{T} \alpha dT \right) \tag{1.3}$$

where σ is the stress, E is Young's Modulus, ε is the true strain, ε_s is the stored strain, α is the coefficient of thermal expansion, and T_o is the initial temperature. The modulus is related to the frozen phase volume fractions as

$$E = \frac{1}{\frac{\phi_f}{E_i} + \frac{1-\phi_f}{E_e}} \tag{1.4}$$

where E_i is the glassy modulus and E_e is the rubbery modulus. The stored strain energy is governed by its temperature dependence, and is defined by a differential equation given in equation 1.5.

$$\frac{d\varepsilon_s}{dT} = \frac{\varepsilon - \varepsilon_s - \int_{T_o}^{T} a dT}{E_e\left(\frac{\phi_f}{E_i} + \frac{1-\phi_f}{E_e} \right)} \left(\frac{d\phi_f}{dT} \right) \tag{1.5}$$

Thus, to fully model the shape memory response the temperature dependence of the frozen volume fraction, $\phi_f(T)$, switching from glassy to its rubbery state must be experimentally fitted. This is naturally done by experimentally measuring the modulus, easily quantified by dynamic mechanical analysis (DMA), and computing the corresponding active/frozen volume fractions.

The elastic modulus of thermally actuated polyurethane based shape memory polymers have been explored by various researchers [108]. One of the key properties of the SMP is the sharp decrease in modulus when the applied temperature approaches T_g. Figure 1.7 shows a typical modulus (E) profile, which is governed by the equation

$$E = E_g \exp\left[a\left(\frac{T_g}{T} - 1 \right) \right] \tag{1.6}$$

where is the applied temperature, T_g is the glass transition temperature, E_g is equal to the value of E at $T=T_g$, T and a is a parametric used to quantify the sharpness of transition. Typical polymers are fabricated such that within +/-5% of T_g a full transition from a glassy to rubbery state, a modulus drop of two orders of magnitude.

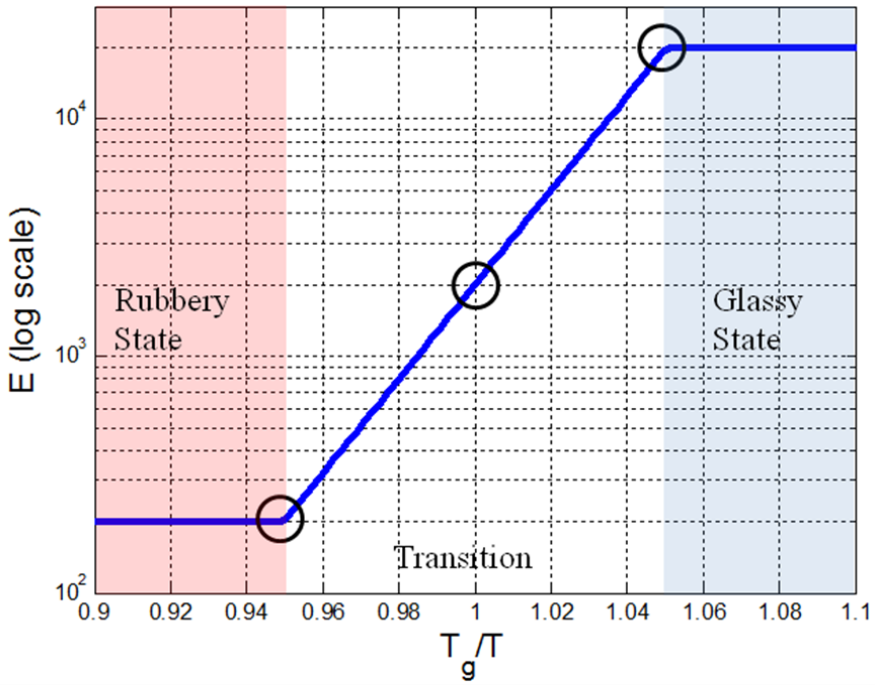

Figure 1.7. *The transitionof elastic modulus from glassy to elastic state with increasing temperature.*

1.2.2.3 Applications of SMPs using Photo-Thermal Heating

Multiple techniques exist for applying thermal energy into the SMP to initiate shape recovery. One promising method is based upon capturing light and transforming it to heat, known as the photo-thermal heating method. This has been demonstrated by dispersing a light absorbing dye into the polymer matrix at the appropriate absorbance wavelength for the corresponding light source. This inherently traps the light energy into the polymer and effectively heats past T_g initiating the shape memory effect.

This original polymer development was performed by *Wilson et al* and its potential use as mico-actuator was demonstrated [110]. *Wilson et al* developed an aliphatic highly crosslinked urethane polymer that has an increased elastic modulus during the rubbery state allowing for good actuation properties [109]. Other design requirements include biocompatibility, optical clarity, and low T_g to mitigate actuation energy (see Chapter 4 for further details). *Maitland et al* used the advantageous properties of the aliphatic SMP for an application to remove neurovascular occlusions, mitigating ischemic stroke [110]. Their design shown in Figure 1.8, consisted of casting the dye mixture SMP into a linear rod and programming to a cork screw geometry. One free end of the SMP device was bonded to a 240 μm fiber optic cable using an optically transparent epoxy. The fiber optic was connected to a high power laser source outputting an infrared wavelength of light at 808 nm. By applying 1 W of power from the laser source with a dye concentration of 0.08 μM, the 4 cm linear rod was able to deform to its cork screw shape in a quick 5 seconds.

It was also noted that by increasing the dye concentration and power supplied, the actuation speed was significantly increased. Other work performed by this group used the photo-thermal heating method to power a microgripper to carry an embriotic coil to a specific site, and applying a laser source to release the gripper. Although photo-thermal heating is a promising form of stimulus, currently only *Wilson, Small, and Maitliad et al* have demonstrated its potential.

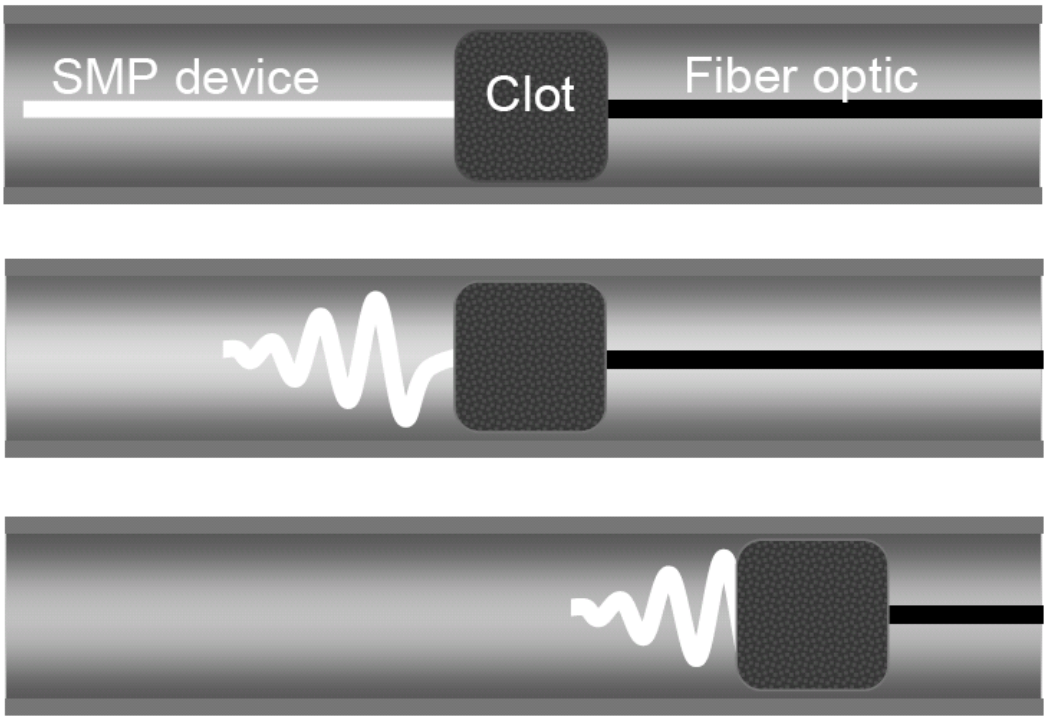

Figure 1.8. *SMP therapeutic device for removing a thormbotic vascular occusion, using photo-thermal heating as the actuation source (Figure from Matiliad et al. [110]).*

1.3 Thesis Overview

Chapter 1 has surveys the literature of each sub-component of the novel autonomous sensing, toughening, and healing material system developed in this thesis. Intensity based fiber optic SHM shows a promising method for real time

crack detection in a polymer matrix, but currently only capable of sensing structural damage and relies on an outside source for repair. Various autonomous self-healing polymer systems are introduced such as inter-molecular diffusion, thermal re-crosslinking, and microencapsulation approach and showpromising healing efficiencies in tensile, crack propagation, and fatigue loading scenarios. All of the systems mentioned required adequate time scales for their healing mechanisms to initiate, with some requiring external forces to allow conformal contact of the fractured surfaces, others requiring excessive stimulus energy (i.e. temperature) globally changing the mechanical properties, while some embed healing agents which lowered the virgin mechanical strength of the host polymer. Further, none of the above methods can defend the propagation of cracks protruding into the polymer matrix in a real time loading environment, and are only effective after damage has been arrested. Thermally responsive shape memory polymers have controllable advantageous mechanical properties such as shape recovery and modulus reduction based upon co-polymer selection and thermal energy. The shape memory effect is a possible self-healing method, although current research has only shown its application to impact dent recovery. The photo-thermal heating method via dispersed light from a fiber optic demonstrates a quick method for actuation. Expanding upon these developments, this thesis will demonstrate a system that can address the above problems by developing an autonomous material system with the capability of autonomously sensing the propagation of damage, toughening to stall it, and subsequently healing, all during operational loading in a real time atmosphere.

Chapter 2 presents a finite element model demonstrating the crack blunting phenomenon used for active toughening in the material system. The model is formulated from linear elastic fracture mechanics with a non-homogenous inclusion at the crack tip. Simulating a heat source at the crack tip location created a radially concentric decrease in elastic modulus. By increasing the temperature at the crack tip past the T_g, the stress at the crack tip dramatically decreases and the stress field is redistributed over a larger surface in the wake of the crack path. This demonstrates the crack blunting phenomenon by dissipating energy at the crack tip ultimately lowering the stress concentration to halt crack propagation. The stress intensity factor is compared to a theoretical value reported for a homogenous inclusion, showing comparable values.

Chapter 3 presents the design and characterization of the novel material system developed here. The synthesis and molding procedures for the SMP fiber optic system is given in detail. The multi-functional use of the fiber optic as both a damage detection sensor and thermal stimulus is characterized. The logic principles of the control algorithm used for active-toughening and self-healing is also demonstrated. Optimum design paramters of the photo-thermal heating method such as dye concentration, applied laser power, and fiber optic placment is determined. These parameters are used maximize the rise time and temperature gradient at the crack location to ensure real time toughening and healing could be performed in operation. The response characteristics between applied load and temperature are evaluated to quantify the photo-thermal stimulus behavior during

real time loading. The general trend shows that increasing the heat decreases load and conversely decreasing heat increases load under a constant applied strain rate.

Chapter 4 experimentally demonstrates the self-toughening and self-healing response of the novel SMP fiber optic material system in continuous real time operation. Upon crack propagation, the embedded fiber optic loses significant power transmission signifying damage to the structure. This system is able to autonomously initiate a toughening algorithm using the fiber optic as a mechanism to deliver stimulus directly to the crack tip without prior knowledge of its location. A laser deposits a controlled amount of thermal energy at the crack location, slowing the crack propagation rate through crack blunting and actively toughening the specimen. Following, the shape memory effect is used to close the crack and subsequently healed the specimen to the original geometric configuration. An evaluation of programming the specimen in a state of global compression before crack propagated occurred in the matrix shows to be a promising healing technique to recover strength. Lastly, both the self-toughening and self-healing mechanisms is demonstrated on the same sample and shows immense toughness and impressive strength recovery.

Chapter 5 concludes this thesis with a brief summary of significant findings throughout each chapter. It provides the relevant contributions to the field of self-healing materials and address recommendations for future work.

CHAPTER 2

Linear Elastic Fracture Mechanics Modeling with Near Tip Non-Homogenous Inclusion

2.1 Introduction

Up to date, the influence of a non-homogenous elastic inclusion surrounding a crack-tip is not well understood. Although research has shown that the varying the elastic modulus of the inclusion and matrix causes a change in the local crack tip stress intensity factor [111], the stress and strain fields on a macroscopic scale are sill unknown. Therefore, Chapter 2 develops a finite element model (FEM) to investigate how the near crack tip non-homogenous inclusion affects the global stress field. It is important to note that the goal of this analysis is to study the effect of a gradient of elastic properties inside a circular inclusion as it applies to multiple new functionally graded materials, not necessarily the specific case of a polymer material system developed in the future sections (i.e. thermal expansion and viscoelastic effects were ignored). The importance of this finite element analysis, as it pertains to the material system presented in Chapter 3, will show the crack blunting phenomena by creating a non homogenous inclusion with a gradient of elastic moduli decreasing radially outward from the crack tip. It was shown that this gradient of material properties locally reduces the stress field at the crack-tip and redistributes the stress concentration into the crack wake. Thus, this type of gradient will be reproduced in the design of the material system, such that active toughening can be achieved during real time loading.

A 2-D plain strain finite element model was created using ANSYS® in order to quantify the crack-tip stress intensity factors and the stress field experienced in the bulk material due to a non homogenous inclusion at the crack tip consisting of a concentric radial gradient of soft elastic moduli. The material properties used for the analysis were based on the temperature dependent elastic modulus of Shape Memory Polymers (SMPs). Dynamic mechanical analysis of the SMP specimens (synthesis procedures will be discussed in section 3.2) was used to obtain the elastic modulus as a function of temperature. The SMP showed a drastic decrease in modulus by two orders of magnitude from glassy to rubbery state as the applied temperature approached the glass transition. Two general temperature gradients where simulated, linear (transient) and sharp transition (steady state), and positioned with the maximum temperature at the crack tip and decreased radially outward. The domain of the circular inclusion was discretized into many concentric layers centered at the crack location in order to accurately simulate the gradient of material properties and granting enough spatial resolution to capture the corresponding stress fields. Following the FE Model, single inclusion theory was introduced to show the effects of one localized soft homogenous inclusion around the crack tip. This theory was compared to the non homogenous gradient performed in the FE Model and showed comparable results.

2.2 Finite Element Model

2.2.1 2-D Symmetric Finite Element Model

A two-dimensional static FE model was constructed in ANSYS® written in Ansys parametric design language (APDL) scripts. The geometry of the model

was based on the geometric constraints for plain strain mode I fracture, outlined in ASTM D 5045. Figure 2.1 shows the two boundary conditions used for this analysis, the applied load and the symmetry condition along the crack axis. A constant load of 100 lbs was placed on the top through-hole key point in the vertical direction, which was found through mechanical experiments (see Chapter 4) as an appropriate value. The model symmetry was enforced by applying a symmetric displacement condition on the line that lies along the crack axis of symmetry, until the crack tip, in order to simulate the crack opening due to the applied load.

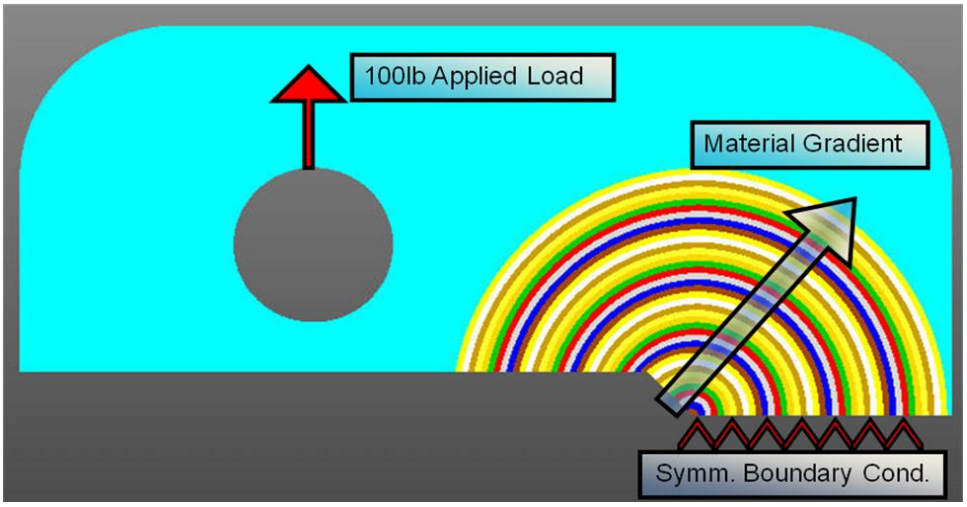

Figure 2.1. *2-D symmetric FEM in the X-Y plane consisting of a layered structure of 40 concentric circular rings representing a material gradient of soft material at the core (crack-tip region) and stiff material in the direction of the arrow.*

2.2.2 Material Models - Methodology

Script files were generated for each case of differing temperature profiles to assign the appropriate isotropic material models to the corresponding 40 layers in the gradient. The material model is constructed by first defining the temperature

profile, either linear or sharp transition into 40 segments to the corresponding material layer in the gradient. The linear gradient (Figure 2.2a) was computed by varying the temperature surrounding the crack-tip from 20°C to 100°C in increments of 5°C and decreasing linearly down to 20°C at the 40^{th} layer. Thus, 17 separate subset cases were studied for this temperature profile. Using the empirical data from dynamic mechanical analysis (DMA), the corresponding modulus could be directly computed and assigned to the material layer. This range encompasses temperatures that are below and above the glass transition temperature of the material, allowing for vast changes in modulus. Figure 2.2b shows that the corresponding modulus drops as high as 2 orders of magnitude as the temperature increases past the glass transition. The sharp transition gradient (Figure 2.2c) is computed by again varying the temperature surrounding the crack-tip from 20°C to 100°C in increments of 5°C but decreasing sharply down to 20°C at the 40^{th} layer using an arctangent shape. Similarly, Figure 2.2d shows that a drastic decrease in modulus is observed but uniquely different from the linear gradient.

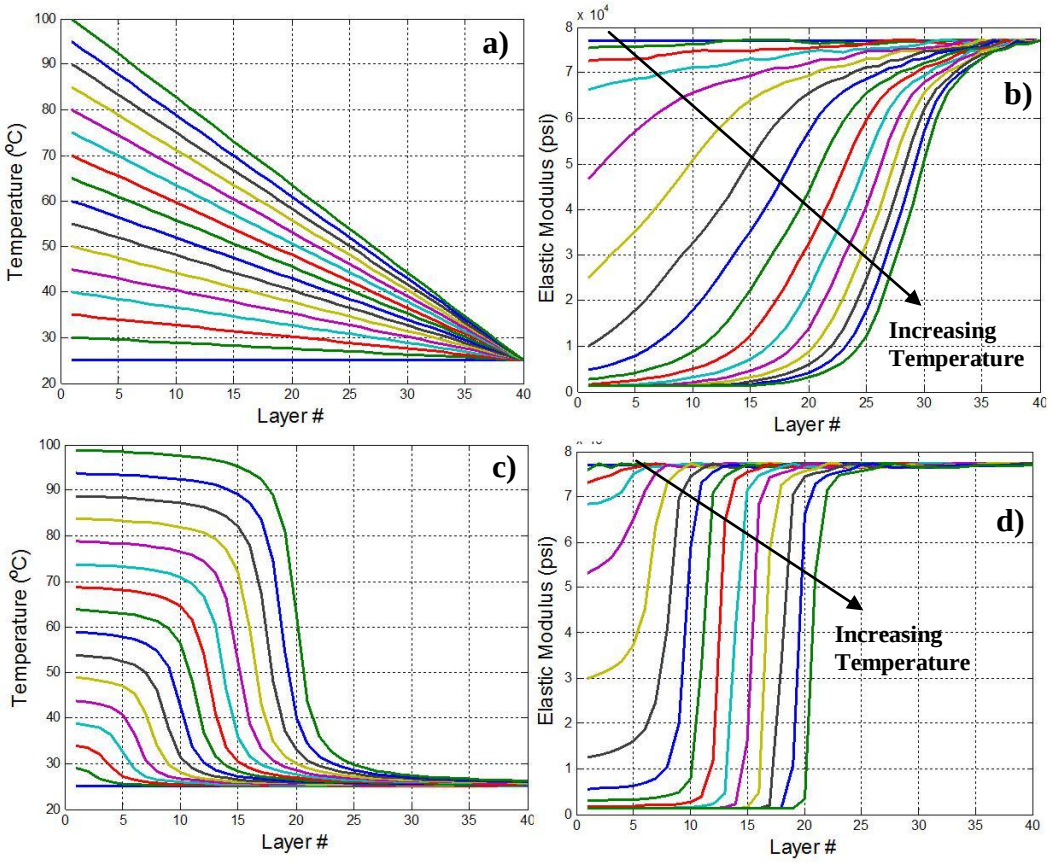

Figure 2.2. *Two temperature profiles studied with several cases evaluated at varying crack-tip temperatures: a) linear temperature gradient, b) corresponding modulus of the linear gradient, c) sharp transition temperature gradient, and d) corresponding modulus of the sharp transition gradient.*

2.2.3 Meshing Procedure for Fracture Analysis

PLANE82 elements (Figure 2.3), plain strain 8-node quadrilaterals (4 vertex and 4 mid-side nodes), were used for meshing of all areas with linear isotropic materials specified for each layer. A 2-D plane-strain analysis was performed in order to quickly create, mesh, and solve the FEM because numerous temperature profiles were required to investigate the blunting phenomenon. *PLANE82* elements can tolerate irregular shapes and can be smoothly fitted to curved contours, which are prevalent in this analysis, unlike simple 4-node quadrilaterals.

Each node has two degrees of freedom (*UX* and *UY*) and a mid-side node can be collocated with two vertex nodes to create a triangular-shaped element. This element was employed because of these aforementioned features, which will prove useful for this analysis consisting of curved boundaries and geometric singularities such as the crack-tip location.

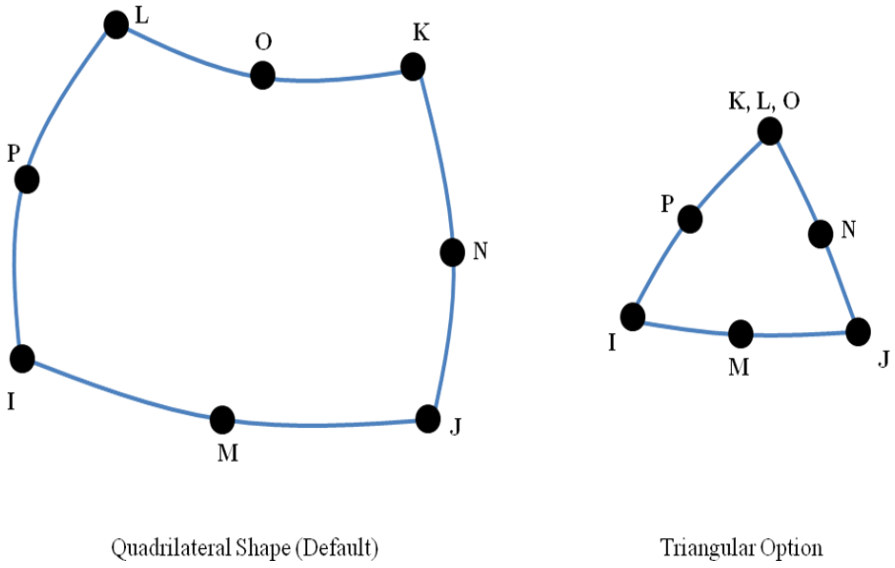

Figure 2.3. *Description of the PLANE82 elements*

Key points were generated at all the geometric vertices such that straight lines and arcs could be defined for the boundaries of the respective areas. It is important to note that adjacent areas in the material gradient share one or more lines with their neighbors. By creating two areas that share a single line, the areas are naturally bonded to each other such that no other bonding constraints are needed between the material gradients creating a continuous material. When the areas are meshed the nodes on the boundary of the two areas will be associated with both of the areas (Figure 2.5). This eliminates the need for creating many

unnecessary lines and does not require a bonded constraint be explicitly specified, reducing the number of equations to be solved.

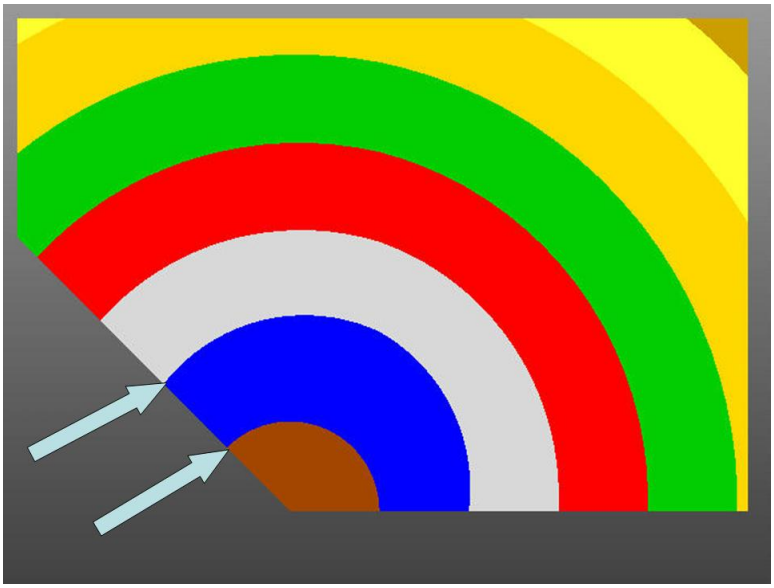

Figure 2.4. *All of the areas of the FEM are created to share lines (i.e. examples shown with arrows of shared lines) in order to eliminate the need for additional bonded constraints for the analysis*

The mesh structure is critical for this type of geometry as it must have a high resolution around the crack tip and capture the stress field through the material gradient. For fracture analysis at the crack-tip stress concentration singularity, the nodes within the vicinity of the crack-tip must be concentrated around the node of failure. Elements were generated circumferentially around and radially away from the crack tip key point. To capture the material gradient, lines of the FEM are selected and then divided into a specified spacing. The areas are subsequently meshed using the *PLANE82* elements and the corresponding material properties assigned by the temperature profile scripts. Free-meshing was used for irregular areas such as the inner core layer that contains the crack-tip and the outer-most

portion of the bulk sample (brown and light blue areas in Figure 2.4). The concentric layers have a regular geometry, therefore mapped meshing was utilized. Each layer is specified to have five nodes through the thickness and sixty nodes along the entire arc length. The mesh generated by this technique creates nodes that are concentrated around the crack and are spaced radially away from the tip (Figure 2.6). The mesh density is very high throughout most of the FEM, with a net total of approximately 90,000 nodes and 30,000 elements.

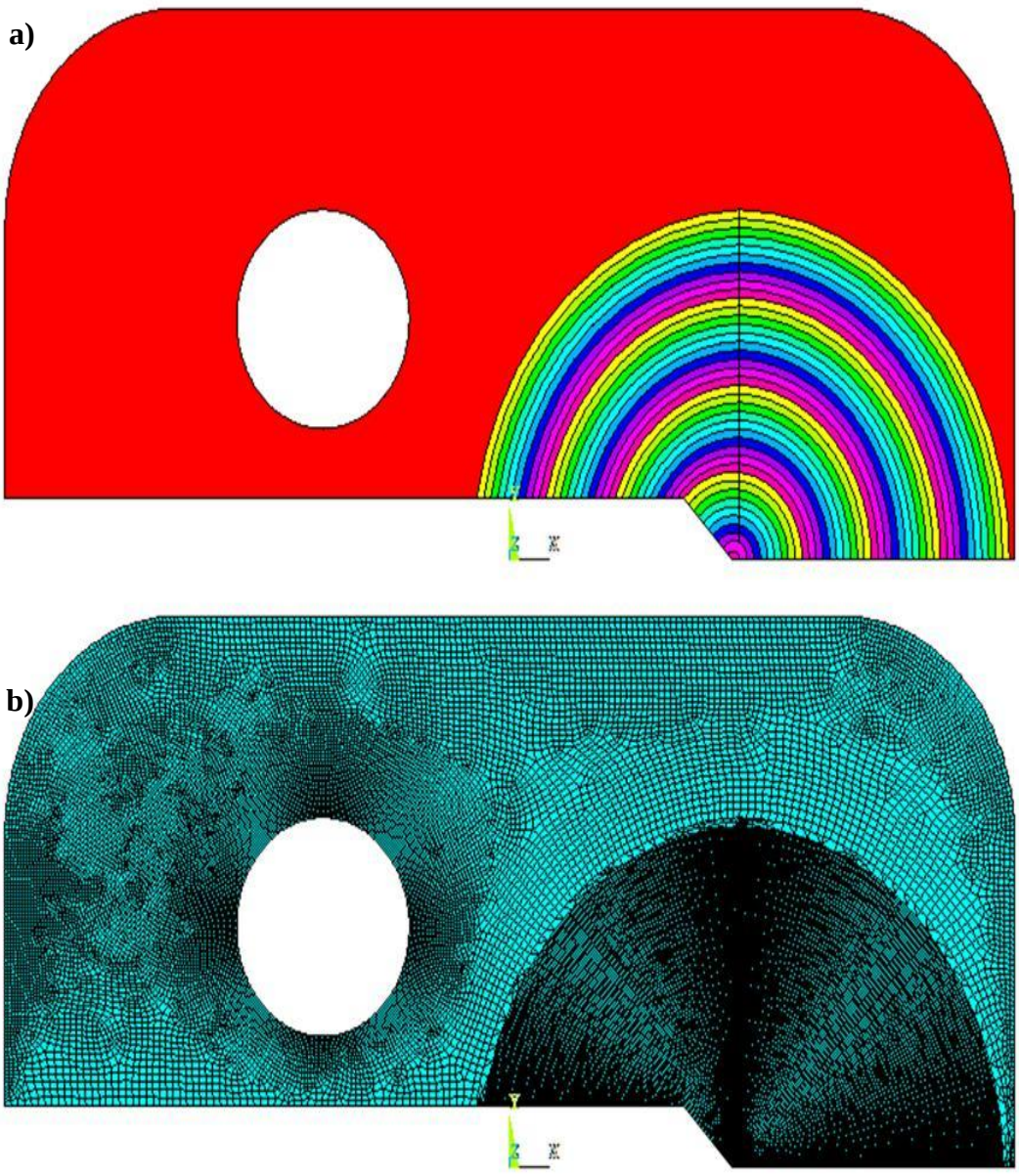

Figure 2.5. *a) Overall model geometry (areas) of the polymer specimen with crack location at center of 40 concentric rings. b) Full mesh of the model.*

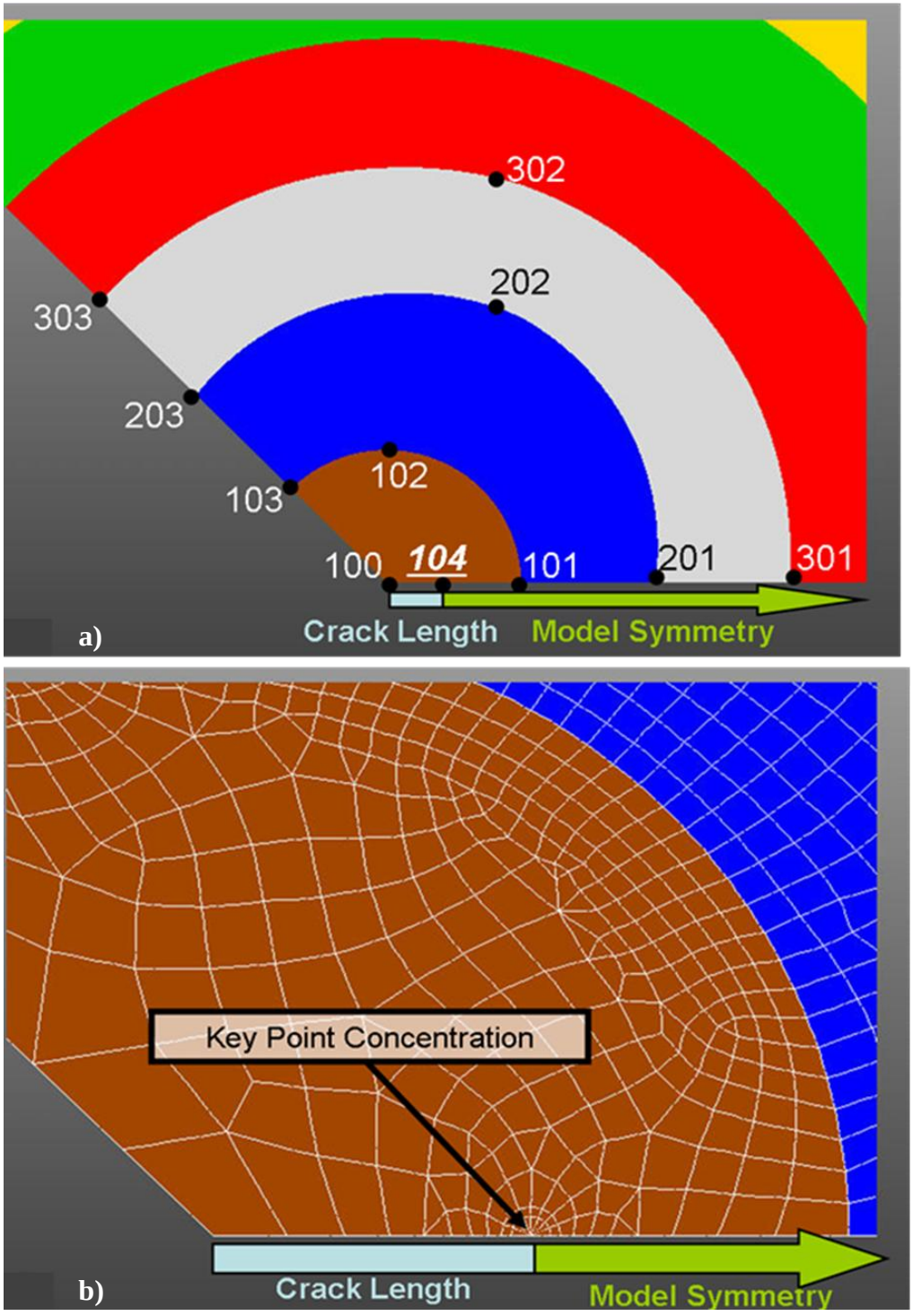

Figure 2.6. *a) Details of crack-tip location and model symmetry with element concentration at the crack-tip (key point 104). b) Mesh concentrated around the crack-tip of the core inclusion material.*

2.3 Finite Element Simulation Results

2.3.1 Linear Temperature Profile

A simulation of various linear temperature profiles was conducted as a simple case for a temperature gradient. As shown in Figure 2.7 shows the linear profile temperature gradient; as the core temperature increases at the crack-tip, the temperature distribution decreases linearly. This is similar to the photo-thermal heating mechanism which will be presented in Chapter 3. This allows for an investigation of the effect of a large gradient of material properties for the inclusion surrounding the crack tip.

The results of the static stress field are presented in Figure 2.8. It shows that at small temperature gradients there is a slight change in stress distribution. At minor temperature shifts there are only slight changes in the gradient of mechanical properties. As the temperature increases closer to the glass transition temperature, the material properties at the crack location start to decrease in elastic modulus by orders of magnitude. In this state, the stress at the crack location begins to decrease dramatically as high stress begin to progress towards the back of the material. The high stress is redistributed towards the back of the polymer in a wake over a larger area such that strain-energy in conserved. This is of particular interest for the crack propagation problem, such that the stress concentration at the crack tip can be reduced below a critical stress to ensure mode I fracture is not initiated.

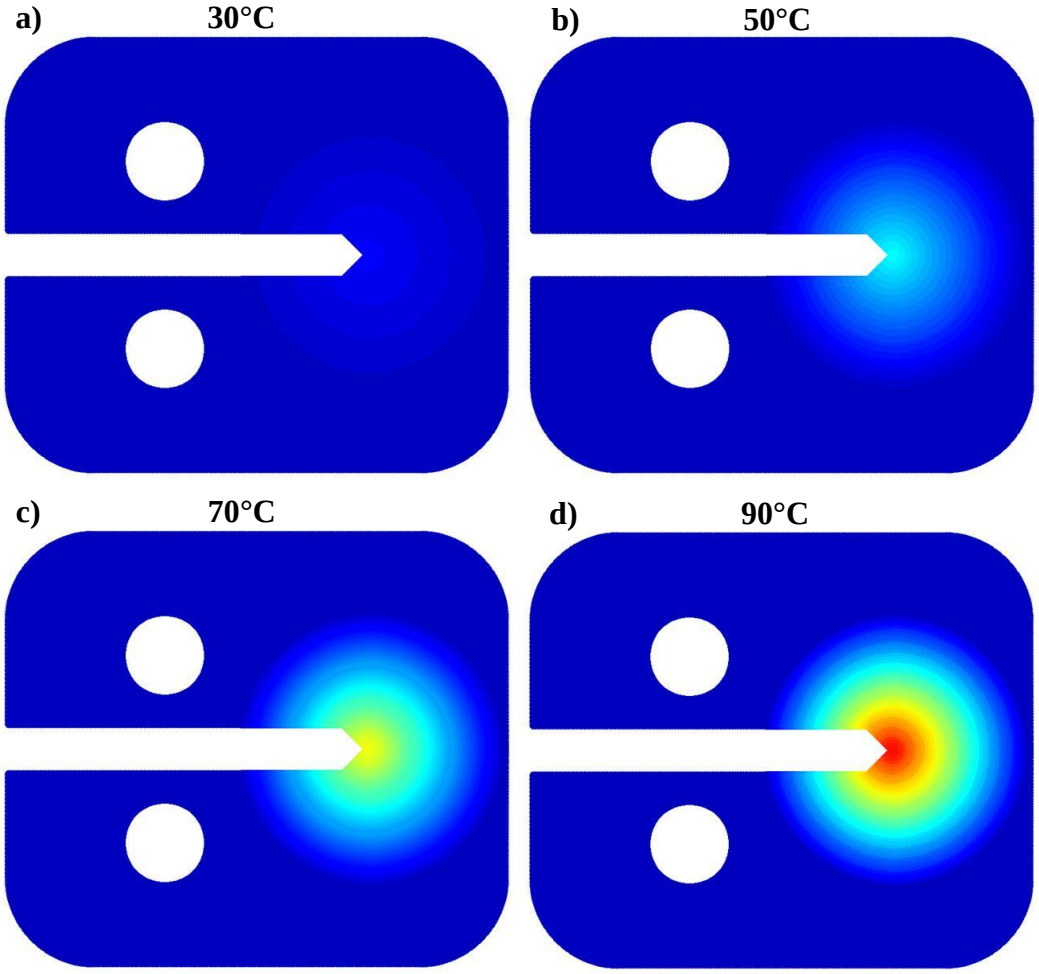

Figure 2.7. *Various Linear temperature gradients with the maximum temperature in the vicinity of the crack at a) 30°C, b) 50°C, c) 70°C and d) 90°C.*

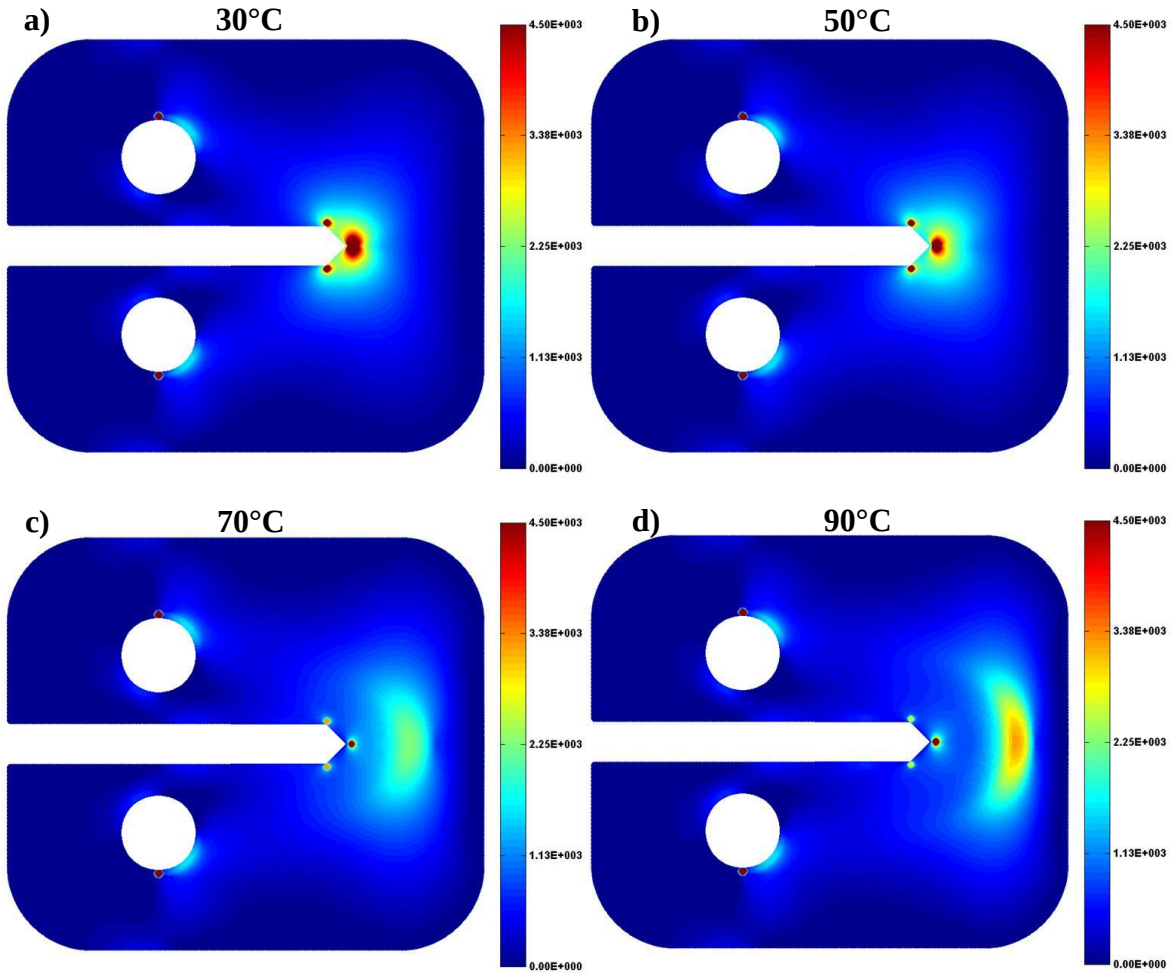

Figure 2.8. *The corresponding principal stress fields for the various linear temperature gradients with the maximum temperature of the crack layer at (a) 30°C, (b) 50°C, (c) 70°C and (d) 90°C.*

2.3.2 Sharp Transition Temperature Profile

The temperature distributions of the sharp transition gradient are presented in Figure 2.9. It shows a "pseudo-single inclusion" formulation, as the temperature is near constant around the crack location and sharply transitions to a cold temperature reaching the room temperature value of the bulk material. This temperature profile was created to study the characteristics of typical steady state heating conditions. This profile was analyzed to compare and contrast the

differences in results between large temperature gradients produced by the linear trend against a sharp decrease in material properties.

The corresponding stress fields for the sharp temperature transition gradient are presented in Figure 2.10. Again the low temperature fields show little change and are similar to the stress distribution at the same low temperatures as the linear gradient. Due to slight changes in elastic modulus at these low temperatures such that the gradient does not cause significant changes in elastic modulus. As the temperature approaches the glass transition temperature, the stress concentration at the crack tip is drastically decreased, and higher stress is redistributed towards the back in the wake of the crack path. The one significant difference between the two temperature gradients is the near stress field around the crack tip. Due to the sharp decrease in elastic properties, the inclusion creates a near zero state of stress in the surrounding layers around the crack tip inclusion while the stress of the linear profile decreases radially away from the crack-tip until it reaches the wake of high stress in the back of the material.

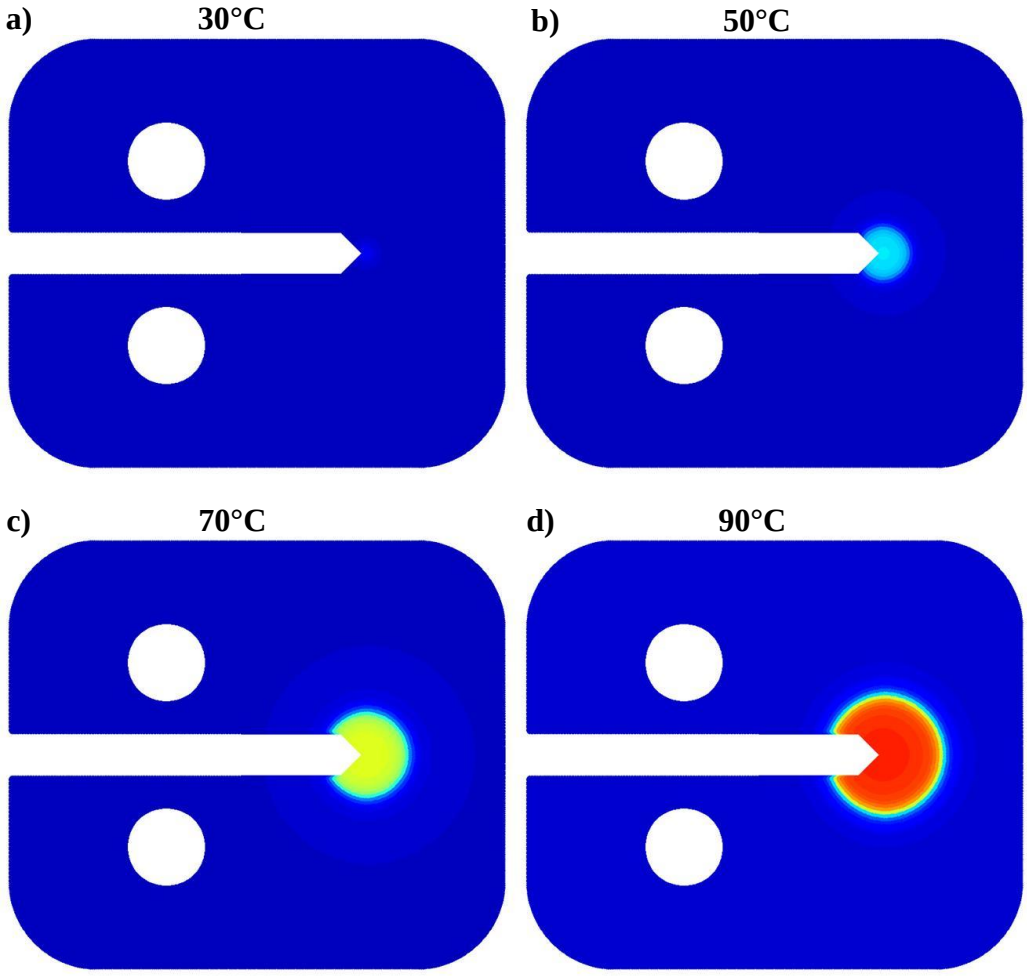

Figure 2.9. *Various sharp transition temperature gradients with the maximum temperature of the crack layer at a) 30°C, b) 50°C, c) 70°C and d) 90°C*

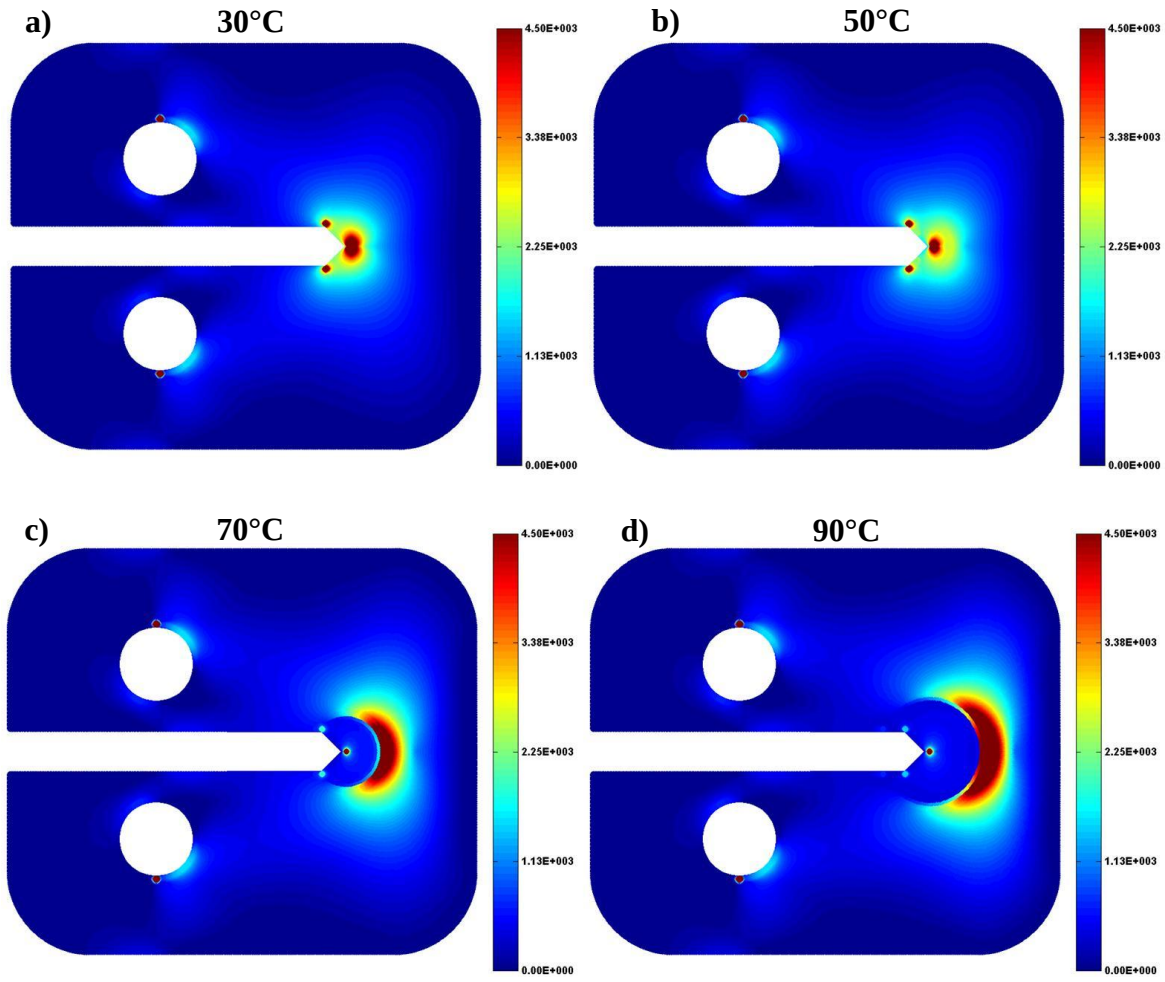

Figure 2.10. *The corresponding principal stress fields for the various sharp transition temperature gradients with the maximum temperature of the crack layer at (a) 30°C, (b) 50°C, (c) 70°C and (d) 90°C*

2.3.3 Stress Field at the Crack Tip

The physics acting at the crack-tip is of particular importance for crack failure. Figure 2.11a shows that the local principal stress concentration at the crack tip decreases as high as an order of magnitude as temperature is increased around the crack-tip. This trend is proportional to the reduction of the stress intensity factor at the crack tip shown in Figure 2.11b. As shown in both the maximum stress found at the crack-tip and the stress intensity factor, there is little

change in both results for the two vastly different temperature gradients; linear versus sharp transition. This implies that the global gradient (far away from the crack-tip) has little influence to the stress concentration at the crack location. Figure 2.11c shows the drastic decrease in the local modulus at the crack tip, and demonstrates the general trend in all three plots in **Error! Reference source not found.** 2.11. This further confirms that only the immediate properties surrounding the crack tip effect the local stress-strain field, such that a global gradient does not affect the local properties of the crack.

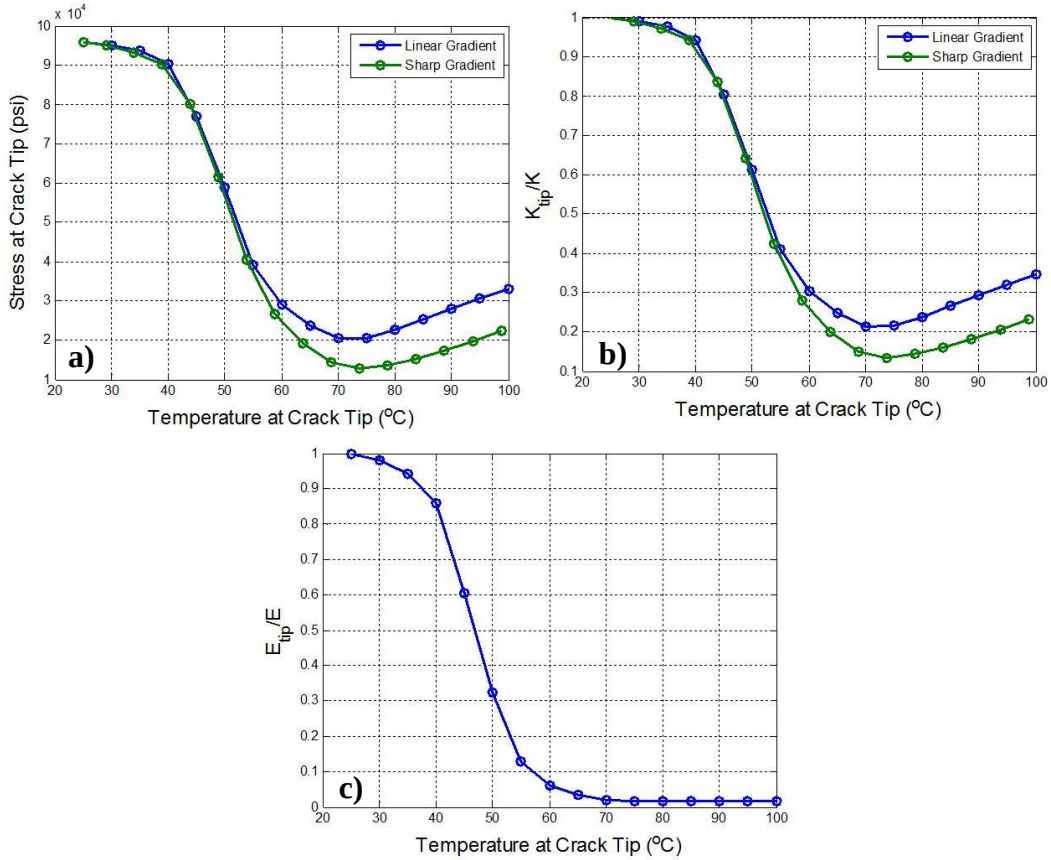

Figure 2.11. *The values of the a) stress, b) mode I stress intensity factor, and c) elastic modulus around the crack-tip as functions of temperature at the crack-tip*

2.4 Comparison to Single Inclusion Theory

2.4.1 Introduction to Theoretical Modeling

The previous results reported in section 2.3 show little significant difference between the near tip stress intensity factors for the two different temperature gradients. This infers that only the local material properties at the crack location affect the stress concentration at the tip. It is therefore natural to compare the results to a single inclusion model, in which the local inclusion is of the same material properties at the crack tip.

It has been well documented that a crack penetrating a low modulus inclusion results in a reduction of stress concentration at the crack tip (K_{tip}). The closed form solution for modeling the stress intensity factor at the crack tip was derived using transformation toughening theory and the Eshelby equivalent inclusion approach, and has been fully investigated elsewhere [112]. Figure 2.12 describes the geometry and problem state of an ellipsoidal inclusion penetrating a crack tip, and is in its closed form solution as

$$\frac{K_{tip}}{K} = C_0\left(1 + \beta_1 C_1 + \beta_2 C_2\right) \tag{2.1}$$

where the *C* terms are related to the mechanical properties of the inclusion and matrix material and are defined as:

$$C_0 = \frac{1}{1 + 0.5C_1 - 0.125C_2}\sqrt{\frac{\alpha(1-\upsilon^2{}_M)}{(1-\upsilon^2{}_I)}} \tag{2.2}$$

$$C_1 = \frac{(1-\alpha)(1-2\upsilon_M)}{(1+\alpha-2\upsilon_M)} \tag{2.3}$$

$$C_2 = \frac{3(1-\alpha)}{2(1+3\alpha-4\upsilon_M\alpha)} \tag{2.4}$$

and the β terms reflect the geometry of the inclusion and are given as:

$$\beta_1 = \frac{1}{\pi}\int_0^{\pi} \ln\left[R(\theta)\right]\cos\left(\frac{\theta}{2}\right)\cos\left(\frac{3\theta}{2}\right)d\theta \tag{2.5}$$

$$\beta_2 = \frac{1}{\pi}\int_0^{\pi} \ln\left[R(\theta)\right]\sin^2(\theta)\cos(\theta)\,d\theta \tag{2.6}$$

where υ represents the Poisons ratio of the material, α is defined as the ratio of the inclusion modulus (E_I) and matrix modulus (E_M), and the subscripts *I* and *M* are with respect to the inclusion and matrix material properties respectively.

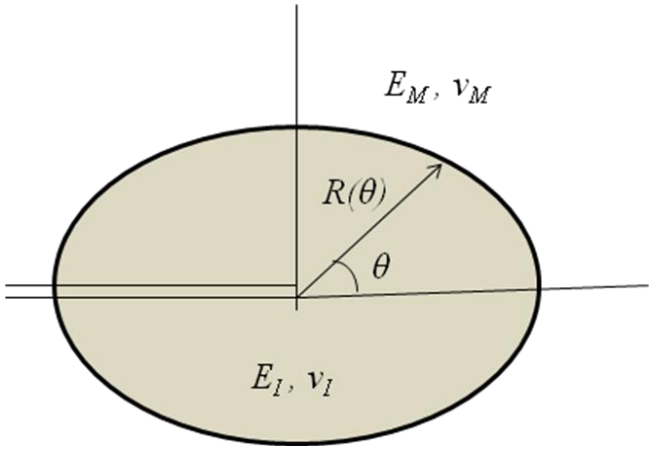

Figure 2.12. *Crack penetrating ellipsoidal inclusion problem diagram*

There are some limiting factors associated with the model that must be considered. First, equation 2.1 is a good approximation for varying poisons ratios

($\upsilon_I \neq \upsilon_M$). Also the model starts to deviate when the ratio of the inclusion radius (*R*) to the crack length (*a*) is larger than 0.15. Lastly it was assumed that both the inclusion and matrix materials were perfectly elastic and isotropic.

2.4.2 Simulated Results

The single inclusion model was used to study the influence of the elastic modulus at the crack-tip, creating a single homogenous inclusion, and the corresponding stress intensity factor. The single inclusion properties were calculated in the same manner as the FEM, based upon the polymer's empirical data for the maximum temperature at the crack tip. For both analyses (FEM and single-inclusion) it was assumed that the Poisson's ratio did not vary with temperature, thus $\upsilon_I = \upsilon_M$. The geometry of the inclusion was taken to be a perfect circle, allowing for a constant radius. Under this constraint, the β terms (the geometric constraints) were forced to zero, allowing for the stress intensity to be a pure function of elastic properties of the inclusion and matrix.

The single inclusion model has fairly good agreement with the nonhomegenous inclusion FE model demonstrated in Figure 2.13. Note that at low temperatures the single inclusion and sharp transition profile have excellent correlation (for $T<50°C$). This is due to the sharp transition gradient having a pseudo single inclusion in which there is a sharp jump in material properties. Above the glass transition temperature, the single inclusion model starts to deviate more substantially but still within a tolerable error. This may be due to large changes in elastic modulus not effectively captured by the single inclusion methodology, such that at large changes in modulus the theory is no longer valid.

Further, the local strain field at the crack tip progresses into more material gradients, such that the homogenized stiffness is higher than the single inclusion. *Li et* al. also reported this discrepancy in the theory, as their simulated results started to deviate for $\alpha > 2$ [112]. Overall, the single inclusion offers a fair estimation of the stress intensity at the crack tip region. For a quick underestimate of the stress intensity factor of a material with graded material properties, the single inclusion model may be sufficient regardless of the far field gradient effects.

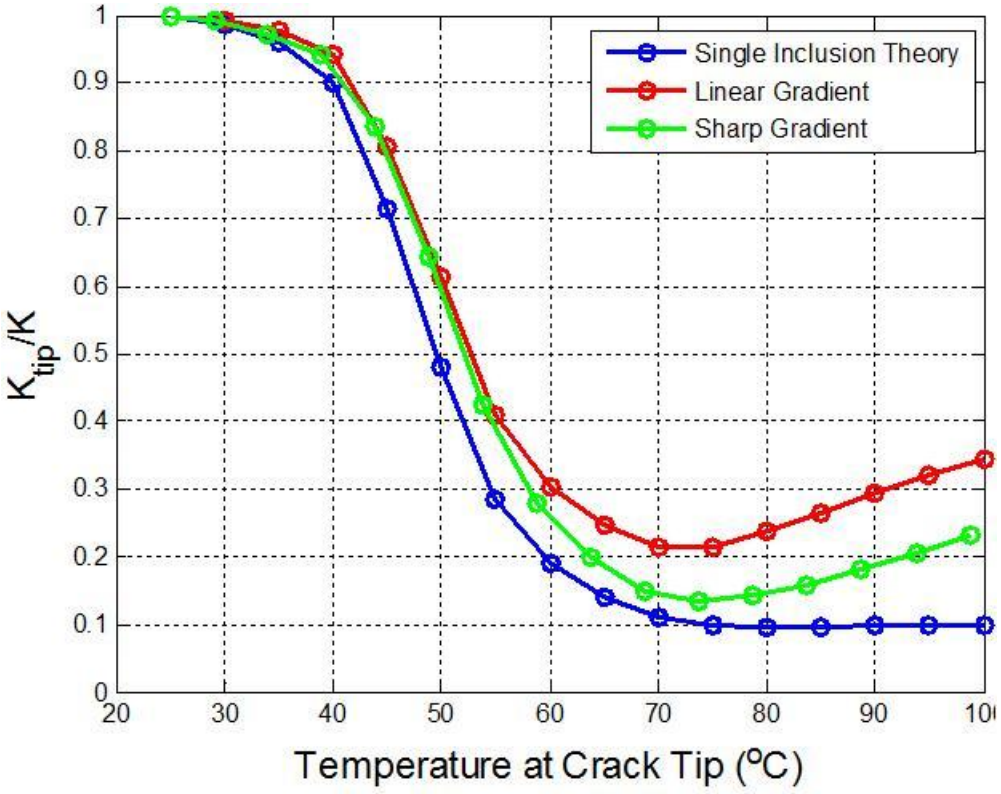

Figure 2.13. *Simulated results of the single inclusion model shown against the FEM for different temperature gradients.*

2.5 Chapter Summary

The solution of the finite element analysis revealed several intriguing aspects and trends for the SIFs at the crack-tip and the stress within the bulk material. It was shown that increasing the temperature surrounding the crack, the stress produced at tip node decreased as high as an order of magnitude. While the maximum stress was located at the crack-tip for all analyses, the reduction in stress with higher temperature is significant and demonstrates that local heating of the crack region can improve the global toughness of the material. It was seen that for two very different temperature profiles, the stress locally surrounding the crack-tip did not vary significantly, but did significantly reduce the stress field around the crack tip such inferring that more energy is required for crack propagation to be initiated. Thus, it is the local heating at the immediate crack location that contributes to the main reduction in the SIFs. Increasing the temperature surrounding the crack location the nonhomogenous inclusion began to radially decrease in elastic modulus. The resulting effect on the stress field is a pushing-back of the high stress away from the crack singularity and into the bulk material creating a crack blunting effect. Finally, good agreement has been demonstrated between the nonhomogenous inclusion FE model and single inclusion theory to determine the near tip SIFs for a crack penetrating an elastic inclusion. Thus, the evaluation of the single-inclusion model provides a good approximation for the K_{tip}/K_{bulk} of a material with graded material properties. Using these results a material system can be developed that uses a similar material gradient in a nonhomgenous inclusion to obtain a decrease in stress concentration

at the crack tip as well as lowering the stress distribution around the crack to increase the global toughness of the material.

CHAPTER 3

Design and Characterization of Autonomous Material System

3.1 Introduction

Chapter 3 presents the design of the novel autonomous material system. The primary objective of the system is to mimic the defense and healing mechanisms found in human bone. The criteria for the system is granting the ablity to detect damage, respond and actively toughen at the crack location impeding crack propagation, and finally recover the induced strain energy, subsequently healing the structure to original strength. To design for this advance structural system each sub-component such as material selection, autonomous control system and stimulus delivery must be engineered to achieve the required demands set forth.

The first section describes the synthesis and development of the SMP specimens. A process described by *Wilson et al* is used to develop uniform aliphatic urethane network SMPs [109]. This network was chosen with monomers composed of high molecular symmetry allowing for a stiffer rubbery modulus when heated past T_g, granting the SMP higher strength. Infrared absorbing dye is homogenously mixed into the SMP to generate localized photo-thermal heating method and to act as the thermal stimulus applied by the control system. The specimens are fabricated according to the compact tension specimen geometry to characterize the strength and mode I toughness of the material system. An optical fiber is integrated into the specimen to sense damage through a drop in transmitted power and respond to structural damage by applying a thermal stimulus.

The design of the autonomous control system is introduced following the development of the material specimens. The section describes the design of the closed loop optical system and sensing elements used during real time operational loading such that autonomous active toughening and healing could be performed. These algorithms are programmed by combining a D Space control board and Simulink's graphical programming language with the optical system. The toughening and healing algorithms used to control the temperature at the damage site delivered by the photo-thermal healing stimulus are discussed.

The effectiveness of the photo-thermal heating method is characterized by measuring both the time dependent temperature profile and the mechanical response. The placement of the fiber optic is shown to produce the required temperature gradient for crack blunting and shape memory recovery around the fractured area. An investigation of dye concentration and applied power is performed to optimize the rise time and temperature gradient from the photo-thermal heating gradient produced by a fractured optical fiber. The mechanical response of the polymer from the photo-thermal heating during operational loading is characterized. A fluctuated heat source at the crack tip with a continuously applied strain is used to demonstrate the relationship between load and temperature and quantify the lead-lag response from the controlled photo-thermal heating method.

3.2 Design of Shape Memory Polymer Specimens

The SMP must have sufficient mechanical properties in both its glassy and rubbery states, so that the overall structural properties of the polymer are not

compromised during a thermodynamic healing cycle. This allows the system to heal during operation, without the need for downtime or separate healing operations. Shape memory alloys are currently used as a shape memory structural material in a wide range of applications [113] because the high stiffness creates greater forces for actuation, however applications are limited to minimal recovery strain (<8%). Shape memory polymers present the converse feature, by having high strain recovery (>300 %), and large changes in elastic modulus upon heating, with low actuation forces. *Wilson et al* has created a SMP with higher mechanical properties in the rubbery state than current polymers, which leads to higher actuation forces and bridges the gap between SMA and SMP applications [109]. The rubbery state modulus is proportional to temperature by the realtionship

$$E \sim n_c RT \sim \frac{RT}{M_c} \tag{3.1}$$

where n_c is the crosslinking density, R is the ideal gas constant, T is the temperature, and M_c is the molecular weight between crosslinks. The polymer was designed to have a high level of cross linking per unit volume to achieve a high stress recovery. Using monomers with high molecular symmetry increased the amorphous cross linking density to create a uniform polyurethane super molecular structure with a T_g ranging between 33°C -87°C. *Wilson et al* also included a multi-functional extender molecule (Triethanolamine) containing three hydroxyl groups instead of the typical molecule, which contains two hydroxyl groups. Incorporating this structure into the molecular chain increases the cross

linking density of the soft segment, ultimately increasing the effective rigid rubbery modulus of the polymer.

3.2.1 Synthesis and Fabrication of Shape Memory Polymers

A process described by *Wilson et al* has been adopted for the synthesis of the SMPs used in this autonomous material system [109]. The uniform aliphatic urethane network SMPs exhibit exceptional shape memory behavior, sharp glass transition temperature, optical clarity, and great mechanical properties making this class of SMPs the ideal candidate for the autonomous material system. A molar ratio of 1:0.30:0.267 of 1,6-hexamethylne diisocyanate (HDI, Sigma Aldrich), N,N,N',N''-tetrakis(2-hydroxypropyl)ethylenediamine (HPED, Sigma Aldrich) and Triethanolamine (TEA, Sigma Aldrich) was chosen for the reported low glass transition temperature (T_g) of 66.4 °C, which makes the laser activated photo-thermal heating processes more rapid and allow for quick fluctuations in modulus and efficient shape memory recovery .

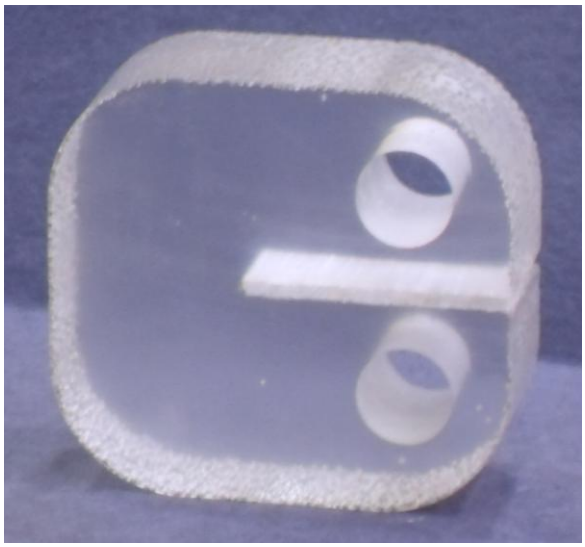

Figure 3.1. *Optical clarity of a syntheisized uniform aliaphatic urethane SMP*

The SMPs are synthesized in a glass jar under nitrogen with great care taken to reduce the presence of moisture. Due to the high viscosity of HPED, it is difficult to accurately dispense a controlled amount of mass, thus it is measured first, with the TEA and HDI added to match the desired molar ratio. An infrared absorbing dye (Epolight 4149) is dispersed at 900 ppm to ensure maximum absorbance of the infrared light provided by the laser source. All components are mixed vigorously for 90 seconds using a high vortex mixer until a consistent viscosity and color is obtained. The mixture is then poured into an aluminum mold, with a mold release agent (Bueler Release Agent) applied to the surface. A 600 μm multimode fiber optic cable (Thorlabs) is placed into the mold before curing such that it was near the location of the tip of the pre-crack. A vacuum oven is purged three times with nitrogen before the samples were placed inside the vacuum oven and degassed at ~1 inch of Hg for 30 minutes. The temperature is ramped to 125 °C at a rate of 1°C/min, followed by a 1 hour dwell at 125°C to ensure full polymerization.

The samples were released from the mold and fabricated into the shape outlined in ASTM D 5045 for Mode I crack propagation. The geometric constraints outlined in this method were strictly adhered to ensuring a plane strain fracture. Compact test specimens, in a pin-pin configuration, were fabricated using a high precision mill. The crack was cut using a 1/32 inch slitting slaw to a length of 0.48 inch, with a precrack notch length of 0.05 inch sawed into the specimen using a razor blade. Lastly, SMA connectors where attached to the both

free ends of the embedded fiber optic to provide for a connection to a laser source. The finished fabricated sample is shown in Figure 3.2.

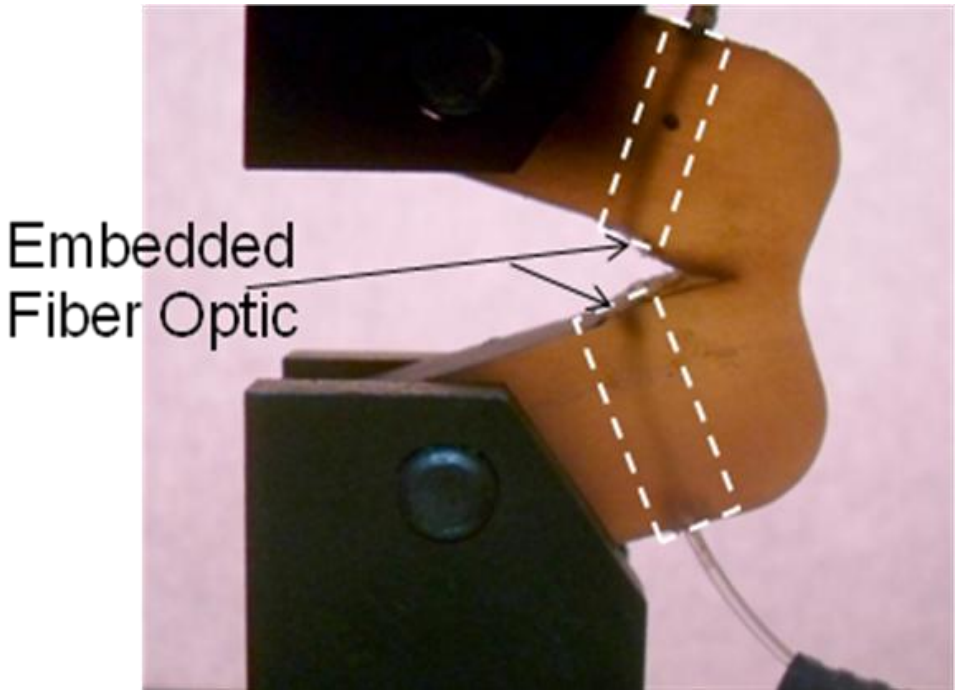

Figure 3.2*. Fully fabricated SMP compact test specimen with an embedded fiber optic undergoing a tensional load.*

3.3 Design of Autonomous Responsive Control System

The complete system designed to sense and respond to damage is shown in Figure 3.3. A high power laser diode (Opto Power Corp), with an infrared wavelength of 808 nm rated for a maximum power output of 15 Watts is selected to allow for adequate properties for photo-thermal heating. The laser diodes infrared light was focused to a 600 μm patch cable by a fiber port coupler to minimize energy loss. A mating sleeve connected the patch cable to the inflow sub-miniature A (SMA) connector to allow light to transmit through the SMP specimen. The outflow SMA connector was connected to a photo-thermal power meter to measure the output power loss across the SMP specimen.

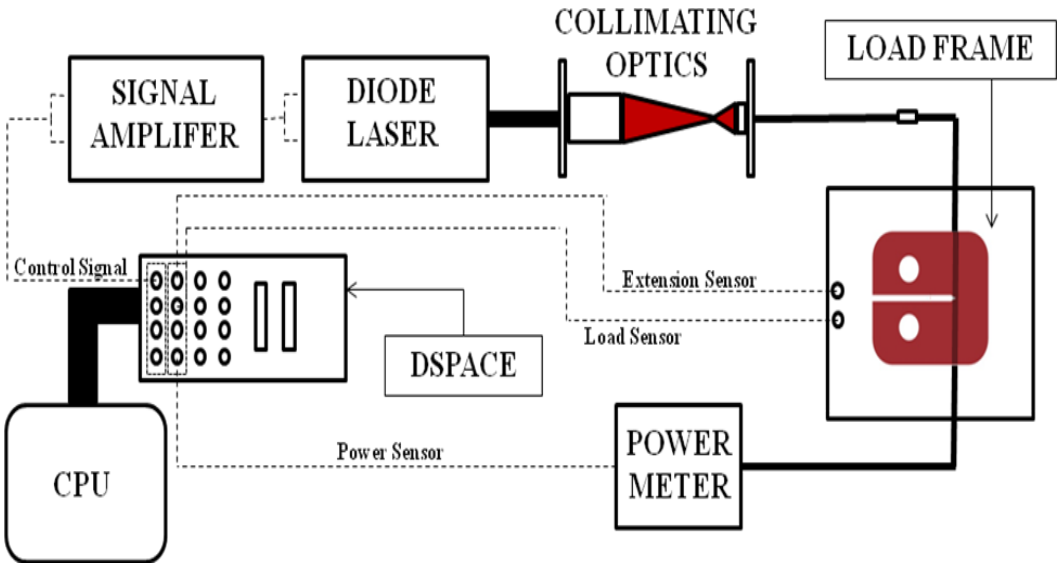

Figure 3.3. *Diagram of the closed loop autonomous control system incorporating the optical photo-thermal heating method.*

The design of the fiber optic system allows the SMP material to achieve two novel properties; the ability to sense and respond to structural damage. The field of structural health monitoring has made numerous technological advances in determining and quantifying damage using fiber optic network arrays [114]. In this system, one intensity based fiber optic SHM monitoring technique was used for simplicity, but can be expanded to incorporate other more advanced SHM methods. Figure 3.4 shows that during crack propagation, the fiber optic cracks significantly lowering the power transmission and signaling that a crack is growing in the structure. This signal is used to autonomously trigger the active toughening and healing mechanisms. The infrared light path is broken at the crack location because the fiber optic cable is fractured, which disperses the light into the dye filled polymer and causes photo-thermal heating at the crack tip. Controlling the amount of energy dispersion allows for a controllable heating

"stimulus" source for toughening and healing. This system is inspired from human bone, in which osteocytes embedded in the bone tissue act as strain sensors for large deformation, sending signals to new cell tissue to defend and rebuild the fractured site [117].

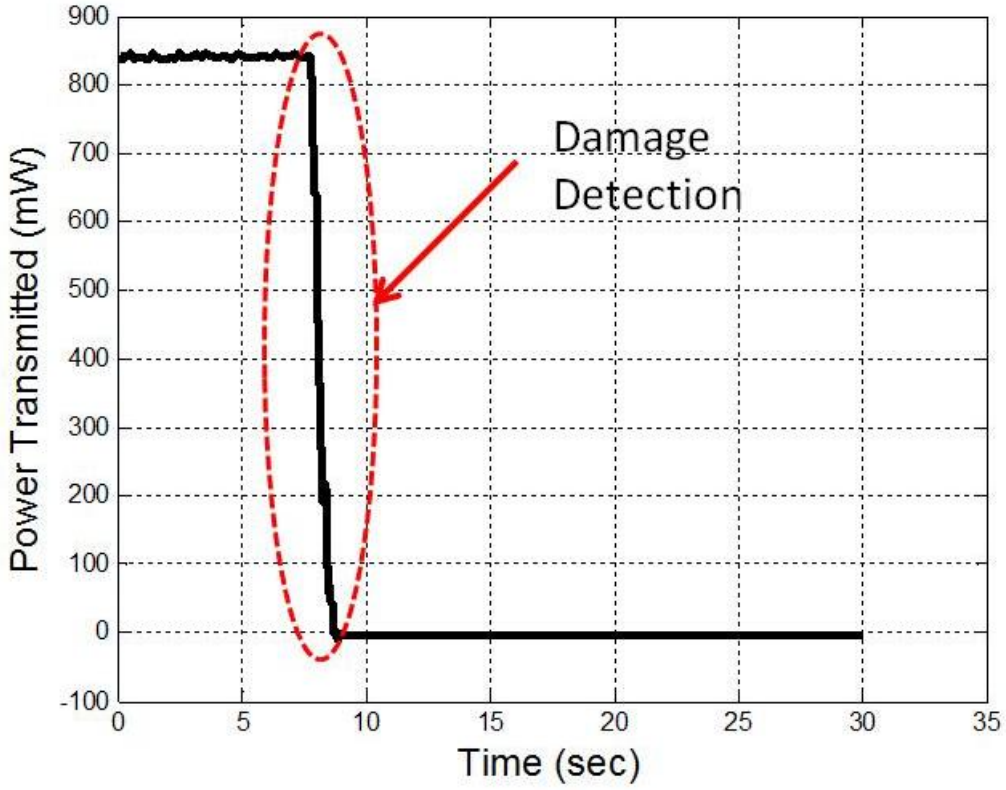

Figure 3.4. *Power loss from the fiber optic during mode I crack propagation of the SMP test specimen.*

Figure 3.5 shows the autonomus control algorthim used to deploy the active toughening and healing mechanisms once fracture has been detected by the system (results of the toughening and healing will be addressed in Chapter 4). The closed loop control system used a DSPACE (model CP1104) real time data acquisition and control board. The control algorithm was developed using SIMULINK's graphical block diagram programming using a library of available

logic blocks. Multiple sensors including load and extension data from the load frame, thermocouples capturing the temperature profiles, and power loss from the power meter where monitored during loading of the SMP specimen.

The toughening mechanism was designed as an on-off controller that produced a pulse width modulated signal with a constant 1W magnitude from the laser source. The switching of the power signal was controlled through a force feedback sensor, in which the load value was tested through a specified interval. If the load is above the “peak load”, photo thermal heating is applied or vice versa if the load was below the critical “low load” the laser was turned off and the polymer is allowed to cool. If the load is between the peak load and low load values, the laser is switched between on and off such that active toughening could be implemented. Once the active toughening algorithm was complete, the load was stopped, and the SMP specimen was released from the load frame into a free-free boundary condition. The laser is simply left in the on position to supply enough thermal energy to actuate the shape memory effect, until full deformation was recovered and the healing transformation was complete.

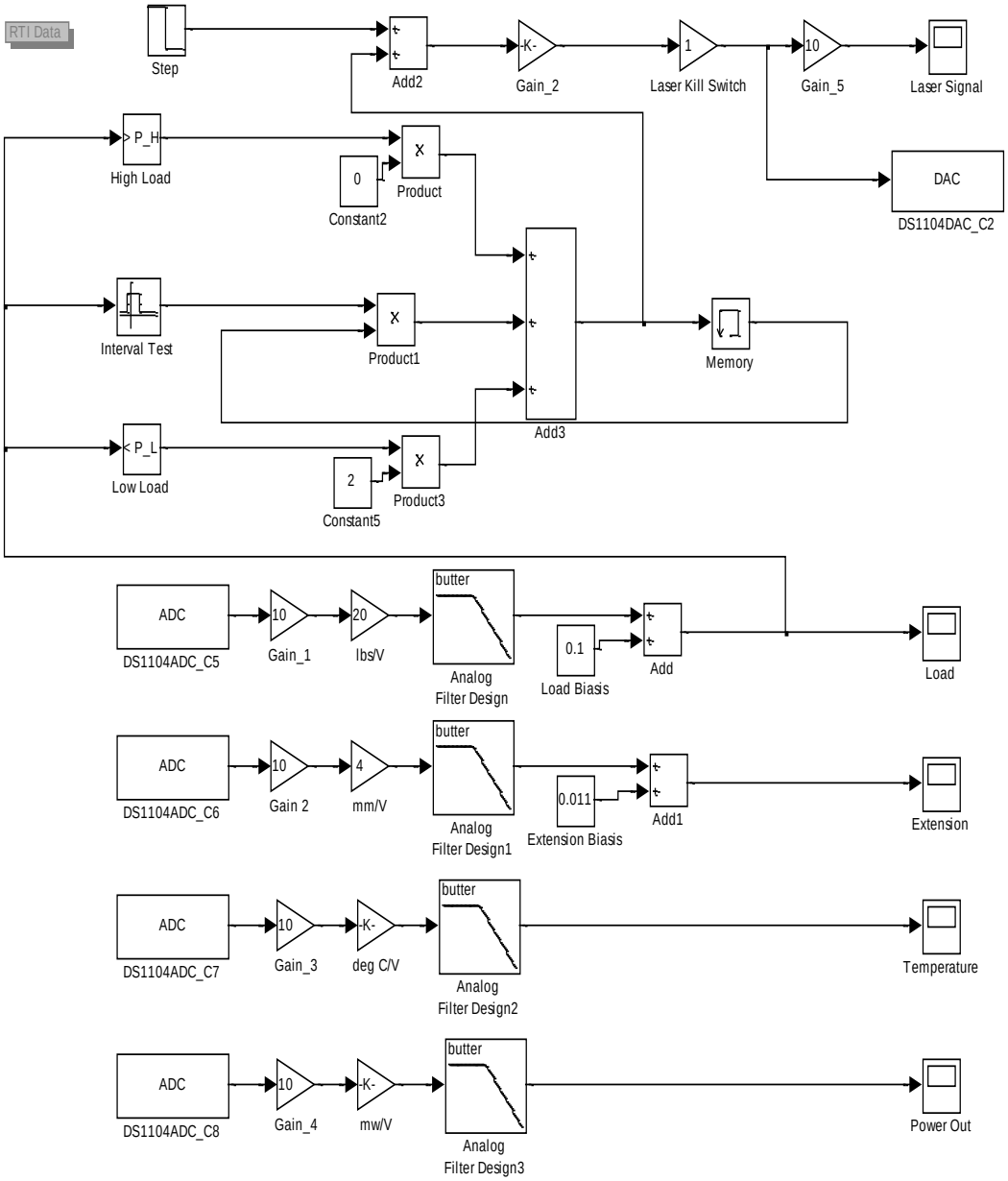

Figure 3.5. *Block diagram programing language used for active toughening and healing algorithms.*

3.4 Photo-Thermal Heating Characteristics at the Crack Tip

3.4.1 Characterization of the Temperature Profile due to Photo-Thermal Heating

Photo-thermal heating was used as the thermal source to actively control the mechanical properties of the crack tip region. Photo-thermal heating is obtained

by concentrating high energy infrared light onto a surface with a matching absorbance coefficient. The light is fully absorbed and transformed to heat creating a temperature gradient at the exposed region. This method has been shown successful as heat source for smaller samples where the exposed surface area of the SMP specimen is on the same order as the fiber optic cross sectional area [115], but has not been characterized for such a large SMP sample or for local heating in a larger polymer matrix. The orientation of the fiber optic, dye concentration, and power supplied greatly influence the temperature profile and ultimately the stimulus responses for toughening and healing. This section aims to quantifying these factors such that an effective photo-thermal heating method is designed for this system.

SMP samples were fabricated in the same fashion as mentioned previously but with a longer pre-crack (~2200 μm) fully cutting through the fiber optic. This configuration was used throughout the following section to generate the initial condition of a crack penetrating the system allowing for photo-thermal heating to be characterized without loading the specimen. Figure 3.6a shows the dispersion of infrared light around the crack tip by supplying 1 W of power from the laser source. Figure 3.6b shows the corresponding temperature gradient captured using a thermal imaging camera (Fluke Ti30) and demonstrates high temperature at the fractured area and concentric circles of lower temperature radially from the heat source. As shown by the finite element (FE) model in Chapter 2, this radial heating gradient can effectively lower the stress concentration at the crack tip exhibiting a crack blunting phenomenon. The placement of the fiber optic and

photo-thermal heating method in this polymer will produce the temperature profile required by the model to actively toughen the polymer. Note that the optical energy is only transmitted through one side of the fiber optic, creating a non-concentric heating profile around the crack tip as propagation occurs. Asymmetric temperature profiles will not degrade the system performance because the FE model in Chapter 2 showed that the local temperature at the crack location is the primary temperature that governs the decrease in stress concentration and leads to toughening in the SMP sample. Chapter 4 will show that this configuration will effectively improve the mechanical properties of this system.

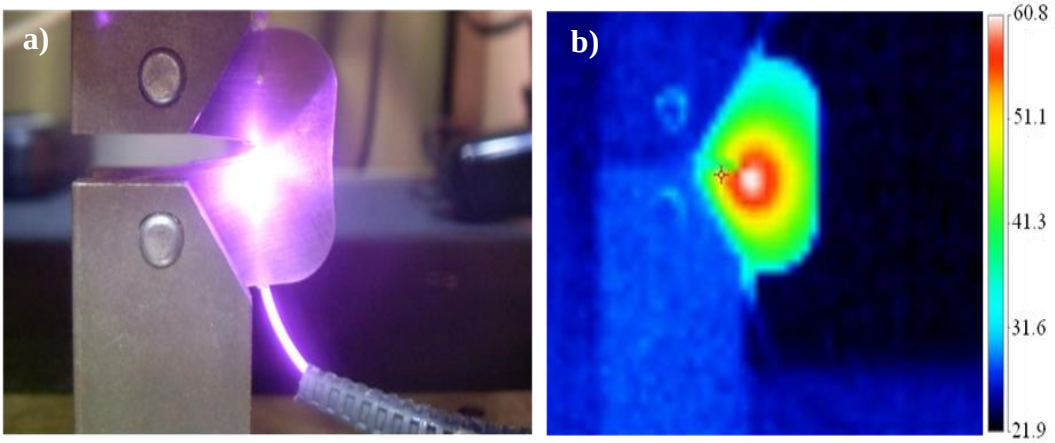

Figure 3.6. *a) Photo-thermal heating at the crack tip of the SMP specimen and corresponding b) thermal image capturing the temperature gradient created by the photo-thermal heating method.*

Rapid heating and cooling is critical to allow for adequate fluctuations in heat because loads are often applied significantly faster than convective heating and cooling. In other words, system response time is directly limited upon the heating and cooling time, thus reducing the heating time will increase the speed of loading

that the system can respond to. It is desired that the heating profile rise quickly to create a high decrease in modulus because temperature at the crack tip is proportional to the decrease in stress concentration. Dye concentration and applied laser power are the two parameters that effectively change the temperature profile of the crack tip. It is well understood that increasing the dye concentration will cause the SMP crack to absorb more energy and generate heat in a small volume. Lab experiments showed that concentrations above 900 ppm generated no increase in the effective absorbance, no increase in steady state temperature, and no change in the heated volume of the polymer. Figure 3.7a shows the effect of increasing the applied power across the fractured crack tip at a 900 ppm dye concentration. As power increases, the maximum temperature at the crack tip increases and the rise time decreases. Figure 3.7b shows that the maximum steady state temperature is linearly proportional to the amount of applied power, which is consistent with the expected behavior for a point heat source in convectively cooled medium. It is necessary for the deformed region around the crack tip to reach the T_g of 66.4 °C, such that shape memory recovery could be performed. Figure 3.9b shows that this is achievable at the crack tip with 800mW applied power and a dye concentration of 900 ppm. Deformation occurs primarily in the crack location during mode I crack propagation; however deformation also occurs in a local radial field surrounding the crack. It was determined through iterative experiments that 1W of power was required to effetely heat the deformed region past T_g to fully recover the applied strain and close the crack tip. Unfortunately if excessive power (1W>) is supplied through

the fiber it will cause the SMP crack to burn, undergoing an unwanted phase transformation changing the mechanical properties. The final configuration of the system uses a dye concentration of 900 ppm with a supplied power of 1 W.

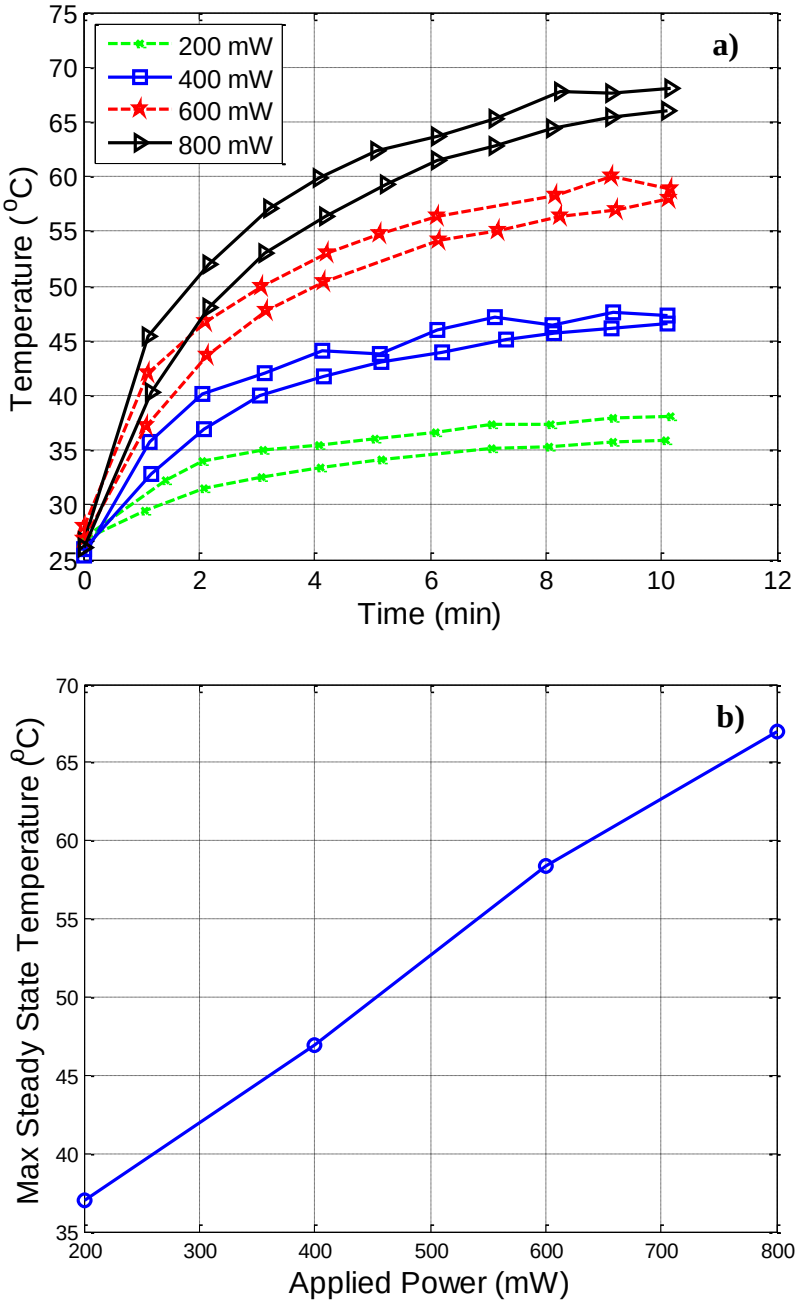

Figure 3.7. *a) Time response of the maximum temperature at the cracked location by increasing applied power from the laser source. b) Linear relationship between the maximum steady state temperature and applied power.*

Figure 3.8 shows a general steady state heating and cooling profile of the maximum temperature due to photo-thermal heating. The crack tip temperature profile follows a simple exponential relationship that is easily fitted to a first order model such as Newton's law of Heating/Cooling. The active control algorithm must be optimized to match the response speed of the material. A pulse width modulated signal (PWM) with constant period and amplitude was sent through the pre-cracked specimen to ensure that the system could track a laser signal with minimal lag in temperature response. An exponential model accurately models the time response of heating, as demonstrated in Figure 3.10. The exponential model can be used as a prediction tool for the maximum applied heat at the cracked location.

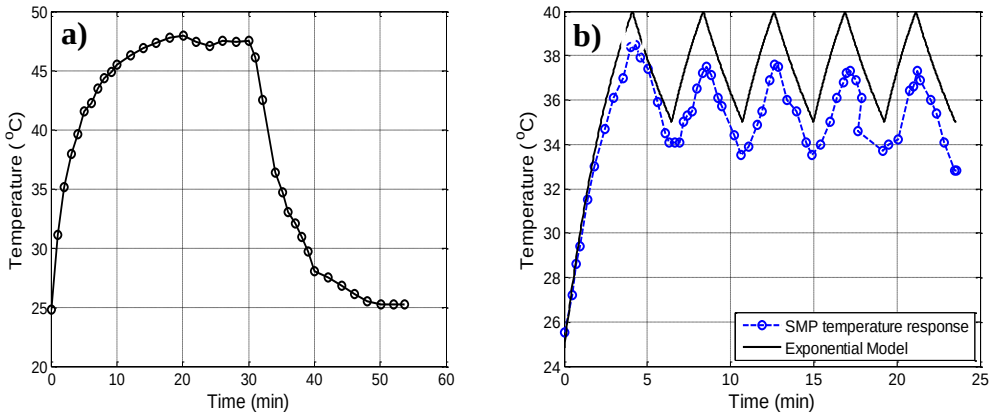

Figure 3.8. *a) The steady state crack tip temperature profile when heated and cooled using photo-thermal heating. b) Temperature response due to fluctuations in applied energy from the photo-thermal heating method.*

3.4.2 Load Response due to Photo-Thermal Heating

The load supported by the SMP specimen varies with the temperature induced modulus fluctuations and this relationship must be elucidated in order to design a

control system. Samples were fabricated with a longer pre-crack, fracturing the fiber optic allowing for the photo-thermal heating method to be effective. A small hole was drilled close to the crack tip location and a thermocouple measures the near field temperature of the polymer, as shown in Figure 3.9. The samples were placed in a load frame in the pin-pined configuration and loaded in tension at a constant extension rate.

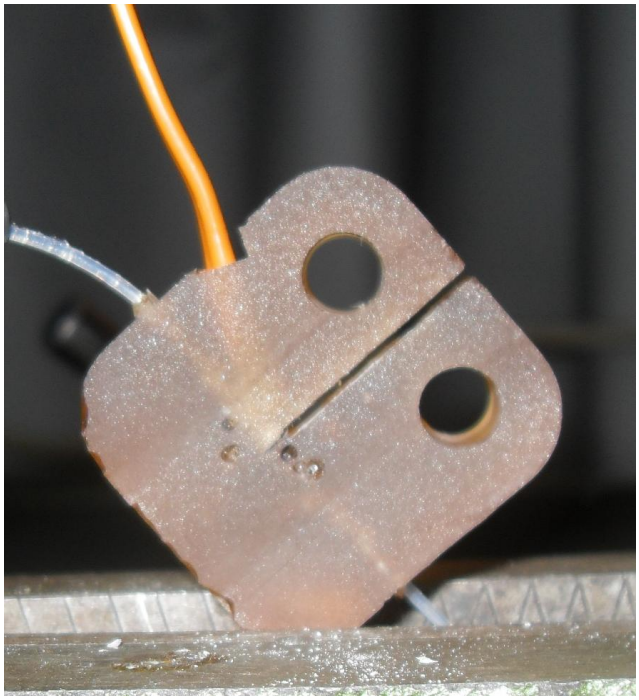

Figure 3.9. *Thermal couple placement used to measure the near field crack tip temperature during real time loading.*

It was desired to see the influence of temperature on applied load in this loading condition, thus a force dependent laser signal was designed such that at a load of 120 lbs the laser system was turned on and at 118 lbs it was turned off. Figure 3.10 shows the time dependent response of load, extension, and temperature for the specimen under controlled loading and heating from the laser. The load responds significantly to the laser signal by small changes in

temperature, which in turn changes the rubbery modulus near the crack tip to blunt the damage and reduce the stress concentration. Increased toughness of the autonomous material system is achieved without necessarily requiring the sample to be heated above 35°C. The benefits of choosing the SMP used in this experiment are realized through the low temperature required to blunt the crack tip and toughen the material system, which will help to minimize energy requirements and improve response time.

Figure 3.11 shows the direct relationship between load and temperature during fluctuation of the laser signal. Figure 3.13a shows the normalized temperature and load values, showing a slight phase lag between the peak temperature and load. This is due to the dissipation/addition of temperature at the crack location is not immediate as the laser source changes from on/off position. This causes the control system to overshoot the designed interval between 120 and 118 lbs; however future systems could easily correct by adding a derivative term into the controller. As shown in Figure 3.13b, the overshoot seems to be more prevalent in the lower load stage, where the laser transitions from the on to off state because the cooling rate is significantly slower than that of the heating rate. It is important to note that the heating temperature range causing the force response is between ~25°C to 36°C. This temperature range is well below the reported T_g ensuring that the shape memory effect is not influencing load response. This confirms that the oscillation in load is purely due to the fluctuating temperature dependent modulus.

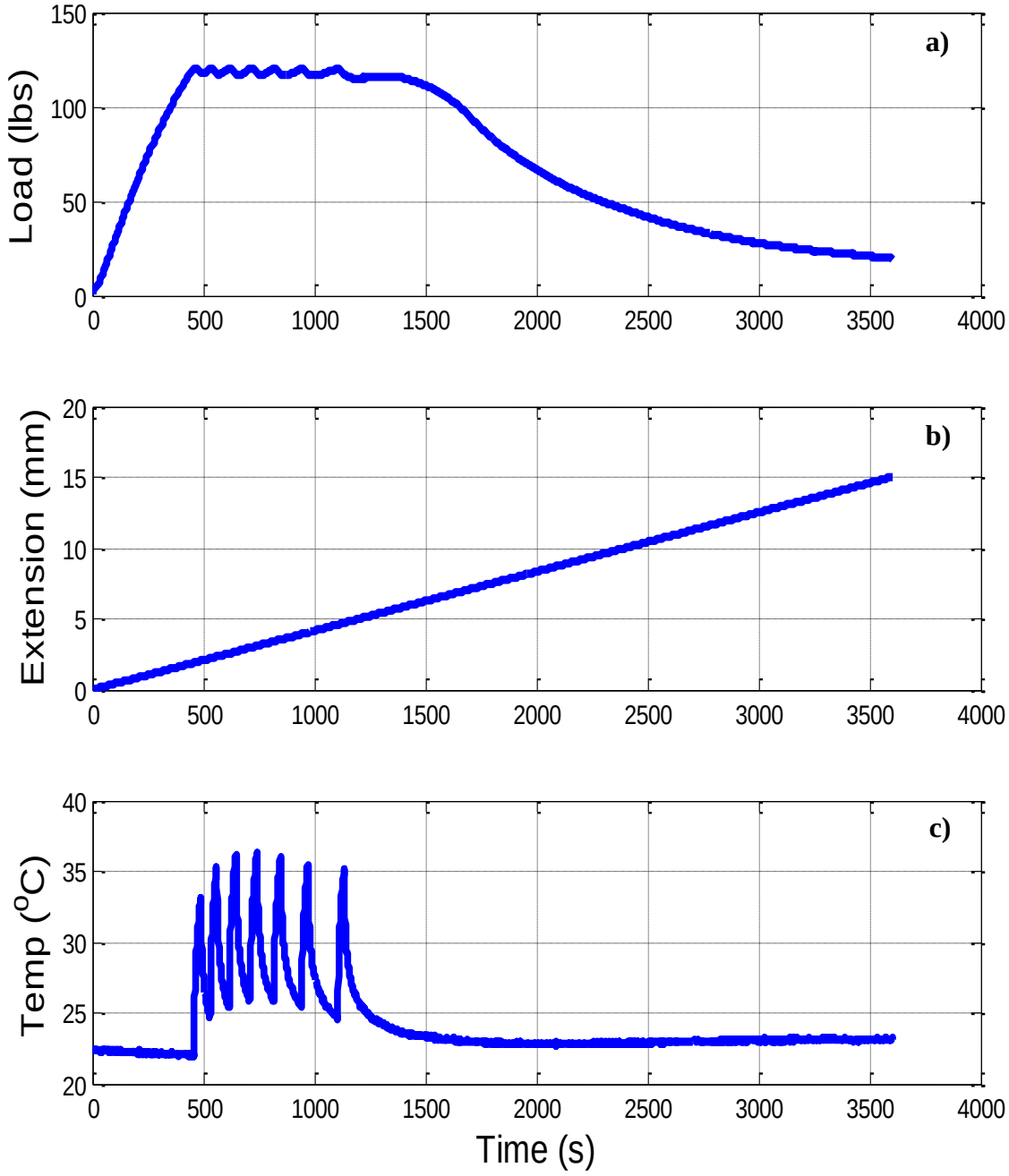

Figure 3.10. *The time dependent a) Load, b) Extension, and c) Temperature characteristics during constant strain with fluctuating laser source.*

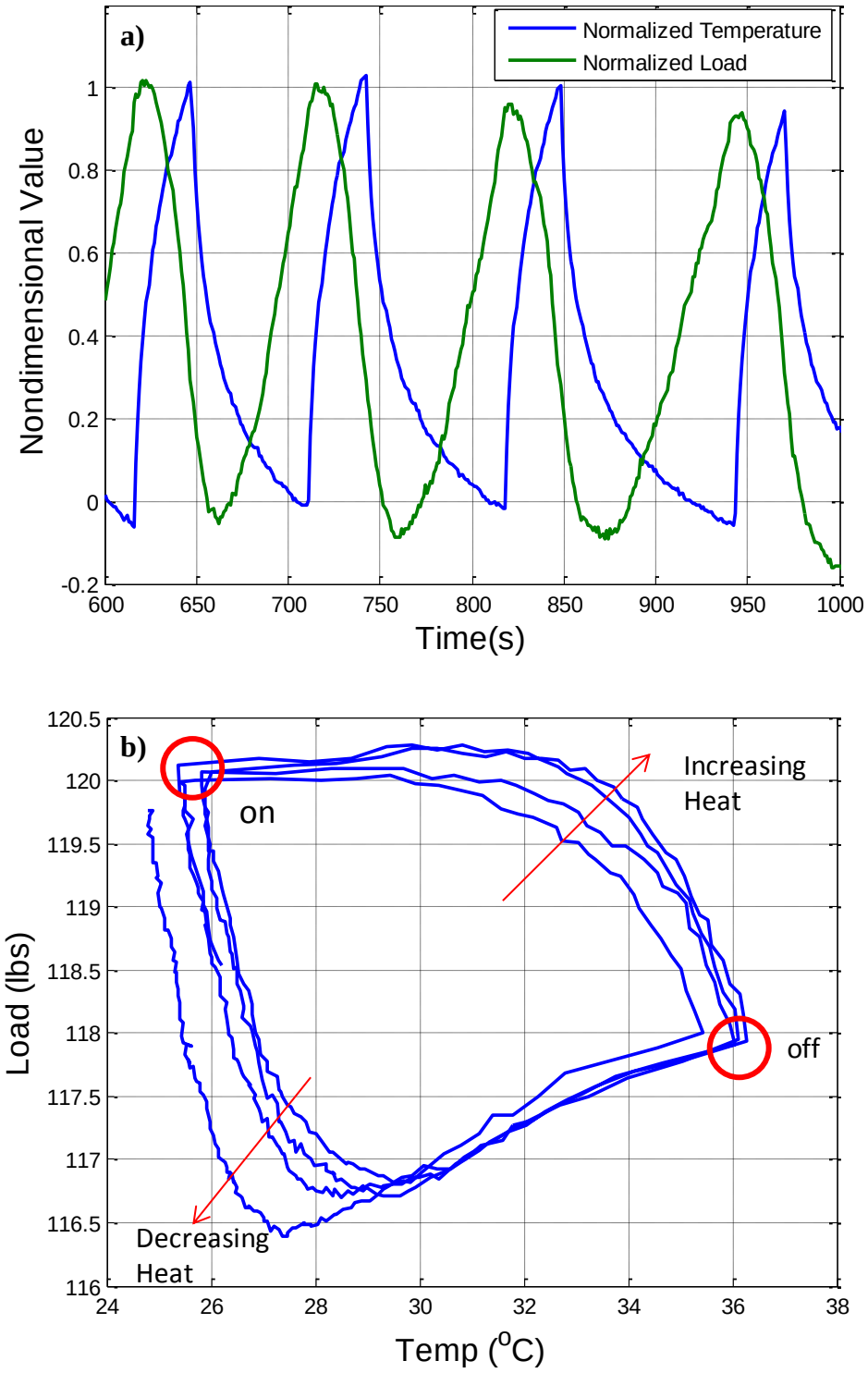

Figure 3.11. *The relationship between load and temperature with a fluctuating heat source demonstrating a) phase lag between applied temperature and responsive load and the b) load hysteresis by switching the heat source from on to off.*

3.5 Chapter Summary

This chapter presented the design and characterization of each sub-component of the automous material system. A SMP was selected that utilized high crosslinking symetry that allowed the SMP to gain a structural advantage of high stifness during its glassy and rubbery states. A strong and stiff polymer in both the rubber and glass state enables the material system to heal during operation, with the need to take the system out of service to heal and toughen. The embedded fiber optic in the SMP specimen is the core element to sense and respond to structural damage by sensing the fracture in the fiber optic and delivering thermal stimulus through light scattering at the fracture point. Damage detection was signaled through transmission loss from the fiber optic once fracture was propogated through the system. Stimulus responsive behavior was shown by a photo-themal heating method, in which a dispersion of light energy from the fractured optic at the crack site was transformed to heat through a dye which absorbed the scattered light. Encorporating a closed loop optical control system allowed for the stimulus response to be autonomusly controlled such that active toughening and healing algorthims were developed and deployed for real time loading scenarios. Design parameters of the photo-thermal heating method such as dye concentration, applied laser power, and fiber optic placment were determined to maximize the rise time and temperature gradient at the crack location to ensure real time toughening and healing could be performed during operation. Using a 900 ppm dye concentraion and a controlled laser power of 1W, the load responded quickly with minimal lag. The general trend showed that

by increasing heat decreases load and conversely decreasing heat increases load under a constant applied strain rate.

CHAPTER 4

Experimental Demonstration of Autonomous Self-Toughening and Self-Healing Mechanisms

4.1 Introduction

The field of structural health monitoring (SHM) has made significant contributions in the field of prognosis and damage detection in the past decade [116]. However, the advantageous use of this technology has not been integrated into operational structures to prevent damage from propagating or to heal injured regions under real time loading conditions. Rather, current systems relay this information to a central processor or human operator, who then determines a course of action such as altering the mission or scheduling repair maintenance. Biological systems exhibit advanced sensory and healing traits that can be applied to the design of material systems. For instance, bone is the major structural component in vertebrates; however, unlike modern structural materials, bone has many properties that make it effective for arresting the propagation of cracks and subsequent healing of the fractured area. The foremost goal for the development of future adaptive structures is to mimic biological systems, similar to bone, such that the material system can detect damage and deploy defensive traits to impede damage from propagating, thus preventing catastrophic failure while in operation. After sensing and stalling the propagation of damage, the structure must then be repaired autonomously using self healing mechanisms motivated by biological systems.

Chapter 4 presents an experimental investigation of the biologically inspired autonomous material system developed in Chapter 3. The following sections show the systems capabilities of active toughening and self healing bridging the gap between the SHM and self healing materials overcoming the limitations posed earlier. All experiments were performed according to the testing methods outlined in ASTM D 5045 for plain strain mode I fracture to simulate a real time loading environment, similar to the loading conditions experienced in continuous operational systems. Throughout the sections various aspects of the toughening and healing mechanisms presented where referenced back to the biological inspiration from human bone.

The first section studies the effective active toughening mechanism due to localized heating at the crack tip via the photo-thermal heating method. The toughening mechanism takes advantage of the SMP's quick fluctuation in modulus from its glassy to rubbery state creating a soft viscoelastic gradient at the crack tip. It shows the problematic brittle nature of the SMP without the use of defense mechanisms, showing instantaneous failure at a critical load. To compensate a non-active controller, producing a steady state thermal gradient at increasing applied constant power, was used to analysis the stress-strain relationship due to an increasingly large thermal equilibrium viscoelastic gradient. A governing relationship was obtained between applied power, or size of the viscoelastic inclusion, and the corresponding stress-strain response when experiencing crack propagation. This relationship was used to develop an active controller, producing a fluctuation in energy, subsequently controlling the

gradient of the viscoelastic inclusion achieving unprecedented toughening characteristics. This toughening mechanism allows the system to defend and impede crack propagation under continuous load demonstrating the system's potential use in real time operational systems.

Following the characterization of active toughening, the second primary property of the SMPs, programmable shape recovery was shown as a self healing mechanism. The system was able to fully recover the induced strain experienced during crack propagation, such that the cracked surfaces were able to conform back in contact. Healing was achieved by programming the SMP into a secondary shape, a state of global configuration in reference to its primary shape, and applying a tensile load in the second shape allowing crack prorogation to occur. By activating the shape memory effect, globally heating beyond the glass transitions temperature, allowed the recovery stresses to pinch the crack close. This original shape memory crack closure healing mechanism shown to double the toughness to that of the original sample.

To complete the system the combination of active toughening and self healing was presented in a real time loading environment. Again the SMP sample was programmed into a secondary shape of global compression. Upon loading, the toughening algorithm was activated below the glass transition to ensure no shape memory recovery was present. This inherently impeded the propagation of cracks mitigating catastrophic failure. Once the load was stopped upon constant localized heating, creating a temperature gradient that surpassed the glass transition temperature (T_g) and encompassed the fractured area, a radial sphere

like geometry was recovered due to the combination of the temperature gradient created by the local photo-thermal heating method and the shape memory recovery. Upon reloading the enhanced geometry of the SMPs crack tip, the specimen was able to fully recover its original strength and further increase the amount of toughening. Thus, the final system offers a solution to the posed problem as it deploys a defense toughening mechanism to defend and impede damage as well as subsequently heals the specimen to its original geometric and mechanical properties all in a continuous loading environment.

4.2 Active Toughening – Viscoelastic Crack Tip Inclusion

4.2.1 Viscoelastic Inclusion Steady State Toughening Effect

The brittle nature of the unheated SMP specimen is demonstrated in Figure 4.1b. When subjected to tensile loads, the SMP specimen shows classic mode I fracture, cracking instantaneously at a critical strain. Figure 4.1a shows the striations forming at the critical point of fracture, in the immediate center where placement of the fiber optic is used for damage detection and stimulus delivery. Figure 4.2b shows the stress-strain response of the polymer by varying the optical power flowing through the fiber optic at the crack tip at several different steady state temperature gradients (as identified by an infrared camera). Steady state implies that the samples were allowed to reach thermal equilibrium under a specific laser power before running the test. Increasing the power output across the crack location allowed for various steady state maximum temperatures to be achieved. Applying a tensile load in this steady state condition, showed that the SMP could experience a much a higher failure strain before crack propagation

was initiated, with the tradeoff of decreased load. Similar results presented by Gall *et al*. showed that by decreasing the rubbery modulus led to an exponential growth in failure strain [111]. The aliphatic urethane SMP has a sharp decrease in elastic modulus when heated, creating a soft viscoelastic inclusion gradient in the direct path of the crack.

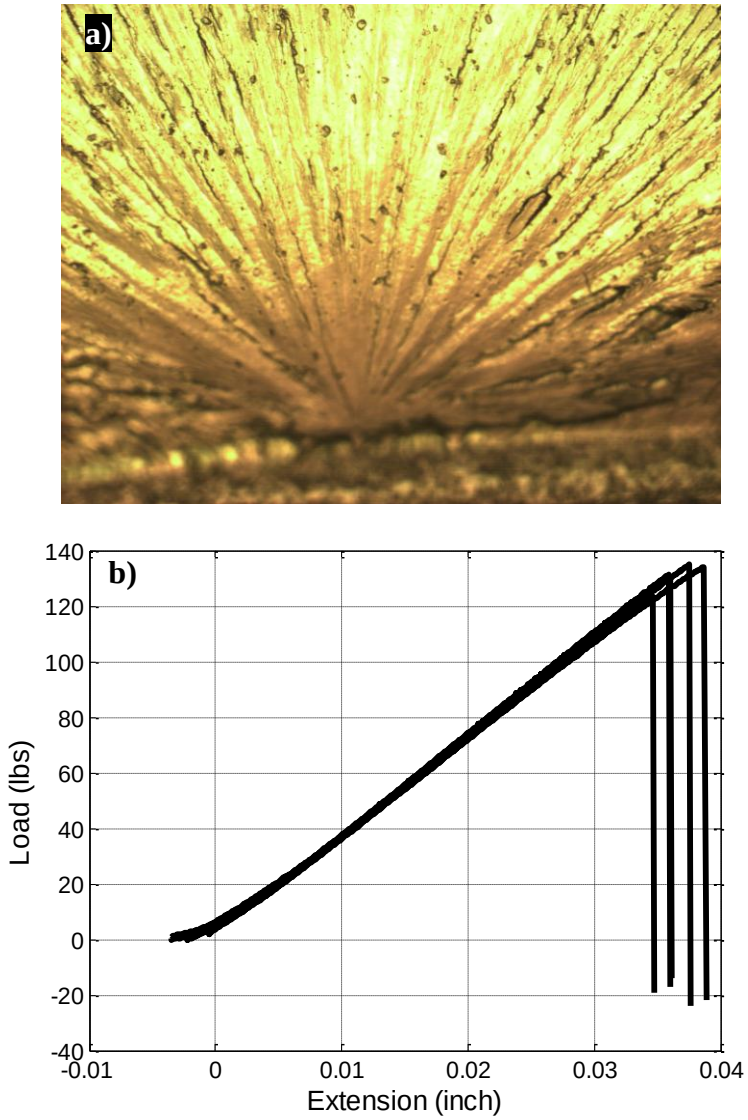

Figure 4.1. *a) Striations pattern generated at a critical point during by Mode I fracture showing optimum placement for stimulus source. b) Stress-strain response demonstrating the brittle nature of the SMP specimens undergoing Mode I fracture testing.*

Bone has been shown to exhibit a similar toughening mechanism by applying a mixed viscoplastic flow impeding crack progression. Polymer bonds have been found between the collagen molecules such that under crack progression, the sacrificial bonds tear dissipating energy at the crack location, inertly toughening bone [117]. This defense mechanism was mimicked in the SMP system by increasing thermal energy at the cracked region, altering the material properties at the fractured area, creating a viscoelastic inclusion within the bulk brittle polymer matrix. The drastic decrease in elastic modulus at the crack tip and the surrounding gradient requires more strain energy for crack propagation to continue. In some instances, the mode of failure switched from mode I to shear crack growth along the fiber optic direction (Figure 4.2a), perpendicular to the pre-cracked path. This further shows the immense toughening that can be achieved using this novel system, physically stalling all crack propagation in the pre-cracked path, forcing the energy to induce fracture in other regions of the sample.

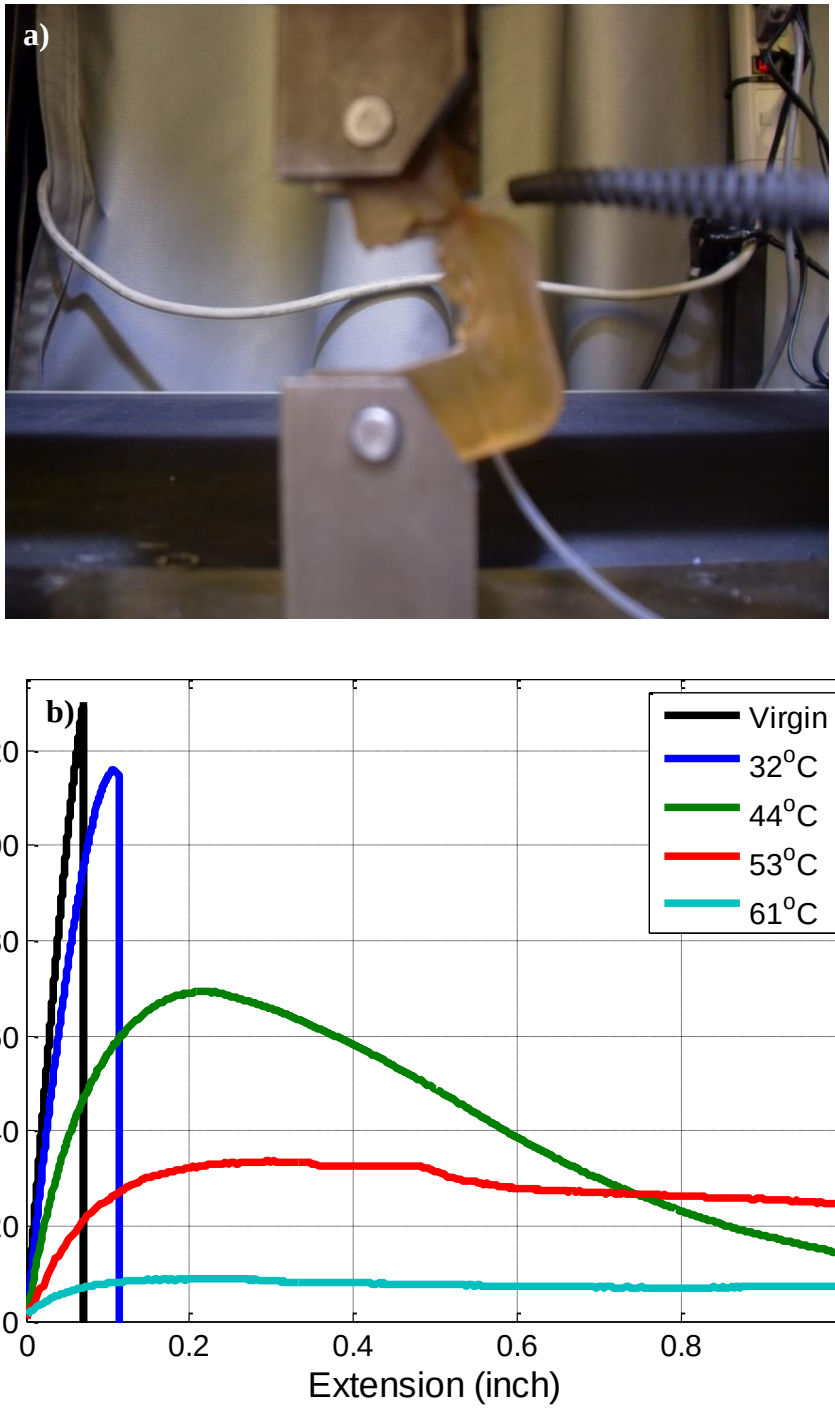

Figure 4.2. *a) Mode of failure switching from mode I to shear crack growth along the fiber optic direction fully blunting the pre notch crack patch. b) Increasing the maximum temperature steady state temperature at the crack location shows an increase in failure strain.*

4.2.2 Active Toughening Using Load Feedback Control

To demonstrate the enormous potential of this autonomous material system, a real time experiment was conducted that used load feedback control to quantify the amount of toughening this material system could achieve during mode I crack propagation. The control system was designed with an on-off controller that produced a pulse width modulated signal with a constant 1W magnitude (Figure 4.3a). The fluctuation in photo thermal heating allowed for the viscoelastic inclusion at the crack tip to be actively controlled such that only local properties were changed allowing the modulus of the sample to be preserved. The fluctuation in the energy deposited by the fractured fiber optic allowed the material properties of the viscoelastic inclusion to be actively controlled, continuously dissipating fracture energy at the damaged site while experiencing continuous strain. Figure 4.3b shows that this type of control algorithm increases the amount of strain-energy required for the system to fail by 11 times more than that of the uncontrolled brittle SMP. The specimen was able to maintain the design load until a critical strain was achieved in which physical limitations of the system prevented further toughness to be controlled. Since the fiber optic is bonded to the polymer matrix, as extension continues, the double cantilever leads to the direction in which light is emitted to be directed away from the crack tip. Effectively the amount of light dispersion still creates a temperature differential behind the crack location allowing the crack to slowly propagate through the viscoelastic wake. This method allows the polymer to transfer fracture patterns

from a brittle fracture leading to ultimate failure, a devastating effect for continuous systems, to slow crack propagation while maintaining a desired load. Using this toughening control algorithm allows the system to remain operational until it can be subsequently healed or repaired.

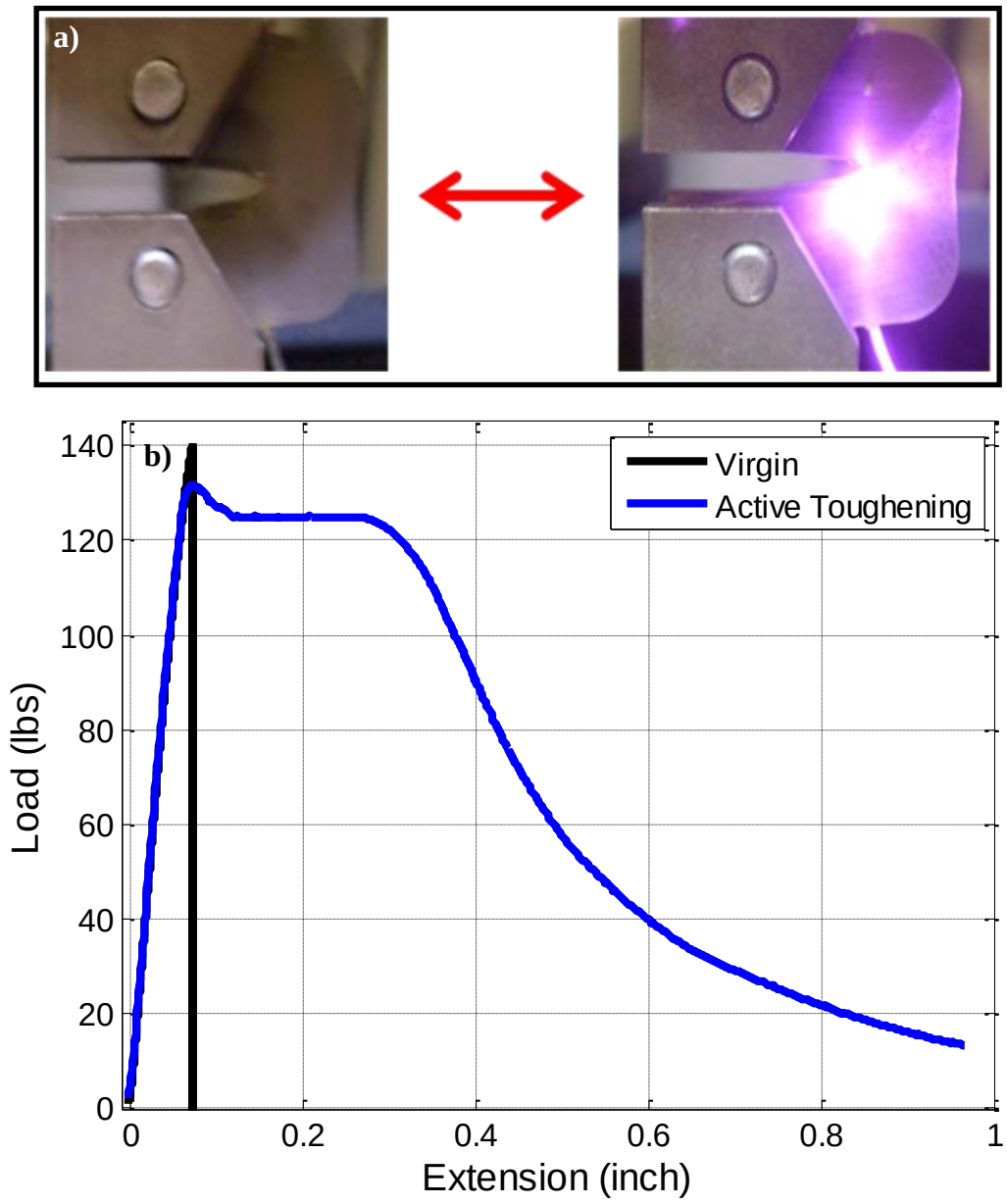

Figure 4.3. *a) Fluctuating the laser energy by the active control algorithm demonstrating exposed by the areas that the photo-thermal heating stimulus used.*

b) Load feedback control to obtain optimum toughening during mode I crack propagation.

4.3 Self-Healing – Shape Memory Crack Closure Effect

The benefit of using SMPs lies in their ability to recover high amounts of strain at relatively low temperatures. Using digital image correlation, the strain field was mapped during mode I fracture. Figure 4.4a shows the global strain field recovery when subjected to heat. In this sequence of images it can be seen that the shape memory effect closes the crack allowing the sample to return to the original geometric condition. The contours are with respect to the original specimen strain and shows that nearly all of the strain induced by the crack propagation could be fully recovered by simply heating the specimen at the crack location. Investigating further, Figure 4.4b confirms that the cracked surfaces on the microscopic level do make contact closing the crack location.

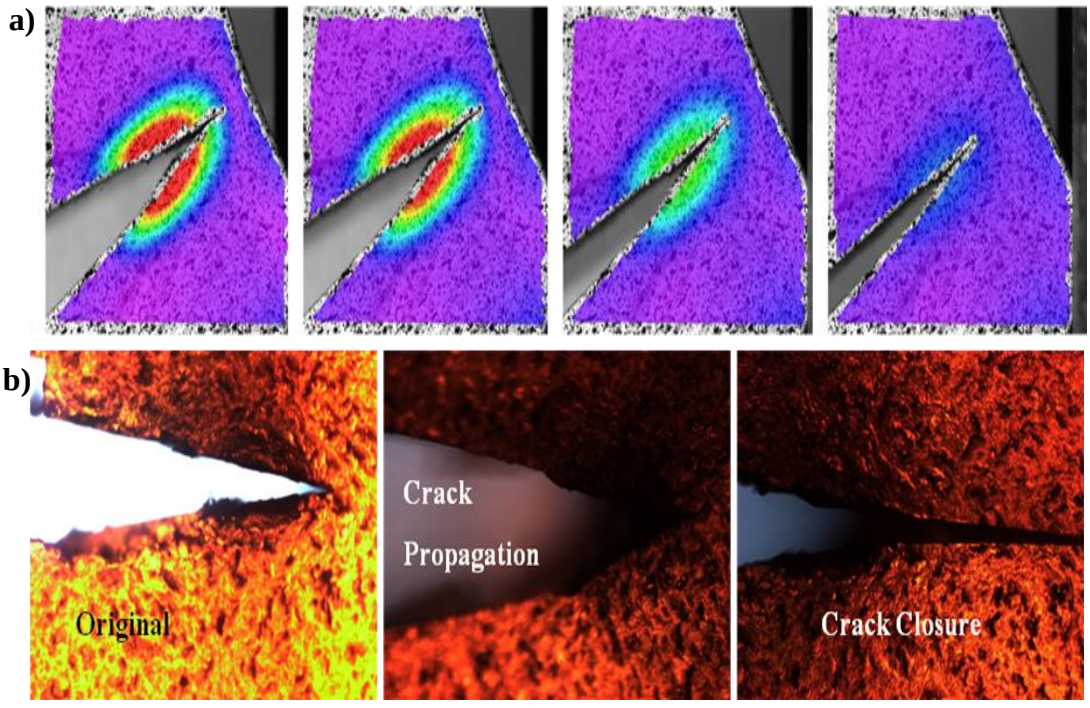

Figure 4.4. *a) Digital image correlation showing the recovery strain due to the shape memory effect around the crack location. b) Optical microscope images showing that the crack completely closed using the shape memory effect.*

Taking advantage of the shape memory phenomenon, the shape memory effect was utilizing the crack closure effect as a new healing mechanism. In this experiment, the curing schedule of the polymers was altered to make the samples viscoelastic at room temperature. Figure 4.5 shows the three different types of samples that were prepared. Sample 1 (Control) and 2 (Healed) were of original geometric configuration. Sample 3 (Prestrained) was heated and programmed in compression in the thickness direction such that the width was compressed uniformly by 20%, then allowed to cool to room temperature freezing the induced strain in the in-plane direction. The three samples where then preloaded at a slow strain rate of 0.25 mm/min to allow the samples to pre-crack to 0.2 inch, before removing them from the load frame in the pre-cracked configuration. Sample 1 was then loaded to show the effect of no crack closure, as if the test was a continuation from the previous. Sample 2 and 3 were placed inside an oven at 100°C to allow the shape memory effect to close the crack and heal the specimen, followed by cooling at room temperature.

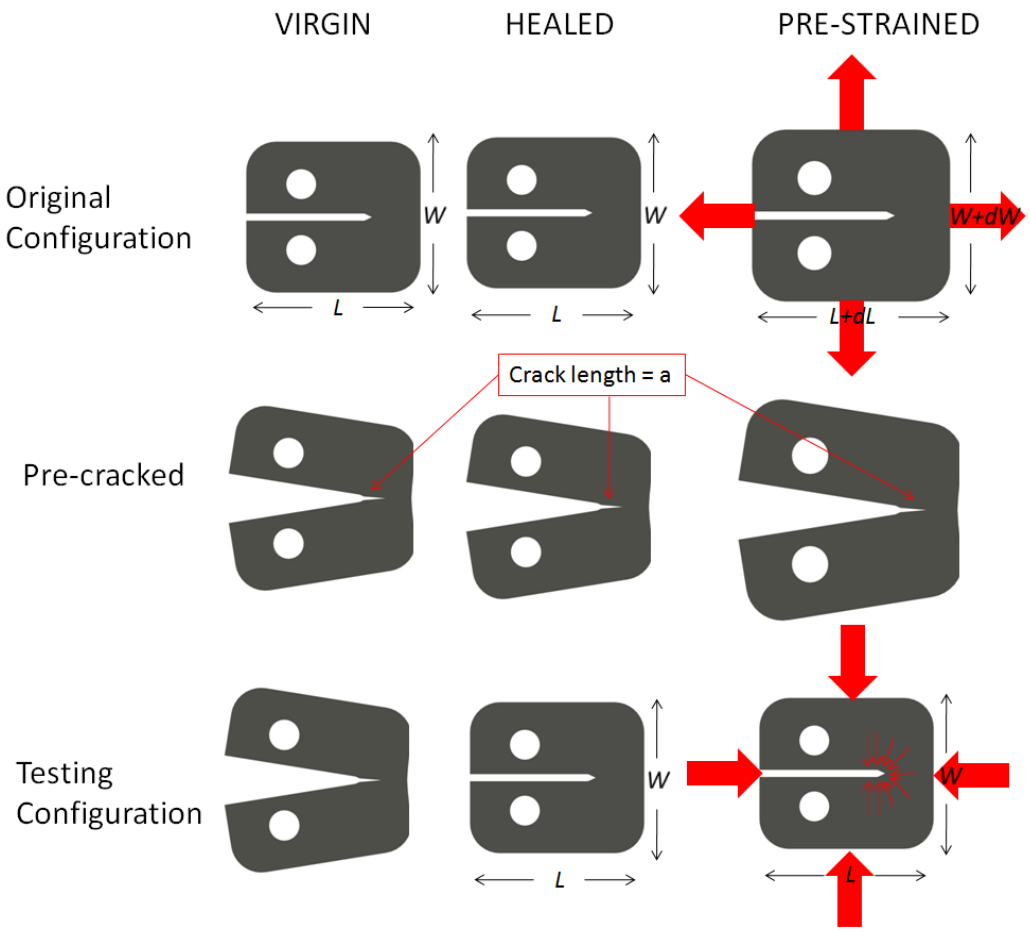

Figure 4.5. *Schematic demonstrationg the 3 different testing configurations used to quantify the shape memory healing mechanism.*

The result of this experiment is shown in Figure 4.6. It demonstrates that by closing the crack location, the SMP specimens exhibits higher strain energy before failure then that of the non closed crack, making pre-straining a candidate as a healing mechanism for mode I crack propagation. Programming a pre-strain field into the polymer greatly influenced the amount of toughening exhibited, nearly doubling that of the control sample. Because the programmed strain field was in the global compression, the recovery strain field not only recovered the strain caused by mode I fracture, but also the contraction in the out of plane direction. This technique "pinches" the crack closed, requiring more energy to

fracture, which further toughens the specimen. This novel healing technique is not in the traditional chemical approaches for self-healing polymers, in which the polymer chains are mended or the system is reinforced by re-polymerization at the crack region. It is based solely on the recovery of mechanical deformation at the crack site taking advantage of the shape memory recovery aspect of SMPs. This was done without optimization of the induced strain field, applying simple compression, and allowing the shape memory effect to recover the induced strain. It is believed that this method may be applied to various other sources of damage, such that the programmed strain field can be altered to help protect each individual system or application.

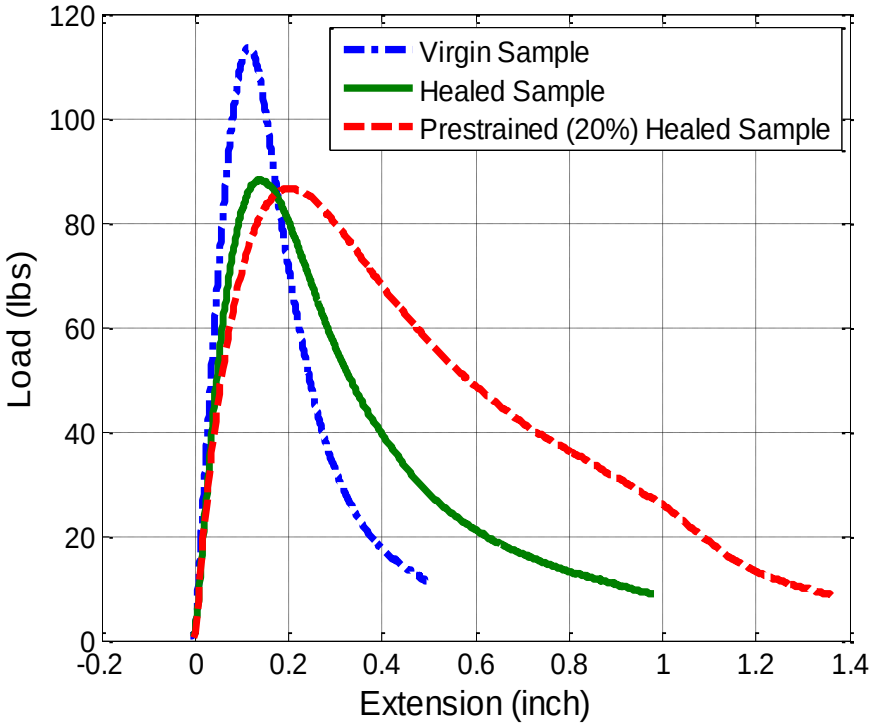

Figure 4.6. *The crack closure effect by using the shape memory recovery around the crack location.*

4.4 Complete System – Autonomous Self-Toughening and Self-Healing

To build the complete autonomous system, both the self toughening and self healing mechanisms must be demonstrated in real time loading condition. Two brittle samples were prepared; both with the same programmed pre-strain across the width allowing the initial geometric configuration to be identical. The uncontrolled sample (virgin) was placed in the load frame, under tensile load, and allowed to fracture in a brittle fashion. The second sample was loaded in tension, but before brittle failure the "toughening" algorithm was activated, pulsing the laser signal, which allowed the polymer to slow the crack propagation by blunting the crack tip. This was done below the glass transition temperature of the shape memory polymer, such that shape recovery was not initiated during the initial toughening cycle. At a generic strain, the load was stopped, and the sample was taken out of the load frame. It was then heated locally by the photo-thermal heating method via the fractured fiber optic to initiate the "healing" process. The strain shape recovery not only closed the crack tip, but produced a radial sphere around the crack location as shown in Figure 4.7. This was due to the programmed in-plane compression pre-strain allowing the shape recovery to form around the crack by the temperature gradient produced by the fiber optic photo thermal heating. The radial sphere strengthens the crack location by enhancing the geometry, requiring more fracture energy for crack propagation and failure to occur. Bone shows a similar tendency, in which the formation of healthy scar tissue enhances the mechanical properties around the cracked region [117].

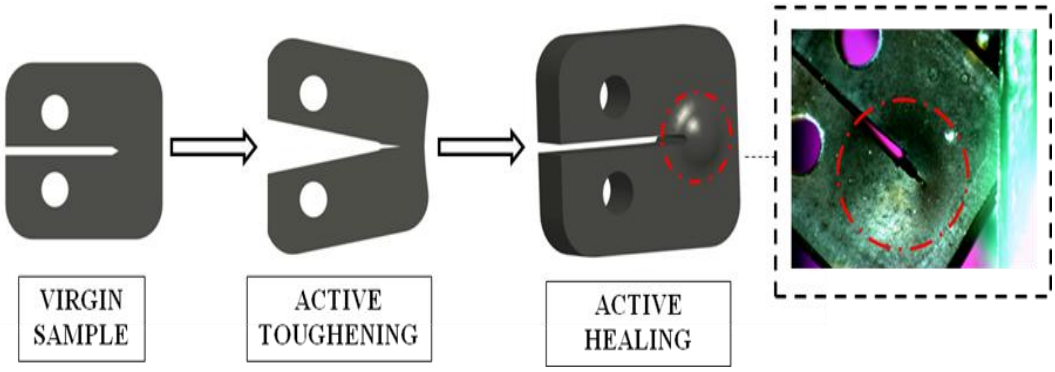

Figure 4.7. *Schematic of complete flow for the combination of active toughening with active healing*

This specimen was then reloaded in tension to test the healing mechanism in this geometric configuration. As shown in Figure 4.8, the healed specimen was able to achieve much higher toughness before failure as well as maintain the same load as the previous virgin sample. The result demonstrates that the healed specimen can recover 96% of the failure load of the virgin sample while increasing the toughness by 4.9 times. It should be noted that the drop in specimen stiffness is due to a smaller gauge length in the crack path, resulting from crack propagation during the significant strain applied under controlled toughening. Due to the increased width of the crack location, the crack propagated in a different direction, taking the curved path around the crack area, showing the toughening ability of this healed specimen. Although the induced strain for this SMP can only be recovered once, the rest of the cycle is fully reversible, allowing the toughening algorithm to stall crack propagation while the shape memory recovery closes the crack allowing existing healing techniques to be subsequently applied to the specimen.

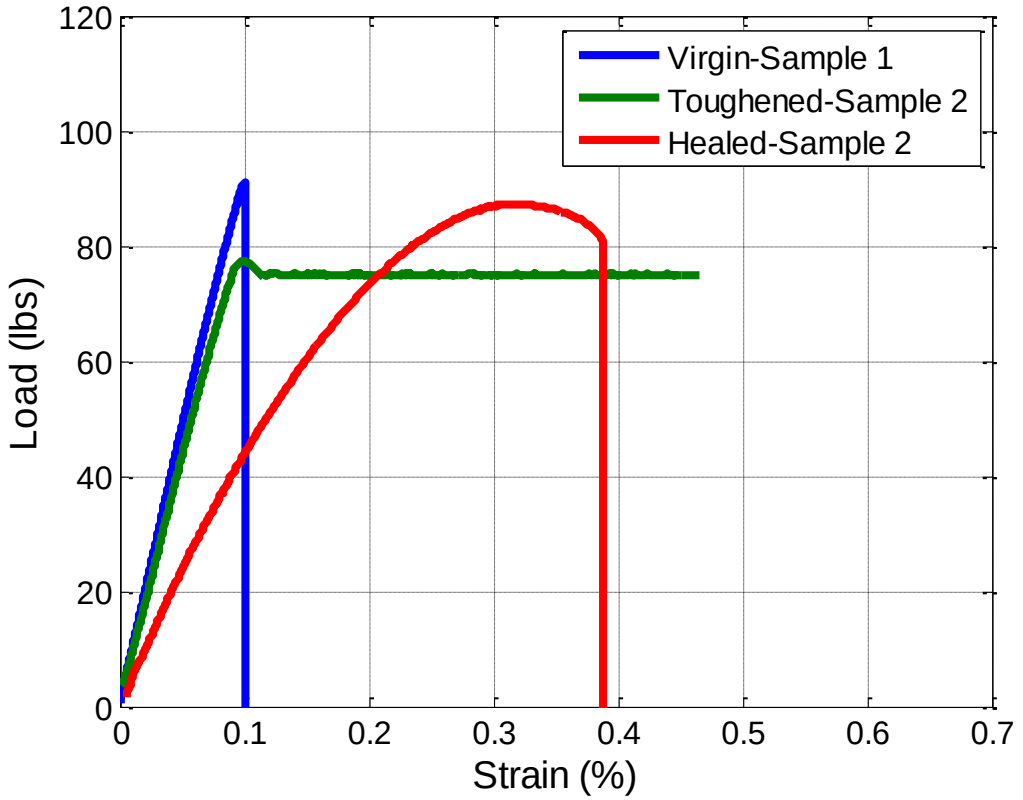

Figure 4.8. *Complete system, using the actively toughening algorithm and crack closure healing technique for a real time application.*

4.5 Chapter Summary

The results presented here demonstrate a paradigm shift in the design of autonomous systems by incorporating toughening mechanisms typically found in biological systems. Past healing modalities have not acted to stop the propagation of damage. If damage is allowed to progress the healing process may act in the wake of the crack leading to little healing effect and ultimately catastrophic failure. The technology presented here provides the key to autonomous material systems as it can (1) detect damage, (2) respond and impede damage from propagating while in operation, and (3) subsequently heal the damaged region of interest, all in an autonomous manner, as bone and other biological systems.

Using shape memory polymers with an embedded fiber optic, a novel system has been developed that was shown to incorporate all three of these techniques in one material system. Upon crack propagation, the embedded fiber optic loses significant power transmission signifying damage to the structure. This system was then able to autonomously initiate a toughening algorithm using the fiber optic as a mechanism to deliver stimulus directly to the crack tip without prior knowledge of its location. A laser was used to deposit a controlled amount of thermal energy at the crack location, slowing the crack propagation rate through crack blunting and actively toughening the specimen. It was shown under operational conditions; the toughness was 11 times larger than that of a virgin sample. Using the shape memory effect to close the crack subsequently healed the specimen to the original geometric configuration. The crack closure effect shows promise as a healing mechanism, as it was able to almost double the strain energy required for failure with an initial induced global pre-strain. Combining both the self toughening and self healing mechanisms resulted in an unprecedented strength recovery of 96% of the original load with 4.9 times more toughness even though the brittle specimen had been strained four times past its un-toughened failure strain.

CHAPTER 5

Conclusions

The field of structural health monitoring (SHM) has grown significantly over the past few years due to the safety and performance enhancing benefits as well as the potential life saving capabilities offered by the technology. Current advances in SHM systems have lead to a variety of techniques capable of identifying damage; however, few strategies exist for using this information to quickly react to the environmental or material conditions to repair or protect the system. Rather, current systems relay this information to a central processor or human operator who then decides on a course of action, such as altering the mission or scheduling a repair operation. Biological systems exhibit advanced sensory and healing traits that can be applied to the design of material systems. For instance, bone is the major structural component in vertebrates; however, unlike modern structural materials, bone has many properties that make it effective for arresting the propagation of cracks and subsequent healing of the damaged region. Self-healing polymers have shown promise using various techniques to mimic the autonomous healing mechanisms found in biological systems. Although these techniques show potential, the large time scales required for re-polymerization/re-cross linking in these self healing mechanisms are not suitable for continuous structures. Also, most of these methods require an external stimulus (i.e. heat) to be deposited to the crack site, requiring knowledge of the crack location, and/or an outside force to connect the fractured surfaces such that healing can be

initiated. Further, none of the above methods can defend against damage in real time, and are only applicable once failure has been completed.

To overcome these issues, this thesis develops a novel autonomous system using shape memory polymers with an embedded optical fiber network that acts as both a damage detection sensor and a network to deliver stimulus to the damage site initiating toughening and healing. This novel autonomous material system provides the missing link in SHM and self-healing materials as it is able to (1) detect damage, (2) respond and actively toughen at the crack location impeding crack propagation, and (3) recover the induced strain energy, subsequently healing the structure to its designed conditions. The following section discusses briefly the relevant results for the autonomous system. It demonstrates a real-time toughness mechanism based on soft crack inclusion, an unprecedented shape memory self-healing technique, all in a real time atmosphere with continuous damage detection capabilities with direct stimulus delivery to the crack site. Following, the system is evaluated and recommendations are made for future work.

5.1 Summary of Thesis and Results

One of the novel mechanisms presented in this thesis is the ability to defend real-time crack propagation by an active-toughening technique. The design of SMP molecular structure allows for a drastic decrease in elastic modulus, as high as two orders of magnitude, once heated past its T_g. Taking advantage of this property, a FE model was created to investigate the influence of a non-homogenous soft inclusion at the crack tip. The solution of the finite element

analysis revealed several intriguing aspects and trends for the SIFs at the crack-tip and the stress within the bulk material. It was shown that by increasing the temperature surrounding the crack, the stress produced at tip node decreased as high as an order of magnitude. While the maximum stress was located at the crack tip for all analyses, the reduction in stress by local heating of the crack region can improve the global toughness of the material. Further, it was shown that the high stress field is redistributed from the crack singularity and into the bulk material over a larger surface area, mitigating fracture energy at the crack tip and creating a crack blunting method. The FE model was compared to a homogenous single inclusion theory, in which the evaluation of K_{tip}/K_{bulk} was validated between the two models showing good agreement.

The FE model demonstrated the ability for the SMP polymer to achieve active toughening by embedding a controlled heat source at the crack location. Thus, the autonomous system was developed and characterized by embedding a fiber optic into the polymer matrix. Embedding a fiber optic into the SMP specimen granted two properties: sensing and response to structural damage. Damage detection was captured through transmission loss from the fiber optic once fracture was propogated through the system. Stimulus responsive behavior was shown by a photo-themal heating method, in which a dispersion of light energy from the fractured optic at the crack site was transformed to heat due to dye absorbance match. Encorporating a closed loop optical control system allowed for the stimulus response to be autonomously controlled such that active toughening and healing algorthims were developed and deployed for real-time

loading scenarios. Optimum design paramters of the photo-thermal heating method such as dye concentration, applied laser power, and fiber optic placment were determined to maximize the rise time and temperature gradient at the crack location to ensure real time toughening and healing could be performed in operation. The response characteristics between applied load and fluctated temperature was evaluated to quantify the photo-thermal stimulus behavior during real time loading. Suitable design requirements using 900ppm dye concentration and a fluctuated applied power of 1W allowed the load to respond quickly with minimal lag. The general trend showed that increasing heat decreased load and conversely, decreasing heat increased load under a constant applied strain rate.

Once the system had been fully characterized, a demonstration of the real-time operational autonomous toughening and healing mechanisms was presented. Upon crack propagation, the embedded fiber optic lost significant power transmission, signifying damage to the structure. This system was then able to autonomously initiate a toughening algorithm using the fiber optic as a mechanism to deliver stimulus directly to the crack tip without prior knowledge of its location. A laser was used to deposit a controlled amount of thermal energy at the crack location, slowing the crack propagation rate through crack blunting and actively toughening the specimen. It was shown under operational conditions that the toughness was 11 times larger than that of a virgin sample. Using the shape memory effect to close the crack subsequently healed the specimen to the original geometric configuration. The crack closure effect shows promise as a healing mechanism, as it was able to almost double the strain energy required for failure

with an initial induced global pre-strain. Combining both the self toughening and self healing mechanisms resulted in an unprecedented strength recovery of 96% of the original load with 4.9 times more toughness, even though the brittle specimen had been strained four times past its un-toughened failure strain. The results presented in this thesis demonstrate a paradigm shift in the design of autonomous systems by incorporating toughening mechanisms typically found in biological systems. Past healing modalities have not acted to stop the propagation of damage. If the damage is allowed to progress, the healing process may act in the wake of the crack leading to little healing effect and ultimately catastrophic failure.

5.2 Recommendations for Future Work

This thesis has successfully developed an autonomous material system capable of defending crack propagation through active toughening and subsequent healing via the shape memory response. Although novel, there is room for optimizing the system's performance.

The innovative use of the fiber optic showed the ability to apply a thermal stimulus by photo-thermal heating as well as detect damage by intensity-based SHM methods. Expanding the fiber optic network to include an array to incorporate the entire polymer matrix would be needed for practical application. This would open new parameters such as fiber optic orientation and spacing such that damage could be sensed and controlled throughout the entire structure. Also, with this embedded fiber optic network existing SHM techniques could be used to monitor the stress and strain fields of the entire structure while in operation.

One of the limiting features of this method is that once the fiber optic has been fractured and the polymer has been subsequently healed, the fiber will still experience significant transmission loss, losing the ability to sense, while also limiting the exposure energy to other downstream cracks along the fiber. This technique limits the repeatability of the system, requiring a repair of the cracked fiber. Little research has demonstrated the ability for fiber optics to self-heal; thus; the demand for a healable/repeatable stimulus and sensing source is needed to purely allow the system to remain autonomous throughout operation, not just strictly during damage.

It is also noted that the shape memory response as a self-healing mechanism has not been fully investigated. It is believed that various sources of damage can be healed by correctly programming the polymer into an optimum geometric configuration (i.e. global compression/tension, radial compression/tension, buckle patterns). Further, investigation of time-dependent heating profiles, would ultimately cause different time-dependent shape memory responses such that damage could be defended before it could progress into the polymer matrix (i.e. allow a radial sphere to be produced behind the crack wake, to deflect crack prorogation). Lastly, the shape memory response allows the cracked surfaces to recover the induced strain and conform back to contact autonomously. Existing self-healing modalities such as micro-encapsulated approach and thermal reversible cross linking could be used to further heal the structure making the polymer matrix more resistant to crack propagation.

REFERENCES

[1] Leka, L.G., Bayo, E., "A Close Look at the Embedment of Optical Fibers into Composite Structures", Journal of Composite Technology, 11, 106-112 (1989).

[2] Kuang, K.S.C., Cantwell, W. J., "Use of Conventional Optical Fibers and Fiber Bragg Gratings for Damage Detection in Advanced Composite Structures: A Review", Applied Mechanics Reviews, 56, 493-513 (2003).

[3] Farrar, C.R., Allen, D.W., Park, G., Ball, S., Masquelier, M.P., "Coupling Sensing Hardware with Data Interrogation Software for Structural Health Monitoring", Shock and Vibration, 13, 519-530 (2006).

[4] Martian, P., "Wound Healing – Aiming for Perfect Skin Regenification", Science, 276, 75-81 (1997).
[5] Varghese, S., Lele, A., Mashelkar, R., "Metal-Ion Healing of Gels", Journal of Polymer Science: Part A: Polymer Science, 44, 666-670 (2005).

[6] Peterlink, H., Roschger, P., Klaushofer, K., Fratzl, P., "From Brittle to Ductile Fracture of Bone" Nature Materials, 5, 52-55 (2006).

[7] Thompson, J. B., Kindt, J. H., Drake, B., Hansma, H. G., Morse, D. E., Hansma, P. K., "Bone Indention Recovery Time Coorelates with Bond Refoming Time", Nature, 414, 773-776 (2001).

[8] Fantner, G. E., Hassenkam, T,m Kindt, J. H., Weaver J. C., Birkedal, H., Pechenik, L., Cutroni, J. A., Cidade, G. A. G., Stucky, G. D., Morse, D. E., and Hansma, P. K., "Sacrafitical Bonds and Hidden Length Dissipate Energy as Mineralized Fibrilis Separate During Bond Fracture", Nature Materials, 4, 612-616 (2005).

[9] Zioupos, P., Curry, J.D., "The Extent of Microcracking and the Morphology of Microcracks in Damaged Bone", Journal of Material Science, 29, 978-986 (1994).

[10] Zioupos, P., Curry J. D., "The Accumulation of Fatigue Microdamage in Human Cortical Bone of Two Different Ages in vitro" Clinical Biomechanics, 11, 365-375 (1996).

[11] Vashishth, D., Tanner, K.E., Bonfield, W., "Experimental Validation of Microcracking-Based Toughening Mechanism for Cortical Bone", Journal of Biomechanics, 36, 121-124 (2003).

[12] Nalla, R.K., Kinney, J. H., Ritchie, R. O., "Mechanistic Fracture Criteria for the Failure of Human Cortical Bone", Nature Materials, 2, 164-168 (2003).

[13] Nalla, R. K., Kruzic, J. J., Ritchie, R. O, "On the Origin of the Toughness of Mineralized Tissue: Microcracking or Crack Bridging?" Bone, 34, 790–798 (2004).

[14] Nalla, R. K., Kruzic, J. J., Kinney, J. H., and Ritchie, R. O, "Mechanistic Aspects of Fracture and R-Curve Behavior and R-Curve Behavior in Human Cortical Bone", Biomaterials, 26, 217-231 (2005).

[15] Liu, D.,Weiner, S., Wagner, H. D., "Anisotropic Mechanical Properties of Lamellar Bone using Miniature Cantilever Bending Specimens", Journal of Biomechanics, 32, 647–654 (1999).

[16] Dry, C., Sottos, N. R., "Passive Smart Self-Repair in Polymer Matrix Composite Materials", Proceedings of SPIE Vol. 1916, 438-444 (1996).

[17] White, S.R., Sottos, N. R., Geubelle, P. H., Moore, J. S., Kessler, M. R., Sriam, S. R., Brown, E. N., Viswanathan S., "Autonomic Healing of Polymer Composites", Nature, 409, 794-797 (2001).

[18] Chen, X., Dam, M. A., Ono, K., Mal, A., Shen, H., Nutt, S. R., Sheran, K., Wudl, F., "A Thermally Re-mendable Cross-Linked Polymeric Material", Science, 295, 1698-1702 (2002).

[19] Park, G., Sohn, H., Farrar, C.R., Inman, D.J., "Overview of Piezoelectric Impedance-Based Health Monitoring and Path Forward", Shock and Vibration, 6, 451-463 (2003).

[20] Sivanesan, P., Sirkis, J., Venkat, V., Shi, Y.C., Reddy, C.J., Sankaran, S., "Simultaneous Measurement of Temperature and Strain using a Single Bragg Grating", Proceedings of SPIE Vol. 3670, 92-103 (1999).

[21] Wood, K., Brown, T., Rogowski, R., Jensen, B., "Fiber Optic Sensors for Health-Monitoring of Morphing Airframes: I Bragg Grating Strain and Temperature Sensor", Smart Material Structures, 9, 163-169 (2000).

[22] Hale, K.F., "An Optical-Fiber Fatigue Crack-Detection and Monitoring System", Smart Material Structures, 1, 156-161 (1992).

[23] Fuhr, P.L., Huston, D.R., Kajenski, P.J., Ambrose, T.P., "Performance and Health-Monitoring of the Stanford Medical Building using Embedded Sensors", Smart Material Structures, 1, 63-68 (1992).

[24] Murukeshan, V.M., Chan, P.Y., Ong, L.S., Asundi, A., "On-line Health-Monitoring of Smart Composite Structures using Fiber Polarimetric Sensor", Smart Material Structures, 6, 113-118 (1999).

[25] Cantwell, W.J., Curtis, P.T., Morton, J., "Impact and Subsequent Fatigue Damage Growth in Carbon Fiber Laminates", International Journal of Fatigue, 6, 113-118 (1984).

[26] Measures, R.M., Glossop, N.D.W., Lymer, J., Leblanc, M., West, J., Dubois, S., Tsaw, W., Tennyson, R.C., "Structurally Integrated Fiber Optic Damage Assesment System for Composite Materials", Applied Optics, 28, 2626-2633 (1989).

[27] Measures, R.M., Glossop, N.D.W., Lymer, J., West, J., Dubois, S., Tsaw, W., Tennyson, R.C., "Fibre Optic Impact Damage Detection of Composite-Material", Proceeding of the Society of Photo-Optics In-strum Engineering, (1988).

[28] Grattan, K.T.V., Meggitt, B.T., "Optical Fiber Sensor Technology", Devices and Technology, Chapman and Hall, 2, (1988).

[29] Kersey, A.D., "A Review of Recent Developments in Fiber Optic Sensor Technology", Optical Fiber Technology: Material, Devices System, 2, 291-317 (1996).

[30] LeBlanc, M., Measure, R.M., "Impact Damage Assessment in Composite Materials with Embedded Fiber-Optic Sensors", Composites Engineering, 2, 573-596 (1992).

[31] Rowe, W.J., Rausch, E.O., Dean, P.D., "Embedded Optical Fiber Strain Sensor for Composite Structure Applications", Proceedings of SPIE Vol. 718, 266-273 (1986).

[32] McKenzie, I., Jones, R., Marshall, I.H., Galea, S., "Optical Fiber Sensors for Health-Monitoring of Bonded Repair Systems", Composite Structures, 50, 405-416 (2000).

[33] Chiu, W.K., Koh, Y.L., Galea, S.C., Rajic, N., "Smart Structure Application in Bonded Repairs", Composite Structures, 49, 433-444 (2000).

[34] Findik, F., Mrad, N., Johnston, A., "Strain Monitoring in Composite Patched Structures", Composite Structures, 49, 331-338 (2000).

[35] Okabe, Y., Yashiro, S., Kosaka, T., Takeda, N., "Detection of Transverse Cracks in CFRP Composites using Embedded Fiber Bragg Grating Sensors", Smart Material Structures, 9, 832-838 (2000).

[36] Badcock, R.A., Fernando, G.F., "An Intensity-Based Optical Fiber Sensor for Fatigue Damage Detection in Advanced Fiber-Reinforced Composites", Smart Material Structures, 4, 223-230 (1995).

[37] Measures, R.M., Glossop, N.D.W., and Lymer, J., Leblanc, M., Dubois, S., Tsaw, W., Tennyson, R.C., "Structurally Integrated Fiber and Optic Damage Assessment System for Composite Materials", Oplied Optics, 28, 2633-2656 (1989).

[38] Glossop, N.D.W., Dubois, S., Tsaw, W., Leblanc, M., Lymer, J., Measures, R.M., Tennyson, R.C., "Optical Fiber Detection for Aircraft Composite Leading Edge", Composites, 21, 71-80 (1990).

[39] Jensen, D.W., Pascual, J., and Augusst, J.A., "Performance of Graphite/Bismalemidine Laminates with Embedded Optical Fibers, Part II: Uniaxial Compression", Smart Material Structures, 1, 31-35 (1992).

[40] Jensen, D.W., Pascual, J., Augusst, J.A., "Performance of Graphite/Bismalemidine Laminates with Embedded Optical Fibers, Part II: Uniaxial Tension", Smart Material Structures, 1, 24-30 (1992).

[41] Blagojevic, B., Tsaw, W., McEwen, and Measures, R.M., "The Influence of Embedded Optical Fibers on the Intralamina Fracture Toughness of Composite Materials", Review of Progress in Quantitative Nondestruction Evaluation, 9, 1213-1218 (1989).

[42] Leka, L.G., and Bayo, E., "A Close Look at the Embedment of Optical Fibers into Composite Structures", Journal of Composite Technology, 11, 106-112 (1989).

[43] Hale, K.F., Hockenhull, B.S., and Christodoulou, G., "The Application of Optical Fibers as Witness Devices for the Detection of Plastic Strain and Cracking", Strain, 16, 150-154 (1980).

[44] Jen, C.K., Farnell, G.W., Parker, M., and Cielo, P., "A Fiber Optic Damage Monitor", Review of Progress in Quantitative Nondestruction Evaluation, 48, 831-838 (1985).

[45] Hofer, B., "Fiber Optic Damage Detection in Composite Structures", Composites, 18, 309-316 (1987).

[46] Glossop, N.D.W., "An Embedded Fiber Optic Sensor for Impact Damage Detection in Composite M0aterials", PhD Thesis, University of Toronto, Toronto, Canada (1989).

[47] Martin, A., Badcock, R., Nightingale, C., Fernando, G.F., "A Novel Optical Fiber-Based Strain Sensor", IEEE Photonics Technology Letters, 9, 982-984 (1997).

[48] Kitade, S., Fukuda, T., Osaka, K., "Fiber Optic Method for Detection of Impact Induced Damage in Composite Laminates", Journal of the Society of Materials Science, 44, 1196-1200 (1995).

[49] Kitade, S., Fukuda, T., Osaka, K., Hamamoto, A., "Detection of Damages in Composite Laminates with Embedded Optical Fibers", Proceedings of US-Japan Workshop on Smart Materials and Structures, (1997).

[50] Takeda, N., Kosaka, T., Ichiyama, T., "Detection of Transverse Cracks by Embedded Plastic Optical Fiber in FRP Laminates", Proceedings of SPIE Vol. 3670, 248-255 (1999).

[51] Osswald, T., Menges, G., "Failure and Damage of Polymers", Materials Science of Polymers for Engineers, Munich: Hanser Publishers, 447–519 (2003).

[52] Chamis, C.C., Sullivan, T.L., "In Situ Ply Strength: An Initial Assessment", Cleveland, OH: NASA Lewis Research Center, 19, (1978)

[53] Wilson, D.J.K., Wells, J.N., Hay, D., Owens, G.A., Johnson, F., "Preliminary Investigation into Microcracking of PMR-15 Graphite Composites—Part I, Effect of Cure Temperature", Proceedings of the 18th International SAMPE Conference, 18, 242-253 (1986).

[54] Jang, B.Z., Chen, L.C., Hwang, L.R., Hawkes, J.E., Zee, R.H., "The Response of Fibrous Composites to Impact Loading", Polymer Composite, 11, 144-157 (1990).

[55] Morton, J., Godwin, E.W., "Impact Response of Tough Carbon Fiber Composites", Composite Structures, 13, 1-19 (1989).

[56] Jud, K., Kausch, H.H., Williams, J.G., "Fracture-Mechanics Studies of Crack Healing and Welding of Polymers", Journal of Material Science, 16, 204-210 (1981).

[57] Espuche, E., Galy, J., Gerard, J.F., Pascault, J.P., Sautereau, H., "Influence of Cross-Link Density and Chain Flexibility on Mechanical-Properties of Model Epoxy Networks", Macromolecules, 93, 107-115 (1995).

[58] Kim, S.L., Skibo, M.D., Manson, J.A., Hertzberg, R.W., Janiszewski, J., "Tensile, Impact and Fatigue Behavior of an Amine-Cured Epoxy-Resin", Polymer Engineering Science, 18, 1093-1100 (1978).

[59] Kim, S.L., Skibo, M.D., Manson, J.A., Hertzberg, R.W., Janiszewski, J., "Tensile, Impact and Fatigue Behavior of an Amine-Cured Epoxy-Resin", Polymer Engineering Science, 18, 1093-1100 (1978).

[60] Kim, N.H., Kim, H.S., "Micro-void Toughening of Thermosets and its Mechanism", Journal of Applied Polymer Science, 98, 1290-1295 (2005).

[61] Kinloch, A.J., Taylor, A.C., "The Mechanical Properties and Fracture Behaviour of Epoxy-Inorganic Micro- and Nanocomposites", Journal of Material Science, 41, 3271-3297 (2006).

[62] Jud, K., Kausch, H.H., "Load Transfer Through Chain Molecules after Interpenetration at Interfaces", Polymer Bulletin, 1, 697-707 (1979).

[63] Lin, C.B., Lee, S.B., Liu, K.S., "Methanol-Induced Crack Healing in Poly(methyl-methacrylate)", Polymer Engineering Science, 30, 1399-1406 (1990).

[64] Wang, P.P., Lee, S., Harmon, J.P., "Ethanol-Induced Crack Healing in Poly(methyl- methacrylate)", Journal of Polymer Science Part B: Polymer Physics, 32, 1217-1227 (1994).

[65] Chung, C.M., Roh, Y.S., Cho, S.Y., Kim, J.G., "Crack Healing In Polymeric Materials via Photochemical [2+2] Cycloaddition", Chemical Materials, 16, 3982-3984 (2004).

[66] Harreld, J.H., Wong, M.S., Hansma, P.K., Morse, D.E., Stucky, G.D., "Self-Healing Organosiloxane Materials Containing Reversable and Energy-Dispersive Crosslinking Domains", University of California, [2004007792-A1] (2004).

[67] Lee, J.Y., Buxton, G.A., Balazs, A.C., "Using Nanoparticles to Create Self-Healing Composites", Journal of Chemical Physics, 121, 5531-5540 (2004).

[68] Tyagi, S., Lee, J.Y., Buxton, G.A., Balazs, A.C., "Using Nanocomposite Coatings to Heal Surface Defects", Macromolecules, 37, 9160-9168 (2004).

[69] Gupta, S., Zhang, Q., Emrick, T., Balazs, A.C., Russell, T.P., "Entropy-Driven Segregation of Nanoparticles to Cracks in Multilayered Composite Polymer Structures", Nature Materials, 5, 229-233 (2006).

[70] Dry, C.M., Sottos, N.R., "Passive Smart Self-repair in Polymer Matrix Composite Materials", Conference on Recent Advances in Adaptive and Sensory Materials and their Applications. Virginia, USA: Technomic, 438-444 (1992).

[71] Dry, C.M., "Procedures Developed for Self-Repair of Polymer Matrix Composite Materials", Composite Structures, 35, 263-269 (1996).

[72] Bleay, S.M., Loader, C.B., Hawyes, V.J., Humberstone, L., Curtis, P.T., "A Smart Repair System for Polymer Matrix Composites", Composites Part A: Applied Science Manufacturing, 32, 1767-1776 (2001).

[73] Pang, J.W.C., Bond, I.P., "A Hollow Fibre Reinforced Polymer Composite Encompassing Self-Healing and Enhanced Damage Visibility", Composite Science Technology, 65, 1791-1719 (2005).

[74] Trask, R.S., Bond, I.P., "Biomimetic Self-Healing of Advanced Composite Structures using Hollow Glass Fibres", Smart Material Structures, 15, 704-710 (2006).

[75] Pang, J.W.C., Bond, I.P., "'Bleeding Composites'—Damage Detection and Self-Repair using a Biomimetic Approach", Composites Part A: Applied Science Manufacturing, 36, 183-188 (2005).

[76] White, S.R., Sottos, N. R., Geubelle, P. H., Moore, J. S., Kessler, M. R., Sriam, S. R., Brown, E. N., Viswanathan S., "Autonomic Healing of Polymer Composites", Nature, 409, 794-797 (2001).

[77] Sanada, K., Yasuda, I., Shindo, Y., "Transverse Tensile Strength of Unidirectional Fibre-Reinforced Polymers and Self-Healing of Interfacial Debonding", Plastics, Rubber, and Composites, 35, 67-72 (2006).

[78] Brown, E.N., Sottos, N.R., White, S.R., "Fracture Testing of a Self-Healing Polymer Composite", Experimental Mechanics, 42, 372-379 (2002).

[79] Brown, E.N., White, S.R., Sottos, N.R., "Retardation and Repair of Fatigue Cracks in a Microcapsule Toughened Epoxy Composite—Part II: In situ Self-Healing", Composite Science Technology, 65, 2474-2480 (2005).

[80] Brown, E.N., White, S.R., Sottos, N.R., "Microcapsule Induced Toughening in a Self-Healing Polymer Composite" Journal of Material Science, 39, 1703-1710 (2004).

[81] Brown, E.N., Sottos, N.R., White, S.R., "Fracture Testing of a Self-Healing Polymer Composite", Experimental Mechanics, 42, 372-379 (2002).

[82] Chen, X., Wudlm F., Mal, A.K., Shen, H., Nutt, S.R., "New Thermally Remendable Highly Cross-linked Polymeric Materials", Macromolecules, 36, 1802-1807 (2003).

[83] Chen, X., Dam, M.A., Ono, K., Mal, A., Shen, H.B., Nutt, S.R., Sheran, K., Wudl, F., "A Thermally Re-Mendable Cross-linked Polymeric Material", Science, 295, 1698-1702 (2002).

[84] Rickborn, B., "The Retro-Diels–Alder Reaction. Part I. C–C Dienophiles", In: Organic Reactions, 1-394 (1998).

[85] Yamaguchi, G., Higaki, Y., Otsuka, H., Takahara, A., "Reversible Radical Ring-Crossover Polymerization of an Alkoxyamine-Containing Dynamic Covalent Macrocycle", Macromolecules, 38, 6316-6320 (2005).

[86] Yamaguchi, M., Ono, S., Terano, M., "Self-Repairing Property of Polymer Network with Dangling Chains", Material Letters, 61, 1396-1399 (2007).

[87] Varghese, S., Lele, A., Mashelkar, R., "Metal-Ion-Mediated Healing of Gels", Journal of Polymer Science Part A – Polymer Chemistry, 44, 666-670 (2006).

[88] Liu, Y., Gall, K., Dunn, M., Greenberg, A. R., and Diani, J., "Thermomechanics of Shape Memory Polymers: Uniaxial Experiments and Constitutive Modeling", Journal of Plasticity, 22, 279-313 (2006)

[89] Tobushi, H., Hashimoto, T., Hayashi, S., and Yamada, E., "Thermomechanical Constitutive Modeling in Shape Memory Polymer Polyurethane Series", Journal of Intelligent Material Systems and Structures 8, 711-718 (1997).

[90] Atli, B., Gandhi, F., and Karst, G., "Thermomechanical Characterization of Shape Memory Polymers", Journal of Intelligent Material Systems and Structures, 20, 87-95 (2009).

[91] Lan, X., Liu, Y., Lv, H., Wang, X., Leng, J., and Du, S., "Fiber Reinforced Shape-Memory Polymer Composite and its Application in a Deployable Hinge", Smart Material and Structures, 18, 1-6 (2009).

[92] Ni, W., Cheng, Y., and Grummon, D., "Recovery of Microindents in Nickel-Titanium Shape-Memory Alloy: A "Self-Healing" Effect", Applied Physics Letters 80, 3310-3312 (2002).

[93] Gao, X., Burton, D. S., and Brinson, L. C., "Finite Element Simulation of a Self-Healing Shape Memory Alloy Composite", Mechanics of Materials 38, 525-537 (2006).

[94] Nji, J., Li, G., "A Self-Healing 3D Woven Fabric Reinforced Shape Memory Polymer Composite for Impact Mitigation", Smart Materials and Structures, 19, 1-9 (2010).

[95] Chang, L.C., Read, T. A., "Plastic Deformation and Diffusionless Phase Changes in Metals- The Gold-Cadmium Beta Phase", Transactions of the American Institute of Mining, 189, 47 (1951).

[96] Buehler, W.J., Gilfrich, J.V., Wiley, R.C., "Effect of Low-Temperature Phase Changes on the Mechanical Properties of Alloys near Composition TiNi", Journal of Applied Physics, 34, 1475-1476 (1963).

[97] Pelrine, R., Kornbluh, R., Pei, Q., Stanford, S., oh, S., Eckerle, J., Full, R. J., Meijer, K., "Dielectric Elastomer Artificial Muscle Actuators: Towards Biomimetic Motion", Proceeding of SPIE Vol. 4685, 126-137 (2002).

[98] Hu, J.L., Ding, X.M. and Tao, X.M., "Shape Memory Polymers and Their Applications to Smart Textile Products", Journal of China Textile University, 19, 89-93 (2002).

[99] Mazzoldi, A., DeRossi, D., "Conductive Polymer Based Structures for a Steerable Catheter", Proceedings of the Electroactive Polymer Actuators and Devices Vol. 3987, 273-280 (2000).

[100] Bar-Cohen, Y., "Editorial: Focus Issue on Biomimetics Using Electroactive Polymers as Artificial Muscles,'' Bioinspiration and Biomimetics, 2, 1-3 (2007).

[101] Scrosati, B., "Application of Electroactive Polymers", Chapman and Hall, London, 29-30 (1993).

[102] Gall, K., Dunn, M.L., Liu, Y., Finch, D., Lake, M., Munshi, N.A., "Shape Memory Polymer Nanocomposites," Acta Materialia, 50, 5115-5126 (2002).

[103] Sokolowski, W.M., Chmielewski, A.B., Hayashi, S. and Yamada, T., "Cold Hibernated Elastic Memory (CHEM) Self-deployable Structures", In: Electroactive Polymer Actuators and Devices Conference, (1999).

[104] Bar-Cohen, Y.. and Zhang, Q., "Electroactive Polymer Actuators and Sensors", MRS Bulletin, 33, 173-181 (2008).

[105] Lendlein, A., Kelch, S., "Shape-Memory Polymers", Angewandte Chemical International Edition, 41, 2034-2057 (2002).

[106] Hu, J., "Shape Memory Polymers and Textiles", Woodhead Publishing Limited, Cambridge, England (2007)

[107] Liu, Y., Gall, K., Dunn, M. L., Greenburg, A. R., and Diani, J., "Thermomechanics of Shape Memory Polymers: Uniaxial Experiments and Constitutive Modeling", International Journal of Plasticity, 22, 279-313 (2006).

[108] Tobushi, H., Okumura, K., Hayashi, S., and Ito, N., "Thermomechanical constitutive model of shape memory polymer", Mechanics of Materials, 33, 545-554 (2001).

[109] Wilson, T.S., Bearinger, J.P., Herber, J.L., Marion, J.E., Wright,W.J., Evans, C.L., Matilad, D.J., "Shape Memory Polymers Based on Uniform Aliphatic Urethane Networks", Journal of Applied Polymer Science, 106, 540-551 (2007).

[110] Maitland, D.J., Metzger, M.F., Schuamm, D., Lee, A., Wilson, T.S., "Photothermal Properties of Shape Memory Polymer Micro-Actuators for Treating Stroke" Lasers in Surgery and Medicine, 30, 1-11 (2002).

[111] Safranski, D. L., and Gall, K., "Effect of Chemical Structure and Crosslinking Density on the Thermo-Mechanical Properties and Toughness of (meth)acrylate Shape Memory Polymers", Polymer, 49, 4446-4455 (2008)

[112] Li Z., and Yang, L., "The Near-Tip Stress Intensity Factor for a Crack Partially Penetrating an Inclusion," Journal of Applied Mechanics, 71, 465-469 (2004)

[113] Morgan, N. B., "Medical Shape Memory Alloys-The Market and It's Products", Material Science and Engineering, 378, 16-23 (2004).

[114] Leka, L. G., Bayo, E., "A Close Look at the Embedment of Optical Fibers into Composite Structures", Journal of Composite Technology, 11, 106-112 (1989).

[115] Small, W., Wilson, T. S., Benett, W. J., Loge, J. M., Maitlad, D. J., "Laser-Activated Shape Memory Polymer Intravascular Thrombectomy Device", Radiology, 13, 8204-8213 (2005).

[116] Chang, P. C., and Chi Liu, S., "Recent Research in Nondestructive Evaluation of Civil Infrastructures", Journal of Materials in Civil Engineering, 15, 298-304 (2003).

[117] Fratzl, P., and Weinkamer, R., “Hierarchical Structure and Repair of Human Bone: Deformation, Remodeling, Healing”, Springer Series in Material Science, 100, 323-335 (2007),